CHEMICAL BEHAVIORS
OF
TIN, ANTIMONY, AND TELLURIUM FISSION PRODUCTS

HIROTAKE MORIYAMA
KYOTO UNIVERSITY
1980

CHEMICAL BEHAVIORS
OF
TIN, ANTIMONY, AND TELLURIUM FISSION PRODUCTS

HIROTAKE MORIYAMA
KYOTO UNIVERSITY
1980

CONTENTS

SYNOPSIS

The present study deals with chemical consequences of nuclear fission, in particular chemical behaviors of fission products in aqueous solutions. The tin, antimony, and tellurium fission products are chosen since their nuclear data and fission yields have been accomplished. The distribution of these fission products between the reduced and oxidized states is studied from the viewpoint of hot atom chemistry.

In Chapter 1, the reviews are made on the chemical consequences of nuclear fission in order to explain the standpoints and motives of the present investigations. Besides, the general theories in hot atom chemistry are briefly reviewed since they are very instructive to discuss the chemical behaviors of fission products.

In Chapter 2, the radiation-induced reactions of antimony and tellurium compounds in sulfuric acid solutions are studied using double tracers for each element. The double tracers are very effective to have information not only on the overall yield but also on the respective yields: G(Sb(III) → Sb(V)), G(Sb(V) → Sb(III)), etc. The reaction mechanisms in aerated solutions are confirmed and some rate constants are evaluated. A possible mechanism of γ-ray-induced reactions in deaerated solutions is proposed, in which Sb(III) is reduced by H and oxidized by OH, Sb(II) is oxidized by H_2O_2 and Sb(IV), and

the disproportionation of Sb(IV) to Sb(III) and Sb(V) follows. In the presence of Sb(V), reduction of Sb(V) by H gives the same stoichiometry. The results on Te(IV) and Te(VI) in dilute sulfuric acid solutions support a similar sequence to that of antimony system, in which the unstable valence states Te(III) and Te(V) play an important part. Besides, both the reactor radiation-induced reactions and the fission-fragment-induced reactions are well elucidated with these mechanisms.

In Chapter 3, the chemical effects of β-decay processes: $^{128}Sn \rightarrow {}^{128}Sb^{m}$, $^{127}Sb \rightarrow {}^{127}Te^{g}$, and $^{129}Sb \rightarrow {}^{129}Te^{g}$ are studied in sulfuric acid solutions. It is confirmed that the results are not of the thermal reactions but of the hot reactions since neither scavenger effect nor temperature-dependence has been observed. Te(IV) are formed with the yield of ∿20 % in the case of $^{127,\ 129}Sb(V) \rightarrow {}^{127g,\ 129g}Te$. The formation of Te(IV) is probably due to bond rupture caused by electronic excitation and ionization since the recoil energies are comparatively low. In the β-decay processes $^{128}Sn(IV) \rightarrow {}^{128}Sb^{m}$ and $^{127,\ 129}Sb(III) \rightarrow {}^{127g,\ 129g}Te$, the essential factors are considered to be the thermodynamic stability of the primary products and their subsequent reactions as well as the electronic excitation and ionization.

In Chapter 4, the oxidation states of tin, antimony, and tellurium isotopes formed predominently(>91 %) by fission are investigated in aqueous solutions of ^{233}U irradiated in a reactor.

Results are corrected for the thermal reactions with the bulk radiolysis products using tracers for each element. In 0.4 M H_2SO_4 solutions containing $^{233}UO_2^{2+}$, Te(IV), and Te(VI), the fraction of Te(IV) is 98 ± 2 % in the absence of oxygen and 92 ± 3 % in the presence of oxygen. In frozen solutions of the same composition, the fraction of Te(IV) is 83 ± 2 % in the absence of oxygen and 81 ± 3 % in the presence of oxygen. Similar differences are also found in the case of the antimony isotopes in 0.4 M H_2SO_4 solutions and the tin isotopes in 1 M HCl solutions. For the interpretation of the differences, the reducing action of the species diffusing from the track of the fission fragments are considered. It is concluded that, in the frozen system, the distribution of the fission products between the reduced and oxidized states is resulted from the hot reactions but that, in the liquid system, there is the possibility of the fission products being involved in the thermal reactions with the diffusing radicals from their own tracks. The results of the hot reactions show two interesting features: (i) the higher the reduction potential is, the larger the fraction of the reduced states is, and (ii) the fraction of the reduced states of Sb and Te isotopes is only 80 % in spite of their high reduction potentials. Considering physical concepts, it is suggested that, together with a very high temperature of the thermal spike of fission, the electronic excitation of the products can allow the fission products to undergo the chemical

reaction requiring a high activation energy.

Chapter 5 describes the analysis of the oxidation states of the antimony and tellurium isotopes formed cumulatively by fission. The differences in the oxidation states of the isotopes are attributed to different modes of formation. The tin and antimony precursors would be oxidized by the radicals formed in the irradiated solutions because of no carrier. The fractions of the tellurium isotopes as Te(IV) formed by β-decay of the antimony precursors in the +5 oxidation state are dependent on the isotopes; the higher β-decay energy is, the more the fraction as Te(IV) is. The differences are attributed to different recoil energies. In contrast to the Te isotopes, the fraction of the Sb isotopes as Sb(III) formed by β-decay of the tin precursors in the +4 oxidation state are nearly constant irrespective of their β-decay energies. This is due to the fact that the newly formed antimony atom in the +5 oxidation state must rearrange its chemical structure. In the separate experiment of the neutron capture reaction $^{130}Te(n, \gamma)^{131}Te^{g}$, higher yields (>90 %) of Te(IV) have been obtained when starting with both Te(IV) and Te(VI). A comparison between fission and neutron capture suggests the importance of the electronic excitation of the products in the case of fission.

In Chapter 6, the conclusive remarks are given for the present investigations. The author's present view is summarized on the overall process of the chemical behaviors of fission products.

CHAPTER 1

GENERAL INTRODUCTION

Fission was chemically discovered by Hahn and Strassman in 1939 (Ha39). Immediately, Meinter and Frisch realized that a large amount of energy would be released as the kinetic energy of the two fragments recoiling from each other (Me39). Frisch was the first to observe the effects of this energy in the large amount of ionization which the recoiling fragments produce in a gas (Fr39). Since that time much research has been given to the physical and chemical aspects of the recoil process (see, for example, Wa57, Mc71a, Wa79).

In spite of much extensive studies on the chemical consequences of fission, the mechanism is still rather illunderstood because it is very complicated. The initial chemical state of the newly formed fission products is not known actually... It would be particularly valuable to know what states they assume in nuclear fuels, but direct information on this topic is difficult to obtain; for the most part we have to be content with inferences from theory or from experiments in which the fuels were dissolved or otherwise destroyed. This limitation often makes the subject complicated together with precursor effects and fission damage.

In the present experimental study, we intend to improve

our knowledge on the chemical behaviors of fission products.

1.1. Chemical Consequences of Nuclear Fission

Fission fragments, including atoms of all the elements in the middle of the periodic table, are all exceedingly energetic when first formed. They dissipate their energy very rapidly in the medium through which they pass, leaving dence tracks of ion-pairs. The fragments lose a large number of electrons in the initial stage, giving them charges in the region of +20. As they slow down, they tend to pick up electrons again from the medium. After slowing down, most of the fission products undergo radioactive decay. Chemical observations on the fission products usually refer to the later members of the decay chains, and these arise mainly through decay of precursors instead of directly in fission. Furthermore, the interaction of the results is often complicated by fission damage.

Nevertheless, the oxidation state of fission products has been the subject of a number of publications since it was first reported for the selenium, tellurium, and iodine fission products (St51). For the iodine fission products most studied, it was shown that the fractions of the reduced states increase in the case of uranyl iodate (Ha61), uranyl nitrate (Sp73), and uranyl chloride (Sp76) in the order of ^{131}I, ^{133}I, ^{135}I. Since the fractional independent fission yield increases in the same

order, a qualitative relationship between the oxidation states of the iodine isotopes and their mode of formation is likely to exist. Another illustration of this relationship was also found in the formation of radioactive methyl iodine by the recoil of the iodine fission products (De63, Pa64).

Interesting results concerning the oxidation state were reported for the tin fission products formed in several liquid and solid media from thermal neutron induced fission of ^{235}U (Br67). In the irradiated solutions, ^{121}Sn is formed mainly in the +4 oxidation state, whereas other isotopes prefer the +2 oxidation state. The difference was attributed to different modes of formation, since ^{121}Sn is known to be formed predominently by β-decay whereas more than one-half of ^{125}Sn is formed independently by fission (Er71). Later, it was shown that the fraction as Sn(II) from β-decay increases with mass number, possibly because of increasing recoil energy, and that it overlaps the fraction as Sn(II) for independently formed tin fission products (Er69a, Li73).

Generally speaking, the fission products formed independently favor the reduced states, whereas the oxidized states tend to persist during β-decay of precursors. Several investigators have attributed the differences to different modes of formation. However, attempts to develop a quantitative situation have often been handicapped by the lack of studies of isotopes formed with known large fractional independent fission yields. In order

to learn more about the nature of high energy chemical reactions, it is of interest to study quantitatively and systematically the oxidation state of the other neighbouring elements in the periodic table.

The present study deals with chemical consequences of fission, in particular chemical behaviors of fission products in aqueous solutions. The reason why aqueous solutions are chosen is that the hot reactions are quantitatively distinguished from the thermal reactions as mentioned later. The tin, antimony, and tellurium fission products were chosen for the following reasons:

(i) They have at least two oxidation states which hardly exchange in aqueous solutions.
(ii) They are adjacent to one another in the periodic table including the most studied iodine fission products.
(iii) Their nuclear data and fission yields have been accomplished very well.
(iv) Some of them have the large fractional independent fission yields in thermal neutron induced fission of ^{233}U.

1.2. General Theories in Hot Atom Chemistry

In this Section, we review the general theories in hot atom chemistry. They are very instructive to discuss the

chemical behaviors of fission products.

Atoms with abnormal kinetic energies and charge are often described as "hot" and the study of their chemical reactions are described as "hot atom chemistry". In coming to equiribrium with their surroundings, the newly formed atoms take part in a variety of physical and chemical processes. The consequences are often striking.

1.2.1. Bond rupture by recoil

Soon after the discovery of the radioactivity, it was known that the products of α-decay carry any kinetic energy by recoil. However, the first remarkable discovery in the field was made by Szilard and Chalmers in 1934 (Sz34). When liquid ethyl iodide was irradiated with neutrons, a proportion of ^{128}I formed in the $^{127}I(n, \gamma)\ ^{128}I$ reaction could be extracted from ethyl iodide. Subsequently, Fermi et al. (Am35) showed that the recoil energy given to the nucleus by the emission of gamma rays following thermal neutron capture was sufficient to break the bonds holding the capturing atom to the remainder of the molecule.

Various pictures of the chemical processes occurring have been proposed, especially in relation to (n, γ) reactions in organic halogen compounds. An elastic-collision model was firstly proposed by Libby (Li47) and extended by Miller, Gryder and Dodson (Mi50). The essential feature of this model is

that the recoil atom loses its energy predominently in "billiard ball" collisions with the atoms of the surrounding molecules. The recoil energies in some nuclear transformations are summarized in Table 1.1.

The billiard-ball model and its modifications have stimulated much experimentation, which has on the whole served to reveal its inadequency rather than to confirm it. The tendency nowadays is to discount the significance of elastic collisions, even sometimes in the gas phase, and to emphasize the energy region around and below 10 eV as the region of hot or epithermal reactions. No attempts is normally made to distinguish hot from epithermal reactions.

A particular difficulty about the billiard-ball model as regards condensed phases is that elastic collisions do not disperse the energy quickly enough. This suggests an approach of a different character, based on the idea of a "hot zone" or "displacement spike", as it is often called in radiation damage studies. The first concept of this kind was the "random fragmentation model" (Wi53). Later versions (Ha58) of the picture emphasize inelastic collisions, more moderate temperatures, the production of relatively few radicals, and chemical reactions in which the parent molecules play important part.

1.2.2 Abnormal charge

The rupture of the C-Br bond was discovered during the

Table 1.1. Approximate recoil energies expected with various nuclear events.

Nuclear Process	Range of recoil energy in eV *
β^- decay	10^{-1} to 10^{2}
β^+ decay	10^{-1} to 10^{2}
α decay	$\sim 10^{5}$
Isomeric transition	10^{-1} to 1
Electron capture	10^{-1} to 10^{1}
n, γ (thermal)	$\sim 10^{2}$
n, p	$\sim 10^{5}$
Fission	$\sim 10^{8}$

* Based on the mass of the hot atom $\sim$ 100 and considering the most probable kinetic energy for a given nuclear process and a range of nuclear energies that are most frequently encountered. See, for details, the literature (Li47).

isomeric transition of $^{80}Br^{m}$ to $^{80}Br^{g}$ by Segre and Seaborg (Se39) and DeVault and Libby (De39). Since the direct recoil is inadequate to explain the phenomena, some other process must be invoked. The accepted theory is that ionization consequent of internal conversion is responsible (Se40).

Later, Wexler (We60) showed using a charge spectrometer that the $^{80}Br^{m}$ atoms are charged up to +13 as shown in Fig. 1.1 and suggested the "Coulomb explosion model". On internal conversion, a K-shell vacancy initiates a cascade of processes in which vacancies in the inner shells are filled by electrons from the outer shells, and X-rays and Auger electrons are emitted (Fig. 1.2). The net result is the loss of least one and usually several vacancy electrons. The loss of these electrons naturally tends to dissolve the chemical bonds, and in addition, when there is a possitive charge of +2 or more, the molecule tends to fly apart under the influence of Coulomb repulsions. Besides the effects associated with the Auger process, it is known that abnormal charges are formed by electron shake off in β-decay and electron capture (Ca60).

1.2.3. Hot and thermal reactions

Besides hot reactions occuring while the atom in question still carries excess kinetic energy, there may also be ordinary thermal reactions, occuring after the atom has come to thermal equilibrium with its surroundings. There are various criteria

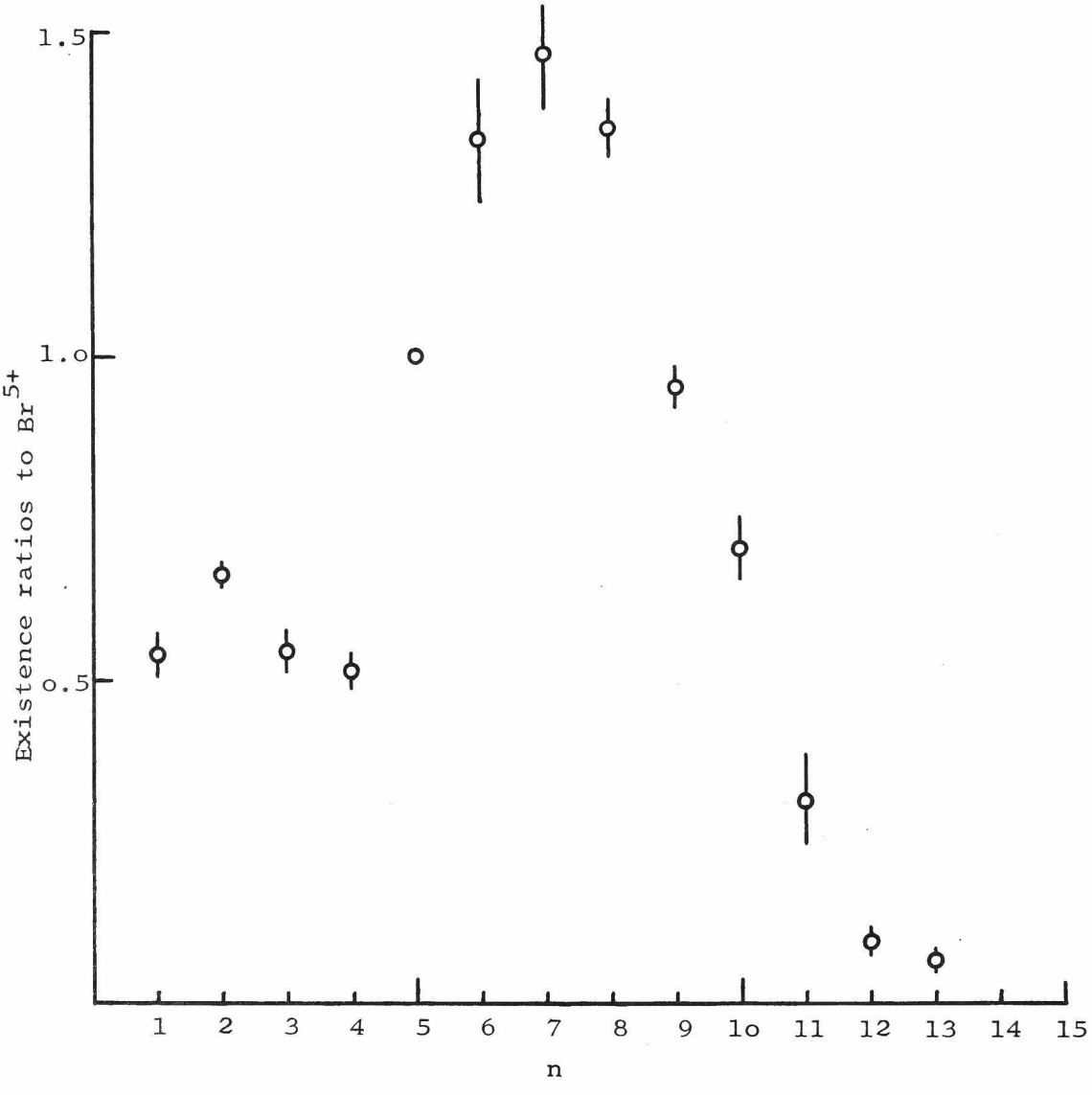

Fig. 1.1. Distribution of Br^{n+} ions produced from isomeric transition of $CH_3{}^{80}Br^m$ (We60).

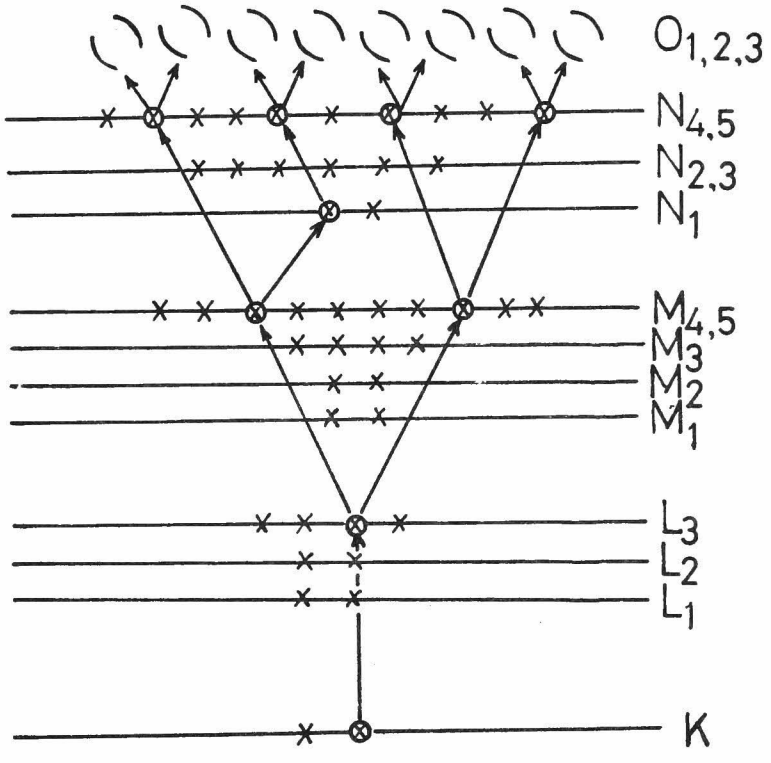

Fig. 1.2. Typical example of a vacancy cascade in Xe.

for distinguishing between the two types.

In the gas phase, thermal and hot reactions can be distinguished by adding to the system "moderates" such as herium and neon. Collisions between the inert gas atoms and the hot atoms remove energy from the latter, tending to reduce them to thermal energies, and favor the occurrence of thermal against hot reactions. Any product whose yield increases on adding inert gas may be assumed to be formed by a thermal reaction, and any whose yield decreases, by a hot reaction. Estrup and Wolfgang (Es60, Wo63) have developed a quantitative theory of hot atom reactions for gas phase, which is often called the "impact model".

The most important technique in liquid-phase investigations is to add small quantities of atom or radical scavengers to the system. Those most commonly used are oxygen, nitric oxide, bromine, and iodine. They act by removing chemically reactive species. A scavenger at a low concentration depends on diffusion of recoil atoms for its effect. However, recoil atoms will be reduced to thermal energies in the course of diffusion. It follows that scavenger-sensitive reactions are thermal reactions and scavenger-insensitive are not.

Another possible criterion for distinguishing hot from thermal reactions is temperature-dependence. The former should be independent of thermal activation, whereas the latter should follow the Arrhenius equation. It has been argued that hot

reactions should be relatively insensitive to phase changes, but that thermal reactions should be sensitive. The idea is that the hot recations occur mainly in a zone of chemical destruction, which would be of similar character whether formed in a solid or a liquid.

In the present study, the measurements are reported of the tin, antimony, and tellurium fission products in the irradiated aqueous solutions. From the viewpoint of hot atom chemistry, the results should be analyzed to distinguish the hot from the thermal reactions. The radiation-induced reactions are considered to be most important in the irradiated solutions. The following criteria are adopted:

(i) With the use of labeled carriers, the newly formed atoms are protected from the thermal reactions including the radiation induced reactions. The labeled carriers may allow us to correct the results for the thermal reactions provided the thermal reactions happen.
(ii) Oxygen is adopted as a radical scavenger, in particular, for the localized reducing species such as in fission tracks.
(iii) Temperature-dependence is studied both at room temperature and at dry ice temperature.

In the following Chapters, the experimental evidences are

described and discussed to improve our knowledge on the chemical behaviors of fission products. Chapter 2 describes the mechnisms of the radiation-induced reactions of the antimony and tellurium compounds in sulfuric acid solutions. Chapter 3 describes the chemical effects associated with β-decay of the tin and antimony isotopes. In Chapter 4 are described the oxidation states of the independently formed fission products. Chapter 5 describes the analysis of the oxidation states of the cumulatively formed fission products. Chapter 6 involves the summary of the improved knowledge of chemical behaviors of fission products.

CHAPTER 2

RADIATION-INDUCED REACTIONS

2.1. Introduction

As mentioned in the previous chapter, there is the possibility of the fission products being involved in the "thermal" reactions within the medium. The radiation-induced reactions are most important in solutions irradiated. This chapter deals with the radiation-induced reactions of the antimony and tellurium compounds in sulfuric acid solutions.

The absorption of radiation by water generates various radical and molecular species (Ma65), notably

$$H_2O \xrightarrow{\gamma} e^-_{aq},\ H,\ OH,\ H_2,\ H_2O_2,\ H^+,\ OH^-. \qquad (2.1)$$

In acidic solutions e^-_{aq} is converted to H atoms (Al60) by the reaction

$$e^-_{aq} + H^+ \rightarrow H, \qquad (2.2)$$

with a rate constant of $2 \times 10^{10}\ M^{-1}\ sec^{-1}$ (Ke64). The equilibrium

$$H^+ + OH^- \rightarrow H_2O, \qquad (2.3)$$

is sufficiently rapidly achieved so that the effects of the radiation-produced H^+ and OH^- can be neglected, particularly in acidic solutions. Thus the species whose effects are to be considered are confined:

$$H_2O \xrightarrow{\gamma} H,\ OH,\ H_2,\ H_2O_2. \qquad (2.4)$$

The yields of radiolysis of several redox systems including Sb(III)-Sb(V) (Ma61, Ka61, A174) and Te(IV)-Te(VI) (Ha63, Ha67, Ha68) have been investigated by the use of γ rays from a ^{60}Co source. Matsuura et al. (Ma61) have reported that Sb(III) in aerated 0.4 M H_2SO_4 and 0.8 M HCl solutions is oxidized to Sb(V) by OH and HO_2 radicals with G(Sb(V)) of $\sim$3. They have also found that the yield of oxidation in deaerated solutions is quite lower than that in aerated solutions. The latter fact suggests that reduction by H atoms takes place in deaerated solutions and competes with oxidation by OH radicals. A similar finding on the tellurium system was reported by Haissinsky et al. (Ha63, Ha67, Ha68). They attributed the decrease of the yield of oxidation to the occurrence of reduction of Te(VI) by H atoms in deaerated solutions. In order to discuss the kinetics in detail, however, it is indispensable to have information not only on the overall yield but also on the respective yields: G(Sb(III) $\rightarrow$ Sb(V)), G(Sb(V) $\rightarrow$ Sb(III)), etc.

In this chapter, γ-ray-induced reactions of Sb(III) and

Sb(V) in 0.4 M H_2SO_4 solutions and those of Te(IV) and Te(VI) in 0.02 M H_2SO_4 solutions are investigated using double tracers for each element. Results are interpreted on the basis of reactions of solutes with H, OH, H_2, and H_2O_2 which are the primary species in acid solutions. The direct absorption of γ rays in the H_2SO_4 is neglected as electron fraction of H_2SO_4 is quite lower than that of water (Se73). The following yields are adopted: $g_H = 3.68$, $g_{OH} = 2.96$, $g_{H_2} = 0.45$, and $g_{H_2O_2} = 0.81$ (Ma58). The unstable valence states Sb(II), Sb(IV), Te(III), and Te(V) are concluded to play an important part in the reaction mechanisms. The radiation-induced reactions in reactors are also discussed.

2.2. Experimental

2.2.1. Preparations

The guaranteed reagents obtained from Nakarai Chemicals, Ltd., were used without further purification. Triply distilled water was used to make up all the solutions. The tracers ^{124}Sb, ^{125}Sb, $^{123}Te^{m}$, and ^{132}Te were produced in the Kyoto University reactor. The solutions of Sb(III), Sb(V), Te(IV), and Te(VI) labeled with ^{124}Sb, ^{125}Sb, $^{123}Te^{m}$, and ^{132}Te, respectively, were prepared. All the specific activities were adjusted to $\sim$1 mCi g^{-1}.

(A) Sb(III) labeled with ^{124}Sb (Sc63a)

About 10 mg of antimony metal was irradiated for 80 hours at a position where the thermal neutron flux was $\sim 4.7 \times 10^{13}$ cm^{-2} sec^{-1}, the epithermal neutron flux was $\sim 2 \times 10^{12}$ cm^{-2} sec^{-1}, the fast neutron flux was $\sim 5 \times 10^{13}$ cm^{-2} sec^{-1}. The antimony metal was dissolved in concentrated hydrochloric acid which contained an adequate amount of antimony to adjust the specific activity. The solution was adjusted to 3 M in HCl and antimony sulfide was precipitated with hydrogen sulfide. The antimony sulfide was dissolved in concentrated sulfuric acid. Complete reduction of the antimony was achieved by passing sulfur dioxide. Excess sulfur dioxide was removed by boiling.

(B) Sb(V) labeled with ^{125}Sb (Sc63a)

About 1 g of tin metal was irradiated for 80 hours at the

same position as that of the ^{124}Sb. After allowing the ^{125}Sn to decay to the ^{125}Sb, the tin metal was dissolved in concentrated hydrochloric acid which contained an adequate amount of antimony carrier. The solution was adjusted to 3 M in HCl and antimony sulfide was precipitated with hydrogen sulfide. The antimony sulfide was dissolved in concentrated sulfuric acid. Complete oxidation was achieved by boiling the solution with hydrogen peroxide repeatedly. Excess peroxide was destroyed by boiling in the presence of platinum metal.

(C) Te(IV) labeled with ^{132}Te (Fe63)

About 0.1 mg of U_3O_8 enriched to 90 % in ^{235}U (obtained from Atomic Fuel Industrial, Ltd.) was irradiated at a position where the thermal neutron flux was $\sim 1.3 \times 10^{13}$ cm^{-2} sec^{-1}, the epithermal neutron flux was $\sim 1 \times 10^{12}$ cm^{-2} sec^{-1}, and the fast neutron flux was $\sim 4 \times 10^{12}$ cm^{-2} sec^{-1}. The U_3O_8 was dissolved in 6 M hydrochloric acid which contained an adequate amount of tellurium carrier. The solution was boiled with hydrozine hydrochloride and adjusted to 2.4 M in HCl with the addition of tartaric acid. The tellurium was reduced to the metallic form by $NaHSO_3$ and dissolved in hot nitric acid. The solution was evaporated to dryness and the residue was dissolved with 10 % potassium hydroxide. The solution was neutralized with dilute nitric acid. The precipitate was filtered and dissolved in concentrated sulfuric acid.

(D) Te(VI) labeled with $^{123}Te^{m}$ (Fe63)

About 1 g of tellurium metal was irradiated for 80 hours at the same position of the ^{124}Sb. The tellurium metal was dissolved in hot nitric acid and oxidized to Te(VI) with potassium permanganate. The insoluble manganese dioxide was dissolved with hydrogen peroxide. After repeated recrystallization of the telluric acid, it was dissolved in a desired solution.

(E) Carriers

The carriers Sb(III), Sb(V), Te(IV), and Te(VI) were made up in the same manner as the corresponding tracers, but the solutions were hydrochloric acid solutions. The concentrations of the carriers were calculated from the weights of the starting materials and were confirmed by a neutron activation method.

2.2.2. Irradiations

Sample solutions were deaerated with oxygen free argon gas and were sealed in 10 ml irradiation vessels. The sample solutions were irradiated for 10 - 100 min at the ^{60}Co γ ray irradiation facility of the Institute for Chemical Research, Kyoto University (Ka70). Doses were determined from G(Fe(III)) = 15.60 (Fr66) for the Fricke dosimeter and the dose rate was 9.5×10^{17} eV l^{-1} sec^{-1}.

2.2.3. Chemical separation of Sb(III) and Sb(V)

The irradiated sample solution, to which 10 mg of Sb(III)

and 10 mg of Sb(V) carriers were added, was adjusted to 1 M in HCl. The solution was passed through an ion-exchange column (2 cm diameter x 5 cm) containing Dowex 1X8 (RCl, 200 - 400 mesh). The column was washed with several free volumes of HCl solutions of the same concentration. Sb(V) which passed through the column was precipitated by H_2S. Sb(III) adsorbed in the column was eluted with 20 ml of 20 % $NaKC_4H_4O_6$ solution which had been made basic with about 1 ml of concentrated NH_4OH and precipitated by H_2S. A typical example of the separation of Sb(III) and Sb(V) is given in Fig. 2.1. The amounts of adsorption of Sb(V) by anion exchanger in 1 M HCl solutions were less than 1 % and those of Sb(III) were more than 99 %. It was also found that negligible exchange reactions between Sb(III) and Sb(V) occurred in 0.4 M H_2SO_4 solutions and in separation process. Chemical yields of Sb(III) and Sb(V) were determined by a neutron activation method and found to be more than 80 %.

2.2.4. Chemical separation of Te(IV) and Te(VI)

The irradiated sample solution, to which 10 mg of Te(IV) and 10 mg of Te(VI) carriers were added, was adjusted to 6 M in HCl. The solution was passed through an ion-exchange column containing Dowex 1X8. Te(VI) which passed through the column was reduced to the metallic form by boiling the solution with hydrazine hydrochloride and $NaHSO_3$. Te(IV) adsorbed in the column was eluted with 20 ml of 0.1 M HCl solution and was

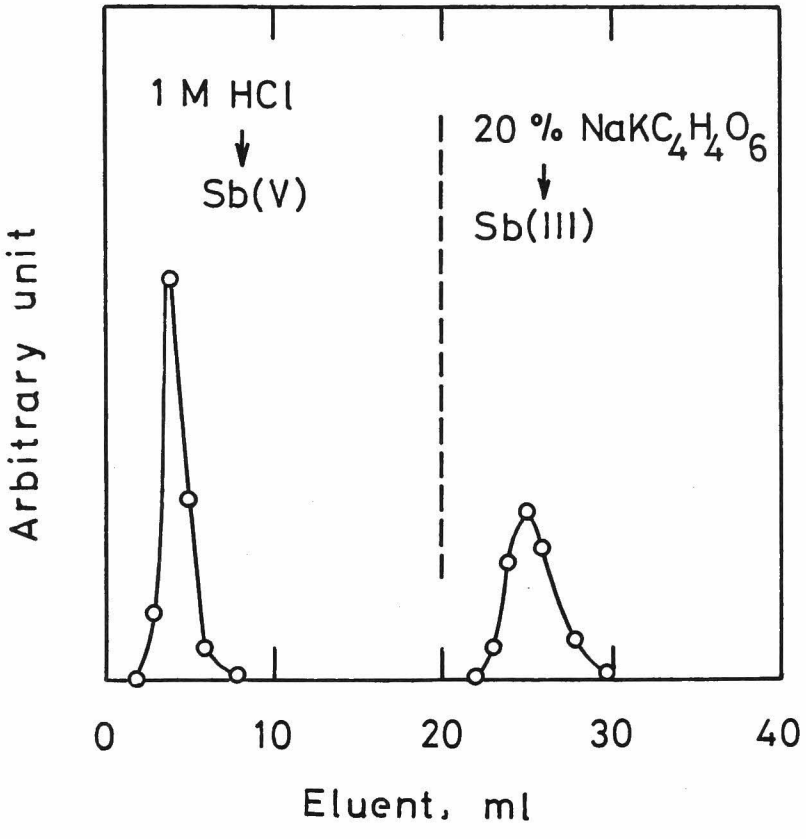

Fig. 2.1. Typical elution curve for anion exchange separation of Sb(III) and Sb(V). See text.

reduced to the metallic form by $NaHSO_3$. A typical example of the separation of Te(IV) and Te(VI) is given in Fig. 2.2. The amounts of adsorption of Te(VI) by anion exchanger in 6 M HCl solutions were less than 0.2 % and those of Te(IV) were more than 99.8 %. It was also found that negligible exchange reactions between Te(IV) and Te(VI) occurred in dilute H_2SO_4 solutions and in separation process. Chemical yields of Te(IV) and Te(VI) were determined by weighing and were found to be more than 90 %.

2.2.5. Measurements

The γ rays associated with each tracer were summarized in Table 2.1 and were analyzed with a 54 cm^3 Ge(Li) detector connected to 400 channel pulse height analyzer. The yields of oxidation of Sb(III) and Te(IV) and those of reduction of Sb(V) and Te(IV) were obtained. The absolute yields were obtained by the equation

$$G = 100N\Delta S/D \qquad (2.5)$$

where, N is the Abogadro's number, ΔS is the difference in concentration of a solute in M, and D is absorbed dose in eV l^{-1}.

The yields of peroxide were also determined by the addition of Fe(II) solution immediately following irradiation. These measurements were performed in 0.8 M HCl solutions since a chain

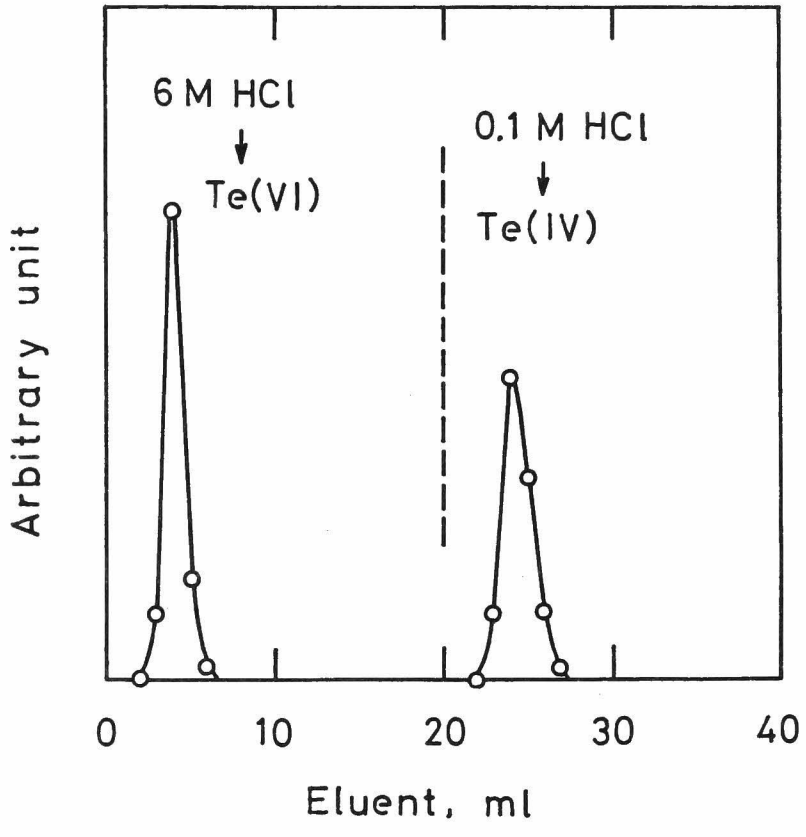

Fig. 2.2. Typical elution curve for anion exchange separation of Te(IV) and Te(VI). See text.

Table 2.1. γ Rays associated with the tracers (B177).

Tracer	Half life	γ-Energy, MeV	γ-Abundance
^{124}Sb	60.2 d	723.	0.106
^{125}Sb	2.73 y	428.	0.304
$^{123}Te^{m}$	117. d	159.	0.841
^{132}Te	78. h	228.	0.88

oxidation of Fe(II) and Sb(III) occurred in aerated 0.4 M H_2SO_4 solutions containing hydrogen peroxide (Ma62). Fe(III) was measured spectrophotometrically and the molar extinction coefficient was 830 M^{-1} cm^{-1} in 0.8 M HCl (Ma62). It was also found by the addition of $KMnO_4$ solution that most of peroxide was composed of hydrogen peroxide. Hydrogen was assumed to be the other product of irradiation and the yields were calculated on the basis of stoichiometry.

The uncertainty (standard deviation) to be assumed to each measurement was arrived at by root-mean-square combination of the variuos individual sources of random error, which were as follows: γ-ray measurements, chemical yield determinations, absorbed dose measurements, etc. When several determinations of a yield were made, the weighted average was obtained by weighting each individual value by the inverse square of its assigned standard deviation σ_i. The uncertainty is the value σ obtained from $1/\sigma^2 = \Sigma(1/\sigma_i^2)$.

2.3. Results and Discussion

For the sake of simplicity and for the lack of information of the exact nature of the chemical species present in solution, the various valence states of the ions are indicated by Roman numerals inclusively. For example, trivalent antimony is represented by Sb(III) even though it may be present as SbO^+ or in some other form in a dilute sulfuric acid solutions (Da70).

2.3.1. Interfering thermal reaction

In the preliminary experiments with the tracers, the thermal reactions excluding the radiation-induced reactions were studied, which would interfere with the exact measurements of the radiation-induced reactions. The separation was carried out following the procedures described above.

(A) Antimony

The most stable oxidation states of antimony in solution are Sb(III) and Sb(V) (Pi57). The thermal reactions which were studied are the oxidation of Sb(III), the reduction of Sb(V), and the exchange between Sb(III) and Sb(V). The results are given in Table 2.2. The exchange reaction in 1 M HCl evidently occurs although none of the other reactions occurs. The exchange rate was obtained to be about 2×10^{-6} M^{-1} min^{-1} using the Mckay's equation (Mc71b)

Table 2.2. Thermal reactions of Sb(III) and Sb(V) at room temperature.*

Solution	$[Sb(III)]_0$, mM	$[Sb(V)]_0$, mM	Time elapsed	Δ[Sb(III)→Sb(V)], mM	Δ[Sb(V)→Sb(III)], mM
0.4 M H_2SO_4	0.5	-	1 week	<0.005	
"	-	0.5	"		<0.005
"	0.5	0.5	"	<0.005	<0.005
1 M HCl	1.0	-	"	<0.01	
"	-	1.0	"		<0.01
"	1.0	1.0	<3 min	<0.01	<0.01
"	1.0	1.0	60 min	0.1	0.1

* All the separations were performed within 1 min.

$$R = - \frac{[Sb(III)][Sb(V)]}{([Sb(III)] + [Sb(V)])t} \ln(1-F) \qquad (2.6)$$

where, F is called the fraction of exchange and t is the time elapsed. The rate of 2×10^{-6} M^{-1} min^{-1} is in fair agreement with the ones which has been reported for 1 M HCl containing 0.66 mM Sb(III) and 0.66 mM Sb(V) (Ka65).

Although no reaction occurs in 0.4 M H_2SO_4 solutions, the exchange reaction between Sb(III) and Sb(V) in 1 M HCl occurs to a fair extent. The exchange reaction might interfere with the exact measurement of the radiation-induced reactions. To avoid the errors, the separation of Sb(III) and Sb(V) should be performed within a few minutes.

(B) Tellurium

The most stable oxidation states of tellurium in solution are Te(IV) and Te(VI) (Ho60). The thermal reactions which were studied are the oxidation of Te(IV), the reduction of Te(VI), and the exchange between Te(IV) and Te(VI). The results are given in Table 2.3. No measurable reaction occurred in sulfuric acid solutions. In 6 M HCl solutions, however, the reduction of Te(VI) occurs considerably. It was found that 6 M HCl reduced Te(VI) to Te(IV) so rapidly that the exchange reaction could not be studied accurately. The reduction of Te(VI) by HCl might interfere with the exact measurement of the radiation-induced reactions. To avoid the errors, the separation should be performed within a few minutes.

Table 2.3. Thermal reactions of Te(IV) and Te(VI) at room temperature*

Solution	$[Te(IV)]_0$, mM	$[Te(VI)]_0$, mM	Time elapsed	Δ[Te(IV)→Te(VI)], mM	Δ[Te(VI)→Te(IV)], mM
0.4 M H_2SO_4	0.2	-	1 week	<0.0004	
"	-	0.2	"		<0.0004
"	0.2	0.2	"	<0.0004	<0.0004
0.02 M H_2SO_4	1.0	-	"	<0.002	
"	-	1.0	"		<0.002
"	1.0	1.0	"	<0.002	<0.002
6 M HCl	1.0	-	"	<0.002	
"	-	1.0	<3 min		<0.002
"	-	1.0	60 min		0.1
"	1.0	1.0	<3 min	<0.002	<0.002
"	1.0	1.0	60 min	<0.002	0.1

* All the separations were performed within 1 min.

2.3.2. Radiation-induced oxidation of Sb(III) in aerated 0.4 M sulfuric acid solutions.

Irradation induced the oxidation of Sb(III) to Sb(V) and the production of hydrogen peroxide. In 9.0×10^{-5} M Sb(III) solution, the initial yield of oxidation $G_i(Sb(V))$ was 2.5 ± 0.2, and hydrogen peroxide was produced at a same time with a yield of $G_i(H_2O_2) = 3.6 \pm 0.3$ (Fig. 2.3). It is easy to explain these figures by taking into consideration the yields of the primary species and admitting the following scheme of reactions proposed by Matsuura et al. (Ma61)

$$H_2O \xrightarrow{\gamma} H,\ OH,\ H_2,\ H_2O_2, \qquad (2.4)$$

$$H + O_2 \xrightarrow{k_7} HO_2, \qquad (2.7)$$

$$Sb(III) + OH \xrightarrow{k_8} Sb(IV) + OH^-, \qquad (2.8)$$

$$Sb(III) + HO_2 + H^+ \xrightarrow{k_9} Sb(IV) + H_2O_2, \qquad (2.9)$$

$$2Sb(IV) \xrightarrow{k_{10}} Sb(III) + Sb(V), \qquad (2.10)$$

$$2HO_2 \xrightarrow{k_{11}} H_2O_2 + O_2. \qquad (2.11)$$

The behavior of SO_4^- radical formed by the reaction (Le67, Ma72)

$$OH + HSO_4^- \rightleftarrows SO_4^- + H_2O, \qquad (2.12)$$

will be qualitatively similar to that of OH radical although the subsequent reactions of SO_4^- radical take place at different rates from those of OH radical (Do67). For simplicity, SO_4^-

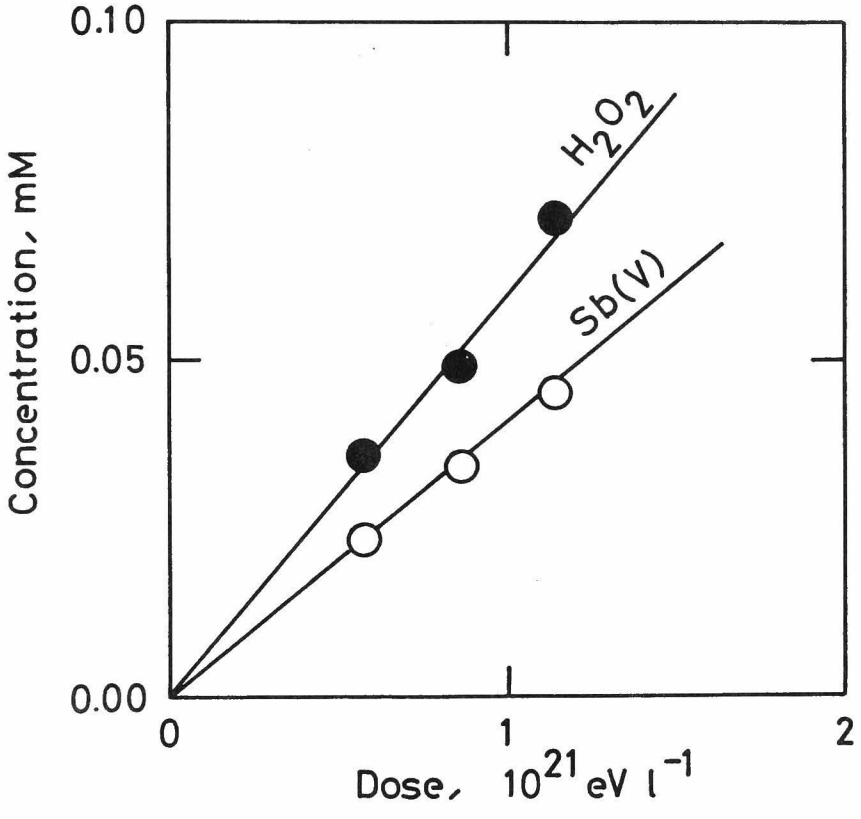

Fig.2.3. Formation of Sb(V) and H_2O_2 in aerated 0.4 M sulfuric acid solutions containing 9.0×10^{-5} M Sb(III) initially. Dose rate is 9.5×10^{17} eV l^{-1} sec^{-1}.

radical is assumed to behave the same as an OH radical. The 2.96 OH radicals lead to 1.48 Sb(V) in reactions 2.8 and 2.10. The remaining 2.5 - 1.48 = 1.02 Sb(V) ions formed in the experiment are therefore the result of reaction 2.9 occurring to the extent of 1.02 x 2 = 2.04. It follows that 3.68 - 2.04 = 1.64 HO_2 radicals are then available for the formation of 0.82 H_2O_2 in reaction 2.11. Altogether, 0.81 + 2.04 + 0.82 = 3.67 H_2O_2 molecules must be formed per 100 eV, and it is equivalent to the measured $G_i(H_2O_2) = 3.6$. This seems to show that H_2O_2 does not react with Sb(IV) any more than with Sb(III) or Sb(V). However, the main interest of this elementary calculation is that it permits deduction of the rate conatant $k_{Sb(III) + HO_2}$. Assuming reaction 2.9 is second-order, we can write

$$\frac{2k_{11}[HO_2]^2}{k_9[Sb(III)][HO_2]} = \frac{1.64}{2.04}. \qquad (2.13)$$

On the other hand, the stationary state hypothesis for HO_2 concentration requires that

$$2k_{11}[HO_2]^2 + k_9[Sb(III)][HO_2] - \frac{g_H I}{100N} = 0, \qquad (2.14)$$

where, I is the absorbed dose rate and N is the Abogadro's number. With $k_{11} = 2.2 \times 10^6$ M^{-1} sec^{-1} (Cz63), [Sb(III)] = 9.0×10^{17} eV l^{-1} sec^{-1}, and $g_H = 3.68$, it follows that $k_9 = k_{Sb(III) + HO_2} \simeq 5 \times 10^3$ M^{-1} sec^{-1}.

2.3.3. Radiation-induced reactions of Sb(III) and Sb(V) in deaerated 0.4 M sulfuric acid solutions

Table 2.4 summarizes the results of the radiation-induced reactions of Sb(III) and Sb(V) in deaerated 0.4 M H_2SO_4 solutions. In the solutions containing Sb(III) only, irradiation induced the oxidation of Sb(III) to Sb(V). Also, the addition of Fe(II) solution following irradiation gave no Fe(III), indicating the absence of peroxide. It was therefore concluded that the net reaction is the oxidation of Sb(III) to Sb(V) with formation of an equivalent amount of hydrogen. Figure 2.4 indicates that the overall yield of oxidation of Sb(III) to Sb(V) $G_i(Sb(V))$ is constant over the range studied. Similar results have been reported by Matsuura et al. (Ma61).

In this case, it should be noted that the initial yield of production of Sb(V) is an overall one

$$G_i(Sb(V)) = G_i(Sb(III)\rightarrow Sb(V)) - G_i(Sb(V)\rightarrow Sb(III)). \quad (2.15)$$

With double tracers, the initial yield of oxidation of Sb(III) to Sb(V) $G_i(Sb(III)\rightarrow Sb(V))$ and that of reduction of Sb(V) to Sb(III) were respectively measured. Two interesting features were obtained: (i) $G_i(Sb(III)\rightarrow Sb(V))$ increases with increasing $G_i(Sb(V)\rightarrow Sb(III))$ as shown in Fig. 2.5, and (ii) $G_i(Sb(V)\rightarrow Sb(III))$ increases linearly with the ratio $[Sb(V)]_0/[Sb(III)]_0$ as shown in Fig. 2.6. The former indicates that the overall yield of

Table 2.4. Oxidation of Sb(III) and reduction of Sb(V) in deaerated 0.4 M H_2SO_4 solutions.

$[Sb(III)]_0$,mM	$[Sb(V)]_0$,mM	G_i(Sb(III)→Sb(V))	G_i(Sb(V)→Sb(III))	G_i(Sb(V))
0.18	-	-	-	0.41±0.02
0.23	-	-	-	0.43±0.02
0.61	-	-	-	0.44±0.02
0.15	0.074	0.48±0.02	0.07±0.01	0.41±0.02
0.20	0.031	0.47±0.02	0.03±0.01	0.44±0.02
0.20*	0.074*	0.48±0.02	0.06±0.01	0.42±0.02
0.61*	0.23*	0.49±0.02	0.06±0.02	0.43±0.03
0.61	0.56	0.56±0.02	0.14±0.03	0.42±0.04

* The ratio $[Sb(V)]_0/[Sb(III)]_0$ is 0.37.

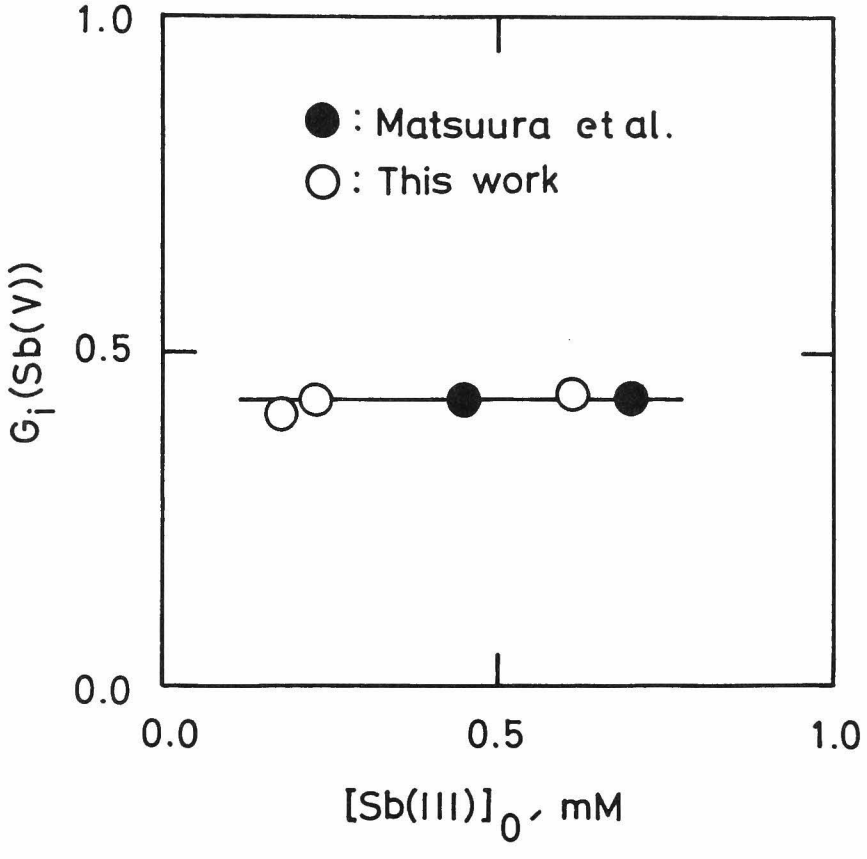

Fig.2.4. Initial yields of oxidation of Sb(III) to Sb(V) in deaerated 0.4 M sulfuric acid solutions containing Sb(III). Dose rate is 9.5 x 10^{17} eV l^{-1} sec^{-1}.

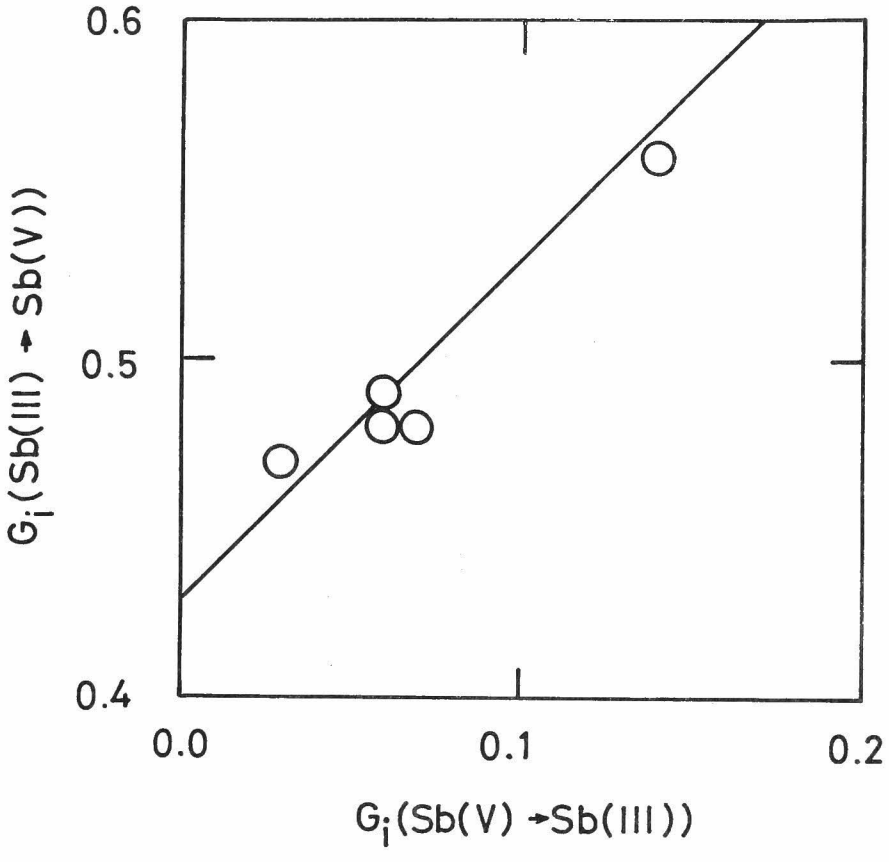

Fig. 2.5. Dependence of G_i(Sb(III) → Sb(V)) on G_i(Sb(V) → Sb(III)) in deaerated 0.4 M sulfuric acid solutions containing both Sb(III) and Sb(V). Line represents a relationship: G_i(Sb(III) → Sb(V)) = G_i(Sb(V) → Sb(III)) + 0.43.

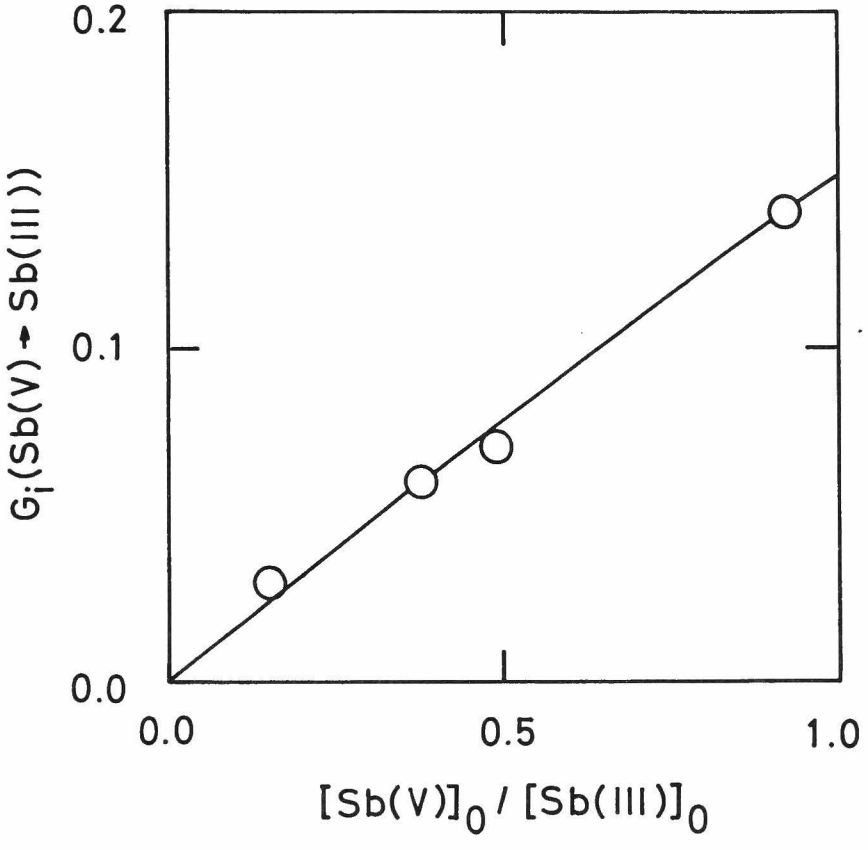

Fig. 2.6. Dependence of G_i(Sb(V) → Sb(III)) on [Sb(V)]$_0$/[Sb(III)]$_0$ in deaerated 0.4 M sulfuric acid solutions containing both Sb(III) and Sb(V). Curve is theoretical and represents least squares fit of the data to eq. 2.29.

Sb(V) $G_i(Sb(V))$ is constant even in a solution containing both Sb(III) and Sb(V). Considering hydrogen to be the other product of irradiation, we should expect the following relationship

$$\begin{aligned} G_i(H_2) &= G_i(Sb(V)) \\ &= G_i(Sb(III) \rightarrow Sb(V)) - G_i(Sb(V) \rightarrow Sb(III)) \\ &\simeq 0.43. \end{aligned} \tag{2.16}$$

The yield $G_i(H_2) \simeq 0.43$ is equivalent to the primary yield of hydrogen $g_{H_2} = (1/2)(g_{OH} - g_H) + g_{H_2O_2}$ and indicates net oxidation by OH and H_2O_2 and net reduction by H. Since H_2O_2 does not react with Sb(IV) any more than with Sb(III) or Sb(V) as mentioned in Section 2.3.2, these features permit the following sequence

$$H_2O \xrightarrow{\gamma} H,\ OH,\ H_2,\ H_2O_2, \tag{2.4}$$

$$Sb(III) + OH \xrightarrow{k_8} Sb(IV) + OH^-, \tag{2.8}$$

$$2Sb(IV) \xrightarrow{k_{10}} Sb(III) + Sb(V), \tag{2.10}$$

$$Sb(III) + H \xrightarrow{k_{17}} Sb(II) + H^+, \tag{2.17}$$

$$Sb(V) + H \xrightarrow{k_{18}} Sb(IV) + H^+, \tag{2.18}$$

$$Sb(II) + H_2O_2 \xrightarrow{k_{19}} Sb(III) + OH + OH^-, \tag{2.19}$$

$$Sb(II) + Sb(IV) \xrightarrow{k_{20}} 2Sb(III), \tag{2.20}$$

$$Sb(II) + Sb(V) \xrightarrow{k_{21}} Sb(III) + Sb(IV). \tag{2.21}$$

A similar sequence proposed by Boyle et al. (Bo59) explains very well γ-ray-induced reactions of Sn(II) in deaerated 0.4 M H_2SO_4 solutions. According to the above mechanism, Sb(III) reacts with both H and OH to form the unstable valence states Sb(II) and Sb(IV), respectively. The unstable valence states then react according to reactions 2.10, 2.19 - 2.21. Reduction of Sb(V) by H gives the same stoichiometry.

Reduction of Sb(V) occurs either in reaction 2.18 or in reaction 2.21. When the ratio [Sb(V)]/[Sb(III)] is constant, the extent of reaction 2.18 will be constant but that of reaction 2.21 will depend on [Sb(V)]. Table 2.4 shows that G_i(Sb(V) → Sb(III)) is independent of the concentration $[Sb(V)]_0$ when the ratio $[Sb(V)]_0/[Sb(III)]_0$ is fixed at 0.37. This fact indicates that reaction 2.21 hardly takes place in this case, because the extent of reaction 2.21 would depend on $[Sb(V)]_0$ even if $[Sb(V)]_0/[Sb(III)]_0$ fixed. Eliminating reaction 2.21, we can calculate the ratio of rate constants k_{17}/k_{18} from the dependence of G_i(Sb(V) → Sb(III)) on $[Sb(V)]_0/[Sb(III)]_0$ as shown in Fig. 2.6. The stationary state hypothesis for H, OH, Sb(II), Sb(IV), and H_2O_2 concentrations requires that

$$\frac{d[H]}{dt} = \frac{g_H I}{100N} - k_{17}[Sb(III)][H] - k_{18}[Sb(V)][H] = 0, \qquad (2.22)$$

$$\frac{d[OH]}{dt} = \frac{g_{OH} I}{100N} + k_{19}[Sb(II)][H_2O_2] - k_8[Sb(III)][OH] = 0, \qquad (2.23)$$

$$\frac{d[Sb(II)]}{dt} = k_{17}[Sb(III)][H] - k_{19}[Sb(II)][H_2O_2] - k_{18}[Sb(V)][H] = 0, \quad (2.24)$$

$$\frac{d[Sb(IV)]}{dt} = k_8[Sb(III)][OH] + k_{18}[Sb(V)][H] - 2k_{10}[Sb(IV)]^2 - k_{20}[Sb(II)][Sb(IV)] = 0, \quad (2.25)$$

$$\frac{d[H_2O_2]}{dt} = \frac{g_{H_2O_2} I}{100N} - k_{19}[Sb(II)][H_2O_2] = 0, \quad (2.26)$$

where, I is the dose rate, and N is the Abogadro's number. On the other hand, the rate of reduction of Sb(V) to Sb(III) $d[Sb(V) \rightarrow Sb(III)]/dt$ is given by

$$\frac{d[Sb(V) \rightarrow Sb(III)]}{dt} = k_{18}[Sb(V)][H] \times \frac{k_{10}[Sb(IV)]^2 + k_{20}[Sb(II)][Sb(IV)]}{2k_{10}[Sb(IV)]^2 + k_{20}[Sb(II)][Sb(IV)]} \quad (2.27)$$

Combination of equations 2.22 - 2.27 gives

$$\frac{d[Sb(V) \rightarrow Sb(III)]}{dt} = \frac{\frac{1}{2}(g_H + g_{OH})g_H \frac{I}{100N}}{g_H + g_{OH} + g_{H_2O_2} + (g_{OH} + g_{H_2O_2})\frac{k_{17}[Sb(III)]}{k_{18}[Sb(V)]}} \quad (2.28)$$

or a more convenient form

$$G(Sb(V) \rightarrow Sb(III)) = \frac{\frac{1}{2}(g_H + g_{OH})g_H}{g_H + g_{OH} + g_{H_2O_2} + (g_{OH} + g_{H_2O_2})\frac{k_{17}[Sb(III)]}{k_{18}[Sb(V)]}} \quad (2.29)$$

The experimental data were fit to equation 2.29 by the method of least-squares and the ratio k_{17}/k_{18} was evaluated to be 21 ± 2. The standard error results mainly from the experimental ones. The curve in Fig. 2.6 represents the least-squares fit of the experimental data to equation 2.29. Although the extent of reaction 2.21 was little in the region studied, it might increase with increasing [Sb(V)].

2.3.4. Radiation-induced oxidation of Te(IV) in aerated 0.4 M sulfuric acid solutions

Irradiation induced the oxidation of Te(IV) to Te(VI), and the production of hydrogen peroxide. In 1.0×10^{-3} M Te(IV) solutions, the initial yield of oxidation $G_i(Te(VI))$ was 3.3 ± 0.2, and hydrogen peroxide was produced at a same time with a yield of $G_i(H_2O_2) = 2.1 \pm 0.2$. These figures support the reaction mechanism proposed by Haissinsky (Ha63, Ha67, Ha68)

$$H_2O \xrightarrow{\gamma} H,\ OH,\ H_2,\ H_2O_2, \quad (2.4)$$

$$H + O_2 \xrightarrow{k_7} HO_2, \qquad (2.7)$$

$$Te(IV) + OH \xrightarrow{k_{30}} Te(V) + OH^-, \qquad (2.30)$$

$$Te(IV) + HO_2 \xrightarrow{k_{31}} Te(VI) + OH, \qquad (2.31)$$

$$2Te(V) \xrightarrow{k_{32}} Te(IV) + Te(VI), \qquad (2.32)$$

$$2HO_2 \xrightarrow{k_{33}} H_2O_2 + O_2. \qquad (2.33)$$

A calculation similar to that carried out in Section 2.3.2 gives $k_{31} = k_{Te(IV) + HO_2} \simeq 20\ M^{-1}\ sec^{-1}$. This value fairly agrees with that of 28 - 63 $M^{-1}\ sec^{-1}$ found by Haissinsky.

2.3.5. Radiation-induced reactions of Te(IV) and Te(VI) in deaerated 0.02 M sulfuric acid solutions

According to Haissinsky (Ha63, Ha67, Ha68), Te(IV) is oxidized to Te(VI) in a yield of $G_i(Te(VI)) \simeq 0.10$ together with the production of hydrogen peroxide ($G_i(H_2O_2) \simeq 0.30$) in deaerated 0.4 M H_2SO_4 solutions containing 5×10^{-4} M Te(IV). The preliminary experiments showed that the yield $G_i(Te(VI))$ increases with the ratio $[Te(IV)]_0/[H_2SO_4]$. Figure 2.7 shows that $G_i(Te(VI))$ reaches a constant value 0.43 when $[Te(IV)]_0/[H_2SO_4] > 0.015$. The following work was carried out in the range where $[Te(IV)]_0/[H_2SO_4] > 0.015$.

Table 2.5 summarizes the results of radiation-induced reactions of Te(IV) and Te(VI) in deaerated 0.02 M H_2SO_4 solutions. The addition of Fe(II) solution following irradiation gave no Fe(III), indicating the absence of peroxide. The net reaction

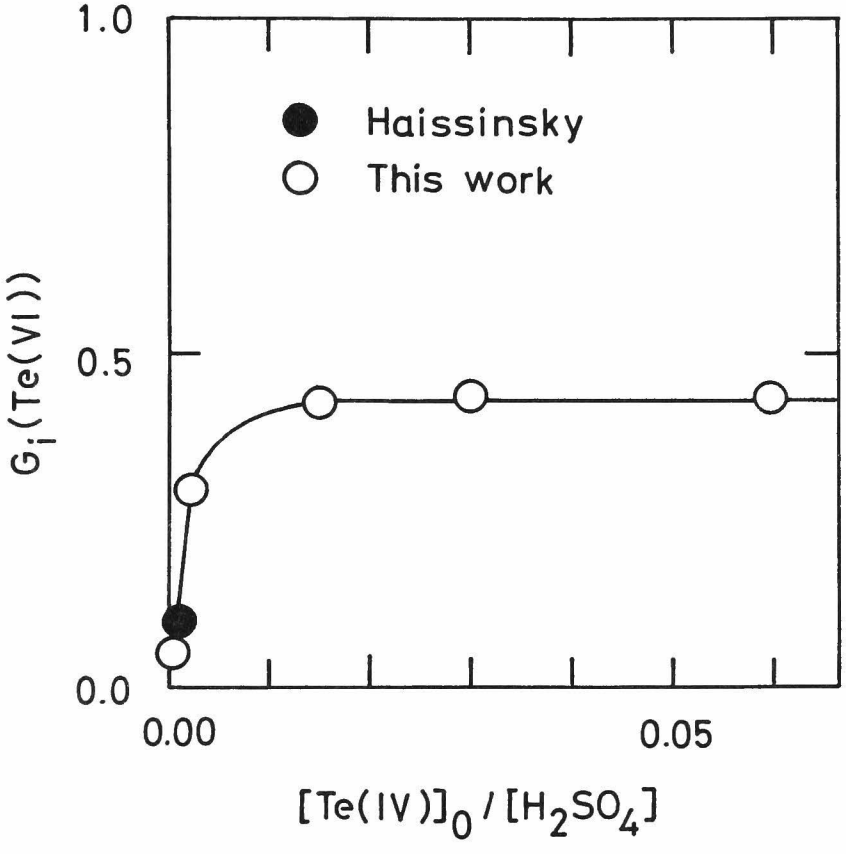

Fig. 2.7. Initial yields of oxidation of Te(IV) to Te(VI) in deaerated sulfuric acid solutions containing Te(IV). Dose rate is 9.5×10^{17} eV l^{-1} sec^{-1}.

Table 2.5. Oxidation of Te(IV) and reduction of Te(VI) in deaerated H_2SO_4 solutions.

$[H_2SO_4]$,M	$[Te(IV)]_0$,mM	$[Te(VI)]_0$,mM	G_i(Te(IV)→Te(VI))	G_i(Te(VI)→Te(IV))	G_i(Te(VI))
0.4	0.22	-	-	-	0.06±0.01
0.04	0.090	-	-	-	0.30±0.01
0.02	0.30	-	-	-	0.43±0.01
0.02	0.60	-	-	-	0.44±0.01
0.02	1.20	-	-	-	0.44±0.02
0.02	0.30	1.30	0.81±0.02	0.38±0.01	0.43±0.02
0.02	0.30	2.60	1.08±0.02	0.65±0.02	0.43±0.03
0.02	0.60	0.64	0.57±0.01	0.15±0.01	0.42±0.01
0.02	0.60	1.30	0.73±0.02	0.30±0.01	0.43±0.02
0.02	0.60	2.60	0.97±0.02	0.53±0.02	0.44±0.03
0.02	1.20	1.30	0.72±0.02	0.28±0.01	0.44±0.02
0.02	1.20	2.60	0.90±0.02	0.46±0.02	0.44±0.03

is the oxidation of Te(IV) to Te(VI) with the formation of an equivalent amount of hydrogen. With double tracers, the initial yield of oxidation of Te(IV) to Te(VI) G_i(Te(IV) → Te(VI)) and that of reduction of Te(VI) to Te(IV) G_i(Te(VI) → Te(IV)) were measured. Some interesting features were obtained: (i) G_i(Te(IV) → Te(VI)) increases with increasing G_i(Te(VI) → Te(IV)) as shown in Fig. 2.8, (ii) G_i(Te(VI) → Te(IV)) increases with $[Te(VI)]_0/[Te(IV)]_0$ (Fig. 2.9), and increases with $[Te(VI)]_0$ (Fig. 2.10). Since H_2O_2 does not react with Te(V) any more than with Te(IV) or Te(VI) (Ha63, Ha67, Ha68), the similar features to those in the case of antimony system permit the following sequence

$$H_2O \xrightarrow{\gamma} H,\ OH,\ H_2,\ H_2O_2, \qquad (2.4)$$

$$Te(IV) + OH \xrightarrow{k_{30}} Te(V) + OH^-, \qquad (2.30)$$

$$2Te(V) \xrightarrow{k_{32}} Te(IV) + Te(VI), \qquad (2.32)$$

$$Te(IV) + H \xrightarrow{k_{33}} Te(III) + H^+, \qquad (2.33)$$

$$Te(VI) + H \xrightarrow{k_{34}} Te(V) + H^+, \qquad (2.34)$$

$$Te(III) + H_2O_2 \xrightarrow{k_{35}} Te(IV) + OH + OH^-, \qquad (2.35)$$

$$Te(III) + Te(V) \xrightarrow{k_{36}} 2Te(IV), \qquad (2.36)$$

$$Te(III) + Te(VI) \xrightarrow{k_{37}} Te(IV) + Te(V). \qquad (2.37)$$

Figure 2.10 shows that G_i(Te(VI) → Te(IV)) increases with $[Te(VI)]_0$ when the ratio $[Te(VI)]_0/[Te(IV)]_0$ is fixed, and that reaction 2.37 takes part in the above mechanism. In the

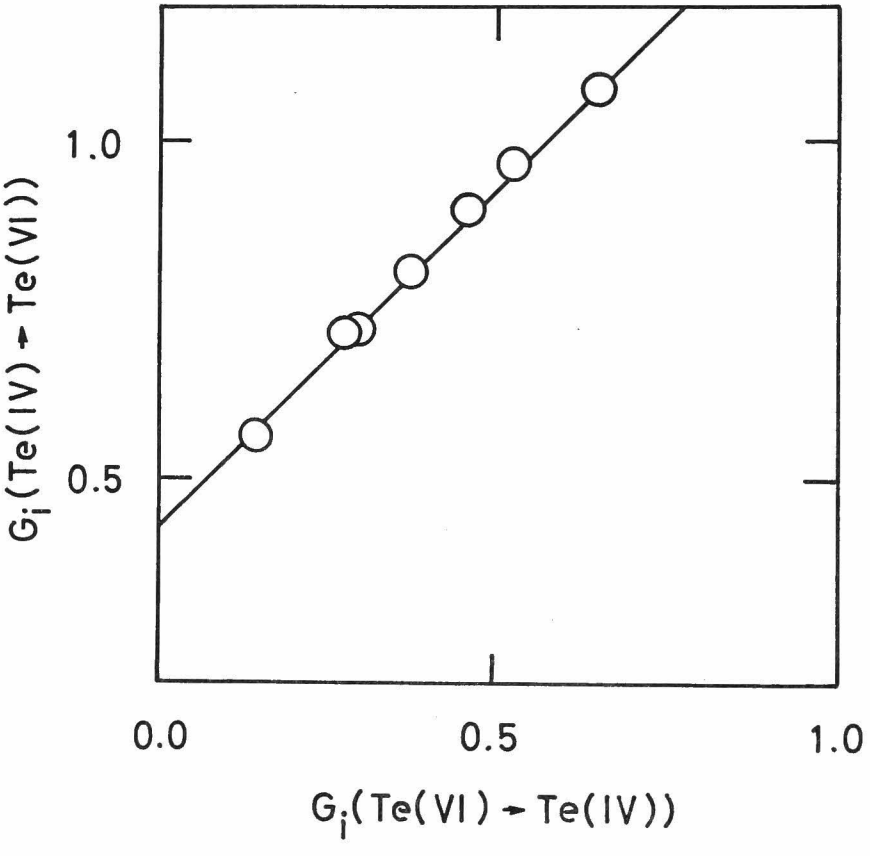

Fig. 2.8. Dependence of G_i(Te(IV) → Te(VI)) on G_i(Te(VI) → Te(IV)) in deaerated 0.02 M sulfuric acid solutions containing both Te(IV) and Te(VI). Line represents a relationship: G_i(Te(IV) → Te(VI)) = G_i(Te(VI) → Te(IV)) + 0.43.

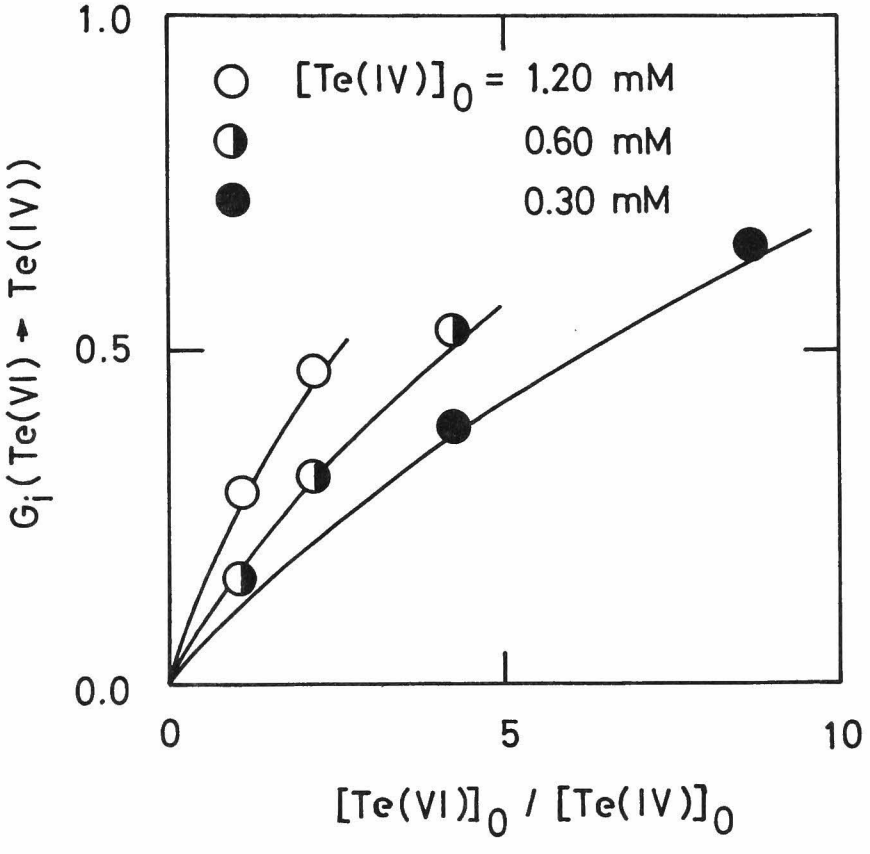

Fig. 2.9. Dependence of G_i(Te(VI) → Te(IV)) on $[Te(VI)]_0/[Te(IV)]_0$ in deaerated 0.02 M sulfuric acid solutions. $[Te(IV)]_0$: 1.20 mM (o), 0.60 mM (◑), 0.30 mM (●). Curves are theoretical and represent least-squares fit of the data to eq. 2.38.

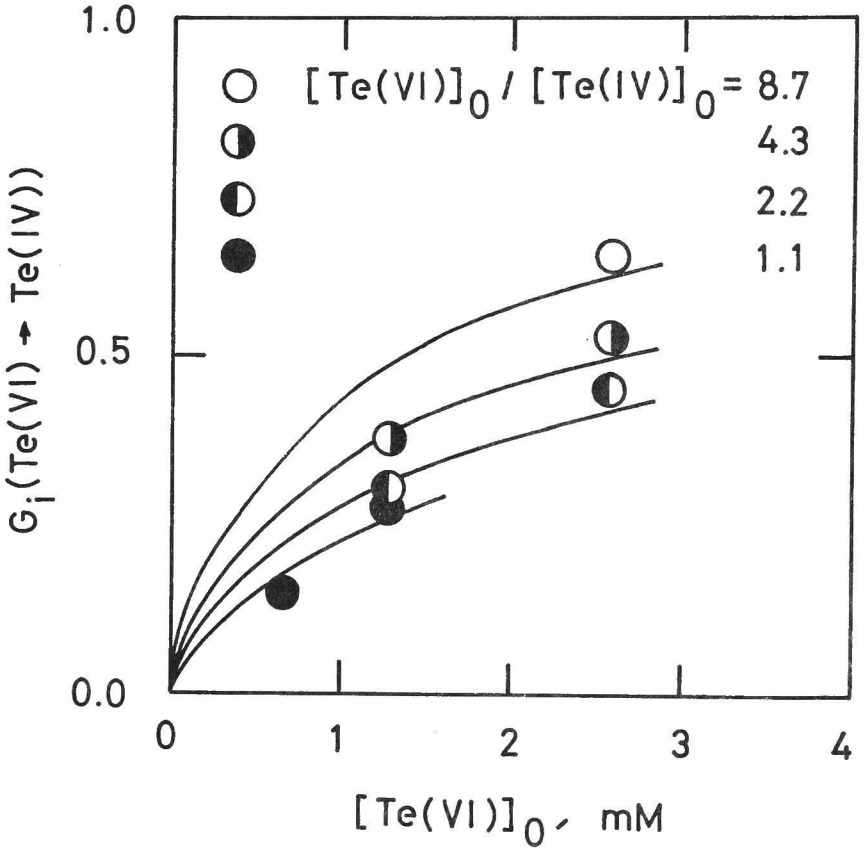

Fig. 2.10. Dependence of G_i(Te(VI) → Te(IV)) on [Te(VI)]$_0$ in deaerated 0.02 M sulfuric acid solutions containing both Te(IV) and Te(VI). [Te(VI)]$_0$/[Te(IV)]$_0$: 8.7 (o), 4.3 (◑), 2.2 (◐), 1.1 (●). Curves are theoretical and represent least squares fit of the data to eq. 2.38.

antimony system. the yield $G_i(Sb(V) \rightarrow Sb(III))$ is independent of $[Sb(V)]_0$ when the ratio $[Sb(V)]_0/[Sb(III)]_0$ is fixed, and reaction 2.21 is eliminated in the analysis. This difference is probably due to the differences of reaction rates and/or those of concentrations of solutes.

The dependence of $G_i(Te(VI) \rightarrow Te(IV))$ on $[Te(VI)]_0/[Te(IV)]_0$ and that on $[Te(VI)]_0$ as shown in Figs. 2.9 and 2.10, respectively, will permit us to calculate some kinetic parameters. The stationary state hypothesis for H, OH, Te(III), Te(V), and H_2O_2 concentrations requires that

$$G(Te(VI) \rightarrow Te(IV)) = \frac{\frac{1}{2}(g_H + g_{OH})\,[\,g_H X + (g_H - g_{H_2O_2})(aA + B)]}{g_H X + [\,g_H + g_{OH} + (g_{OH} + g_{H_2O_2})\frac{X}{B}\,]\,(aA + B)}, \qquad (2.38)$$

where, X denotes $k_{36}[Te(V)]/k_{37}$ and is a real solution of the third-order equation

$$bX^3 + bBX^2 + [\,\frac{1}{2}(g_H - g_{OH}) - g_{H_2O_2} - \frac{g_H B}{aA + B}\,]\,\frac{IX}{100N} - \frac{1}{2}(g_H + g_{OH})\frac{BI}{100N} = 0,$$

$a = k_{33}/k_{34}$, $b = k_{32}k_{37}^2/k_{36}^2$, $A = [Te(IV)]$, and $B = [Te(VI)]$. The experimental data were fit to equation 2.38 by the method

of least-squares. The iterative procedure was employed assuming that all G_i(Te(VI) → Te(IV)) had a constant percentage error. The kinetic parameters a and b were evaluated to be 48 ± 7 and (8.6 ± 2.3) x 10^{-5} M^{-1} sec^{-1}, respectively. The value of X which denotes $k_{36}[Te(V)]/k_{37}$ was around 0.014 M. The curves in Figs. 2.9 and 2.10 represent the least-squares fit of the experimental data to equation 2.38 and the agreement between the experimental data and theoretical value is excellent.

2.3.6. Radiation-induced reactions in reactors

The radiation-induced reactions of antimony and tellurium compounds were investigated in the solutions irradiated in the Kyoto University reactor. In order to know the effects of phase changes, the difference between the liquid and the frozen solutions was studied. Also, in order to know the fission-fragment-induced reactions, the samples containing fissile materials were irradiated. Although the details of the experimental procedures are described in the related Sections of Chapter 4, the results are interpreted here according to the reaction mechanisms given in this Chapter.

(A) Reactor-radiation-induced reactions

Irradiation in the reactor induced the oxidation of Sb(III) and Te(IV) and the reduction of Sb(V) and Te(VI). Tables 2.6 and 2.7 summarizes the yields of the reactor-radiation-induced reactions of the antimony and tellurium compounds in the reactor, respectively. The absorbed doses were determined from G(Fe(III)) = 8.20 (Fr66) for the oxigen-free ferrous sulfate dosimeters which had been irradiated with the sample solutions. The dose rate was about 2×10^{18} eV ml^{-1} sec^{-1}. Although the radiations in the reactor are various (i.e., γ rays, β rays, recoil protons, etc.), it was estimated that those are mainly (>90 %) composed of γ rays.

Tables 2.6 and 2.7 show that the yields in deaerated liquid solutions are in good accordance with the ones measured by ^{60}Co

Table 2.6. Reactor-radiation-induced reactions of Sb(III) and Sb(V) in 0.4 M sulfuric acid solutions containing 0.5 mM Sb(III) and 0.5 mM Sb(V).

Phase	Oxygen	$G(Sb(III) \rightarrow Sb(V))_r$	$G(Sb(V) \rightarrow Sb(III))_r$
Frozen	Deaerated	0.2 ± 0.1	<0.1
Frozen	Aerated	0.3 ± 0.1	<0.1
Liquid	Deaerated	0.4 ± 0.1	<0.1

Table 2.7. Reactor-radiation-induced reactions of Te(IV) and Te(VI) in 0.4 M sulfuric acid solutions containing 1.5 mM Te(IV) and 1.5 mM Te(VI).

Phase	Oxygen	$G(Te(IV) \rightarrow Te(VI))_r$	$G(Te(VI) \rightarrow Te(IV))_r$
Frozen	Deaerated	<0.05	0.10 ± 0.05
Frozen	Aerated	<0.05	<0.05
Liquid	Deaerated	0.10 ± 0.03	0.15 ± 0.03
Liquid	Aerated	1.5 ± 0.1	<0.1

γ rays as shown in Tables 2.4 and 2.5, respectively. This indicates that the reaction mechanisms given in the preceding Sections can also elucidate the yields in the reactor. However, some differences between ^{60}Co γ rays and reactor radiations were observed. These differences are probably caused by the differences of dose rates. For instance, the yields of oxidation of Te(IV) is about 3 for ^{60}Co γ rays and 1.5 for reactor radiations in aerated liquid solutions. As mentioned in Section 2.3.4, Te(IV) is oxidized by OH and HO_2 radicals in aerated solutions. In the case of a high dose rate of the reactor, the HO_2 radicals prefer the reaction $HO_2 + HO_2$ to the oxidation Te(IV) + HO_2 because the rate constant $k_{HO_2 + HO_2}$ is considerably larger than the rate constant $k_{Te(IV) + HO_2}$. On the other hand, the OH radicals oxidize Te(IV) completely. Accordingly the yield of oxidation of Te(IV) in the reactor becomes close to $g_{OH}/2 = 1.48$.

In the solid phase, $G(Sb(III) \rightarrow Sb(V))_r$ is lower than that in the liquid phase as shown in Table 2.6, and $G(Te(IV) \rightarrow Te(VI))_r$ diminishes as shown in Table 2.7. The influence of the phase changes on the yields of oxidation evidently indicates that the yields of the primary species are much lower in the solid phase than in the liquid phase (Er70, Th69). The difference between $G(Sb(III) \rightarrow Sb(V))_r$ and $G(Te(IV) \rightarrow Te(VI))_r$ is probably due to the differnce of the rate constants: for example, the rate constant $k_{Sb(III) + OH} = 1.3 \times 10^9\ M^{-1}\ sec^{-1}$ (Ma62, Sc63a)

is quite larger than $k_{Te(IV) + OH} = 4.7 \times 10^6\ M^{-1}\ sec^{-1}$ (Ha68).

(B) Fission-fragment-induced reactions

When the solutions containing fissile materials such as ^{233}U are irradiated in the reactor, fission fragments induce the radiolysis of the solutions together with the reactor radiations mentioned above. Since uranyl ions were not changed by irradiation, they were assumed not to take part in the reaction mechanisms. The yields of the fission-fragment induced reactions as shown in Tables 2.8 and 2.9 were obtained assuming that the observed yields are linear combinations of two radiolysis yields:

$$G_{obsd} = F_r G_r + F_f G_f. \qquad (2.39)$$

The coefficients, F_r and F_f are the respective fractions of energy deposited by reactor radiations and fission fragments. Values for G_r were taken from Tables 2.6 and 2.7. The energy absorption from fission fragments was calculated from their average released energy (Va73) with the total number of fission events. The rate of energy absorption from fission fragments was about 3×10^{18} eV ml^{-1} sec^{-1}.

Table 2.8 shows that fission fragments apparently induced the oxidation of Sb(III) to Sb(V). Although a fission fragment yields a radical sheath with a diameter of $\sim$120 Å (Mo69),

Table 2.8. Fission-fragment-induced reactions of Sb(III) and Sb(V) in 0.4 M sulfuric acid solutions containing 0.5 mM Sb(III), 0.5 mM Sb(V), and 4.3 mM UO_2^{2+}.

Phase	Oxygen	$G(Sb(III) \rightarrow Sb(V))_f$	$G(Sb(V) \rightarrow Sb(III))_f$
Frozen	Deaerated	0.2 ± 0.1	<0.1
Frozen	Aerated	0.3 ± 0.1	<0.1
Liquid	Deaerated	0.5 ± 0.1	<0.1

Table 2.9. Fission-fragment-induced reactions of Te(IV) and Te(VI) in 0.4 M sulfuric acid solutions containing 1.5 mM Te(IV), 1.5 mM Te(VI), and 4.3 mM UO_2^{2+}.

Phase	Oxygen	$G(Te(IV) \rightarrow Te(VI))_f$	$G(Te(VI) \rightarrow Te(IV))_f$
Frozen	Deaerated	<0.05	<0.05
Frozen	Aerated	<0.05	<0.05
Liquid	Deaerated	<0.03	<0.03
Liquid	Aerated	<0.1	<0.1

the cumulative volume of tracks or sheaths is so small that intertrack reactions cannot elucidate the yields quantitatively. It was concluded that the yields of oxidation is mainly due to the species escaping track reactions. According to Bibler (Bi75), H atoms as well as OH radicals do not escape fission fragment tracks to react with solutes at millimolar concentrations. The following estimates for the respective species escaping track reactions have been reported: $G(H_2) = 2.1$, $G(H_2O_2) = 0.96$, $G(HO_2) = 0.5$, $G(OH) = 0$, and $G(H) = 0$. The yield of oxidation of Sb(III) in deaerated liquid solutions is 0.5 and is in good accordance with the yield of HO_2 radicals. This indicates that Sb(III) was oxidized in reaction 2.9 by the HO_2 radicals escaping track reactions.

As shown in Table 2.8, the yield of oxidation of Sb(III) in the solid phase is smaller than that in the liquid phase. The decrease is probably caused by the decrease of the yields of the species escaping track reactions since the mobilities of the species diminishes in the solid phase (Er69b, Th69). In contrast with the antimony system, there is no fission-fragment induced reaction of Te(IV) and Te(VI) as shown in Table 2.9. The difference shows that the rate constant $k_{Te(IV) + HO_2}$ is quite lower than the rate constant $k_{Sb(III) + HO_2}$. In the preceding Sections, the rate constants $k_{Sb(III) + HO_2}$ and $k_{Te(IV) + HO_2}$ have been given to be $\sim 5 \times 10^3$ M^{-1} sec^{-1} and $\sim 2 \times 10$ M^{-1} sec^{-1}, respectively. The yield of oxidation of Te(IV) might increase with increasing [Te(IV)].

2.4. Conclusions

The radiation-induced reactions of antimony and tellurium compounds in sulfuric acid solutions were investigated using double tracers for each element. The chemical separation of Sb(III) and Sb(V) and that of Te(IV) and Te(VI) were performed with anion exchange methods. In the preliminary experiments, it was confirmed that no other thermal reaction interferes with the exact measurements of the radiation-induced reactions.

First, the reaction mechanisms in aerated solutions were studied. The results on Sb(III) and Te(IV) in 0.4 M sulfuric acid solutions supported the mechanisms proposed by Matsuura (Ma61) and Haissinsky (Ha63, Ha67, Ha68), respectively. An interesting feature was presented: hydrogen peroxide which is formed does not react at all in this medium, with any of Sb(III), Sb(V), Te(IV), and Te(VI). Also, the rate constants $k_{Sb(III) + HO_2}$ and $k_{Te(IV) + HO_2}$ were evaluated to be $\sim 5 \times 10^3$ M^{-1} sec^{-1} and ~ 20 M^{-1} sec^{-1}, respectively.

Next, the reactions in deaerated solutions were studied. The initial yield of reduction $G_i(Sb(V) \rightarrow Sb(III))$ increased linearly with the ratio $[Sb(V)]_0/[Sb(III)]_0$, that of oxidation $G_i(Sb(III) \rightarrow Sb(V))$ increased with increasing $G_i(Sb(V) \rightarrow Sb(III))$, and the overall yield of oxidation $G_i(Sb(V)) = G_i(Sb(III) \rightarrow Sb(V)) - G_i(Sb(V) \rightarrow Sb(III))$ was constant and equivalent to the primary yield of hydrogen $g_{H_2} = (1/2)(g_{OH} - g_H) + g_{H_2O_2}$.

There was no measuable yield of hydrogen peroxide. A possible mechanism of γ-ray-induced reactions in deaerated solutions was proposed, in which Sb(III) was reduced by H and oxidized by OH, Sb(II) was oxidized by H_2O_2 and Sb(IV), and the disproportionation of Sb(IV) to Sb(III) and Sb(V) followed. In the presence of Sb(V), reduction of Sb(V) by H gives the same stoichiometry. The results on Te(IV) and Te(VI) in 0.02 M H_2SO_4 solutions support a similar sequence to that of antimony system, in which the unstable valence states Te(III) and Te(V) play an important part. The ratios of the rate constants $k_{Sb(III) + H}/k_{Sb(V) + H}$ and $k_{Te(IV) + H}/k_{Te(VI) + H}$ were evaluated to be about 20 and 50, respectively. It is especially noteworthy that the rates of reduction of Sb(III) and Te(IV) by H atoms are more rapid than those of Sb(V) and Te(VI), respectively.

Finally, the radiation-induced reactions in the reactor were analyzed. The reactor-radiation-induced reactions were elucidated well with the mechanisms mentioned above. Some differences were attributed to the differences of the dose rates. It was also shown that the yields of radiation-induced reactions were very sensitive to the phase changes. The analysis of the fission-fragment-induced reactions presented some interesting features: solute of millimolar concentrations can react only with the species escaping track reactions, and the yields of the reactions depend on the rate constants and the mobilities of the species.

CHAPTER 3

CHEMICAL EFFECTS ASSOCIATED WITH BETA-DECAY

3.1. Introduction

Generally speaking, most of the fission products undergo radioactive decay. Except in certain paticular instances, the fission products arise through decay of precursors instead of directly in fission. This means, of course, that the phenomena observed are the consequences as much of β-decay (and ITs) as fission itself. Thus, it would be particularly valuable to know what effects are associated with β-decay. This chapter deals with the chemical effects associated with β-decay of the tin and antimony precursors in sulfuric acid solutions.

Beta-decay involves the simultaneous ejection of a neutrino and an electron. It causes recoil of the nucleus, but with very much less energy than in fission. As regards the initial charge of the product atom, we might expect emission of a β^--particle to raise the net charge by one unit. However, as well known, electronic excitation energy frequently induce electron shake-off and Auger effects which cause additional loss of electrons. In general, then, β-decay can cause chemical effects in three ways: through the change in atomic

number, through recoil, and through electronic excitation and ionization (Mc71a, Ha79). The relative importance of these processes is expected to vary greatly from one case to another. The phenomena observed are therefore much more complicated, and our picture is still far from complete.

Several investigators have focussed their attention on the chemical effects of the following decay processes in the solid system: $^{125}Sn \rightarrow {}^{125}Sb$ (An66), $^{121}Sn^{m} \rightarrow {}^{121}Sb$ (Le70, Am75), and $^{125}Sb \rightarrow {}^{125}Te^{m}$ (Ne62, Ne64, Am71). However, there has been no work on the chemical effects of β-decay of the tin and antimony isotopes in solutions. In this chapter, the chemical effects of the β-decay processes: $^{128}Sn \rightarrow {}^{128}Sb^{m}$, $^{127}Sb \rightarrow {}^{127}Te^{g}$, and $^{129}Sb \rightarrow {}^{129}Te^{g}$, are investigated in sulfuric acid solutions. The results are compared with one another and the mechanism of the chemical effects are discussed.

3.2. Experimental

3.2.1. Preparations

The guaranteed reagents obtained from Nakarai Chemicals, Ltd., were used without further purification. Triply distilled water was used to make up all the solutions. The isotopes ^{128}Sn, ^{127}Sb, and ^{129}Sb were produced by the fission of the uranium enriched to 90 % in ^{235}U (obtained from Atomic Fuel Industrial, Ltd.,) in the Kyoto University reactor. The tracers and carriers were prepared following the procedures described in Section 2.2.1.

3.2.2. Procedures

(A) $^{128}Sn \rightarrow {}^{128}Sb^{m}$

About 0.1 mg of U_3O_8 was irradiated for 60 minutes at a position where the thermal neutron flux was $\sim 1.3 \times 10^{13}$ cm^{-2} sec^{-1}, the epithermal neutron flux was $\sim 1 \times 10^{12}$ cm^{-2} sec^{-1}, and the fast neutron flux was $\sim 4 \times 10^{12}$ cm^{-2} sec^{-1}. After cooling of about 30 minutes, the U_3O_8 was dissolved in concentrated hydrochloric acid containing 5 mg of tin carrier. The solution was adjusted to 3 M in HCl and 1 mg of Sb(V) was added to the solution. After the complete reduction of Sb(V) to Sb(III) with NH_2OHHCl, Sb_2S_3 was precipitated by passing H_2S. The filtrate which contained Sn(IV) was diluted to 1 M in HCl and SnS_2 was precipitated by H_2S. In order to diminish

the contamination, the SnS_2 was dissolved in 6 M HCl and was purified repeatedly. Finally, the SnS_2 was dissolved in concentrated sulfuric acid and was adjusted to 0.4 M in H_2SO_4. The ^{128}Sn solution, which also contained 0.5 mM Sb(III) and 0.5 mM Sb(V) carriers, was aerated or deaerated.

The solution was allowed to stand at room temperature or dryice temperature for a length of time long enough for transient equilibrium to be established. Then, Sb(III) and Sb(V) were separated following the procedure described in Section 2.2.3. Chemical yields of Sb(III) and Sb(V) were determined by a method of neutron activation.

(B) $^{127}Sb \rightarrow {}^{127}Te^g$ and $^{129}Sb \rightarrow {}^{129}Te^g$

About 0.5 mg of U_3O_8 was irradiated for 60 minutes at the same position as that of ^{128}Sn. After cooling of about 3 hours, the U_3O_8 was dissolved in concentrated hydrochloric acid containing 5 mg of Sb(V) carrier. The solution was adjusted to 3 M in HCl. After the complete reduction of Sb(V) to Sb(III) with NH_2OHHCl, Sb_2S_3 was precipitated. The Sb_2S_3 was dissolved in concentrated hydrochloric acid and the antimony was purified by distilling SbH_3 as shown in Fig. 3.1 (Gr63). The hydrides of antimony, selenium, tellurium, and arsenic are volatilized by a burst of nascent hydrogen generated by pouring the Sb-HCl solution to zinc powder. Selenium and tellurium were separated from arsenic and antimony by absorbing the first two elements

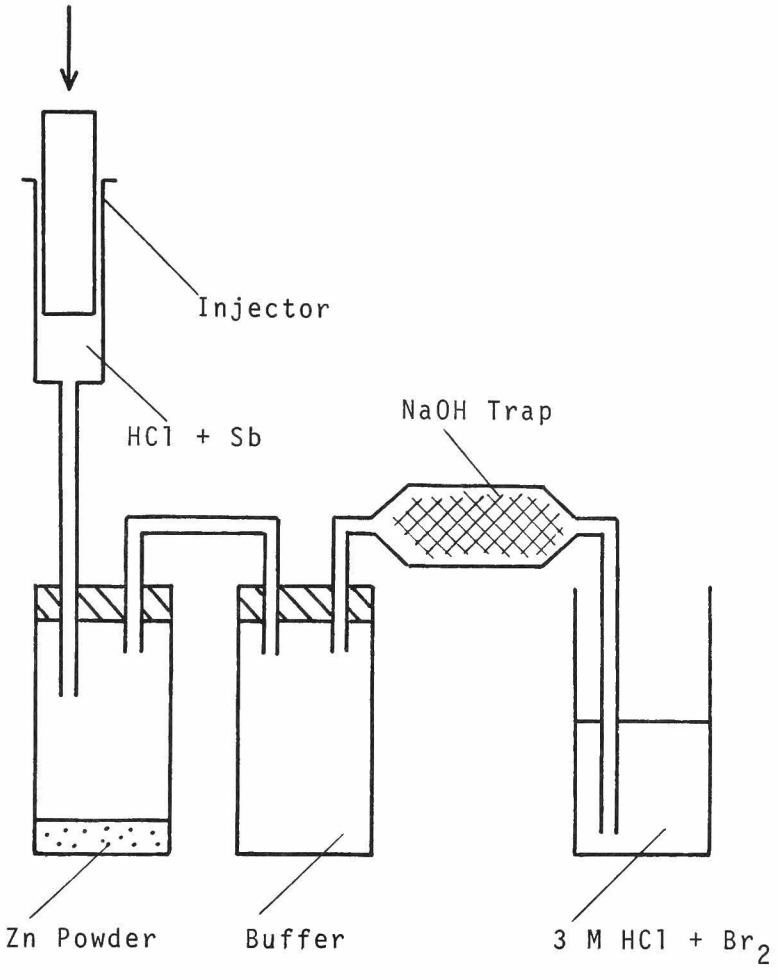

Fig. 3.1. Apparatus for the separation of antimony from fission products.

on glass wool coated with 1 M NaOH. The gas burst escaping the NaOH trap was passed through a 3 M HCl containing Br_2 which decomposed the hydrides and oxidized arsenic and antimony. The purification of antimony from arsenic was not performed since the latter hardly interfere with the measurement of the radioactivities of the former. After excess bromine was removed by boiling, the antimony sulfide was precipitated with H_2S.

Sample solutions of Sb(III) and Sb(V) were prepared with the antimony sulfide following the procedures in Section 2.2.1. The sample solutions containing 1.5 mM Te(IV) and 1.5 mM Te(VI) carriers were allowed to stand for a length of time enough for transient equilibrium to be established under various conditions (i.e., aerated or deaerated at room temperature or dry ice temperature). Then, Te(IV) and Te(VI) were separated following the procedure in Section 2.2.4. Chemical yields of Te(IV) and Te(VI) were determined by weighing.

3.2.3. Measurements

The radioactivities in each fraction were followed with a calibrated 38 cm^3 Ge(Li) detector connected to a 4096 channel pulse height analyzer. The γ rays associated with $^{128}Sb^m$, $^{127}Te^g$ and $^{129}Te^g$ are summarized in Table 3.1.

In order to know the yields of the radiation-induced reactions (i. e., β-ray-induced reactions), the tracers mentioned in Section 2.2.1 were used. There was no measurable yield.

Table 3.1. Nuclear data used in the analysis of chemical effects of β-decay.

Nuclide	Half life*	γ-Energy*, in KeV	Intensity*	Branching fraction in % to		
^{129}Sb	4.32 h	813.	0.435	$^{129}Te^{m}$	16.6	(Ho72)
$^{129}Te^{m}$	34.1 d			$^{129}Te^{g}$	63.6	(Ho72)
$^{129}Te^{g}$	69.6 m	460.	0.0714			
^{128}Sn	59.1 m			$^{128}Sb^{m}$	100.	(Im75)
$^{128}Sb^{m}$	10.0 m#	743.	1.00	$^{128}Sb^{g}$	3.6	(Im75)
$^{128}Sb^{g}$	9.1 h#	743.	1.00			
^{127}Sb	3.85 d			$^{127}Te^{m}$	17.4	(Au72)
$^{127}Te^{m}$	109. d			$^{127}Te^{g}$	97.6	(Au72)
$^{127}Te^{g}$	9.35 h	417.	0.00741			

* Taken from Ref. (B177).

\# Taken from Ref. (Im75).

3.3. Results

The daughter $^{128}Sb^{m}$ was formed in both the +3 and +5 oxidation states, and the daughters $^{127}Te^{g}$ and $^{129}Te^{g}$ were in both the +4 and +6 oxidation states. The percentage of an isotope in the reduced state F_r is defined as

$$F_r = 100A_r/(A_r + A_o), \qquad (3.1)$$

where, A_r and A_o are the radioactivities of the isotope in the reduced and oxidized states at the chemical separation, respectively. The results are shown in Tables 3.2 - 3.4. The reproducibilities of several runs was very good. The uncertainty was arrived at by the method described in Section 2.2.5.

The excellent reproducibilities of the results with the liquids can be attributed to the presence of carriers. A newly formed atom becomes chemically equivalent to carrier atoms in a very short time, and thus could undergo only the chemical changes that were followed with labeled carriers. However, in the frozen system, newly formed atoms can not be similarly protected by carriers. The newly formed atoms can be trapped in the frozen system in unstable as well as stable oxidation states and, therefore, can be reactive not only in the frozen system but also in the solid-liquid interface during the dissolution process. Contrary to expectation,

the agreement between data for most duplicate samples was obtained. This fact seems to show that the results in the frozen system are not of the thermal reactions but of the hot reactions since the thermal reactions are expected to depend greatly on the subtle differences among the experimental atmospheres (see below).

Table 3.2. Percent as Sb(III) of $^{128}Sb^{m}$ formed by β-decay of ^{128}Sn in the +4 oxidation state in 0.4 M sulfuric acid solutions containing 0.1 mM Sn(IV), 0.5 mM Sb(III), and 0.5 mM Sb(V) carriers.

Phase	Temperature	Oxygen	Percent as Sb(III)	
			^{125}Sb	$^{128}Sb^{m}$
Frozen	Dry ice	Deaerated		40 ± 4
Frozen	Dry ice	Aerated		39 ± 4
Liquid	Room	Deaerated		41 ± 4
Liquid	Room	Aerated		40 ± 4
Solid	Room		10 - 90*	

* In solid $K_2{}^{125}SnCl_6$ (An66). See text.

Table 3.3. Percent as Te(IV) of $^{127}Te^{g}$ and $^{129}Te^{g}$ formed by β-decay of ^{127}Sb and ^{129}Sb, respectively, in the +3 oxidation state in 0.4 M sulfuric acid solutions containing 0.1 mM Sb(III), 1.5 mM Te(IV), and 1.5 mM Te(VI) carriers.

Phase	Temp.	Oxygen	Percent as Te(IV)		
			$^{125}Te^{m}$	$^{127}Te^{g}$	$^{129}Te^{g}$
Frozen	Dry ice	Deaerated		<95	<98
Frozen	Dry ice	Aerated		<95	<98
Liquid	Room	Deaerated		<95	<98
Liquid	Room	Aerated		<95	<98
Solid	Room		28*		

* In solid $^{125}SbR_3$ (R = phenyl or toryl), 60 % of the daughter $^{125}Te^{m}$ was found as TeR_2 (Ne62, Ne64).

Table 3.4. Percent as Te(IV) of $^{127}Te^{g}$ and $^{129}Te^{g}$ formed by β-decay of ^{127}Sb and ^{129}Sb, respectively, in the +5 oxidation state in 0.4 M sulfuric acid solutions containing 0.1 mM Sb(V), 1.5 mM Te(IV), and 1.5 mM Te(VI) carriers.

Phase	Temp.	Oxygen	Percent as Te(IV)		
			$^{125}Te^{m}$	$^{127}Te^{g}$	$^{129}Te^{g}$
Frozen	Dry ice	Deaerated		20 ± 9	22 ± 5
Frozen	Dry ice	Aerated		18 ± 9	20 ± 5
Liquid	Room	Deaerated		23 ± 9	27 ± 5
Liquid	Room	Aerated		25 ± 9	25 ± 5
Solid	Room		90*		

* In solid $^{125}SbR_3Cl_2$ (R = phenyl or toryl) (Ne62, Ne64).

3.4. Discussion

As well known, the chemical effects associated with β-decay vary greatly from case to case. Tables 3.2 - 3.4 give a remarkable variety of the chemical effects of β-decay. The Tables also show the results of other β-decay processes (An66, Ne62, Ne64) although it is difficult to compare the present results with those because of the different β-decay processes. In order to know some details of the mechanism, the similarities and the differences among the results are speculated.

3.4.1. Distinction between hot and thermal reactions

Anderson et al. (An66) have reported that the Sb valence distribution in solid $K_2{}^{125}SnCl_2$ depends critically on the preparation and purification procedure. The yield of Sb(III) in crude crystals was 90 %, but in high purified material went below 10 %. This dramatic change is obviously related to the differing contents of impurity atoms and crystal defects introduced in synthesis and is probably due to thermal reactions.

It is very important to distinguish the hot from the thermal reactions prior to discussion of the mechanism of the hot reaction. The tracer experiments showed that any thermal reaction including the radiation-induced reaction did not occur in all the cases. Furthermore, no scavenger effect was observed in both the liquid and the frozen systems. Tables 3.2 - 3.4 shows that the results

in the deaerated samples agrees with the ones in the aerated samples within the experimental errors. Thesefacts suggest that the results are not of the thermal reactions but of the hot reactions.

Another fact supports the above suggestion. According to the hot-zone model (see, for example, Ha79), the hot reaction should be relatively insensitive to phase changes, but the thermal reactions should be sensitive. The idea is that the hot reactions occur mainly in a zone of chemical destruction, which would be of similar character whether formed in a liquid or a solid. As shown in Tables 3.2 - 3.4, the results in the frozen system are in good accordance with the ones in the liquid system. Therefore, it concludes that the results shown in Tables 3.2 - 3.4 are almost of the hot reactions.

3.4.2. Factors in chemical effects of β-decay

In general, β-decay can cause chemical effects in three ways: through the change in atomic number, through recoil, and through electronic excitation and ionization (Mc71a, Ha79). It is discussed here what factor is essential in the chemical effects of the β-decay processes: $^{128}Sn \rightarrow {}^{128}Sb^{m}$, $^{127}Sb \rightarrow {}^{127}Te^{g}$, and $^{129}Sb \rightarrow {}^{129}Te^{g}$.

(A) Change in atomic number

As regards the initial charge of the product atom, we

might expect emission of a β^--particle to raise the net charge by one unit. For example, the β-decay of the ^{128}Sn in the +4 oxidation state would result in the $^{128}Sb^m$ in the +5 oxidation state. It is very important whether Sb(V) is stable or unstable chemically in the medium. If Sb(V) is unstable, the β-decay can not lead to the product Sb(V). As shown in Table 3.5, Sb(V), Te(IV), and Te(VI) are stable in sulfuric acid solutions (Da70, Ho60), which might be primarily formed in the β-decay of Sn(IV), Sb(III), and Sb(V), respectively.

Tables 3.2 - 3.4 show that

$$^{128}Sn(IV) \xrightarrow{\beta^-} \begin{matrix} ^{128}Sb^m(III) & (\sim 40\ \%), \\ ^{128}Sb^m(V) & (\sim 60\ \%), \end{matrix} \qquad (3.2)$$

$$^{127,\ 129}Sb(III) \xrightarrow{\beta^-} \begin{matrix} ^{127g,\ 129g}Te(IV) & (>95\ \%), \\ ^{127g,\ 129g}Te(VI) & (<5\ \%), \end{matrix} \qquad (3.3)$$

$$^{127,\ 129}Sb(V) \xrightarrow{\beta^-} \begin{matrix} ^{127g,\ 129g}Te(IV) & (\sim 20\ \%), \\ ^{127g,\ 129g}Te(VI) & (\sim 80\ \%). \end{matrix} \qquad (3.4)$$

As expected, an apparent memory effect was observed, which leads to large yields of the primary products.

In a dilute sulfuric acid solution, Sb(V) is probably present as a mixture of $Sb(OH)_6^-$ and $[Sb_3O_6(OH)_6]^{3-}$ (Da70), and Te(VI) as a mixture of H_6TeO_6 and H_2TeO_4 (Ho60). The similarity

Table 3.5. Chemical species of tin, antimony, and tellurium compounds in sulfuric acid solutions.

Compound	Species	Reference
Sn(IV)	$SnSO_4^{2+}$	Br55
Sb(III)	SbO^+	Da70
Sb(V)	$[Sb(OH)_6]^-$, $[Sb_3O_6(OH)_6]^{3-}$	Da70
Te(IV)	$HTeO_2^+$, H_2TeO_3	Ho60
Te(VI)	H_2TeO_4, H_6TeO_6	Ho60

between the chemical structures of $Sb(OH)_6^-$ and H_6TeO_6 may support that the antimony species $Sb(OH)_6^-$ leads to the tellurium species H_6TeO_6 through the β-decay process 3.4 without bond rupture. Thus, ∿20 % as Te(IV) is probably due to bond rupture caused by the recoil and the electronic excitation and ionization. On the other hand, Table 3.5 shows that the β-decay processes 3.2 and 3.3 are necessarily accompanied with the changes of the products in chemical structure, which complicate the results.

(B) Recoil

Table 3.6 shows the nuclear data and the estimated maximum effective recoil energies E_{eff}^r following β-decay. The E_r^β in Table 3.6 is the maximum recoil energy calculated by the use of the general equation (Li47)

$$E_r^\beta = \frac{536}{M} E_\beta (E_\beta + 1.02), \qquad (3.5)$$

where, E_β is the energy of the β^--particle in MeV, and M is the mass of the daughter atom in a.m.u. The E_{eff}^r values are calculated by the use of the Suess's equation

$$E_{eff}^r = E_r^\beta \frac{X}{M + X}, \qquad (3.6)$$

where, M and X are the mass of daughter atom and ligand ion in

Table 3.6. Maximum β^--particle energies and recoil energies.

Process	E_β, * MeV	Branching fraction*	E_r^β, eV	E_{eff}^r, # eV
$^{128}Sn \rightarrow {}^{128}Sb^m$	0.63	0.84	4.4	
	0.48	0.16	3.0	
$^{127}Sb \rightarrow {}^{127}Te^g$	1.10	∿0.2	9.8	5.5
	0.91	∿0.4	7.4	4.1
	0.82	∿0.3	6.4	3.5
	Others	∿0.1		
$^{129}Sb \rightarrow {}^{129}Te^g$	1.80	∿0.1	21.1	11.8
	1.53	∿0.1	16.2	9.0
	1.38	∿0.1	13.8	7.7
	0.62	∿0.3	4.2	2.4
	0.52	∿0.2	3.3	1.9
	Others	∿0.2		

* Taken from Ref. (Br78).

The chemical species was assumed to be H_6TeO_6 for Te(VI).

a.m.u., respectively. The chemical species was assumed to be H_6TeO_6 for Te(VI). The average value of effective recoil energy is estimated to be half of the maximum one and is comparatively low (<10 eV).

The recoil energy by γ-ray emission E_r^γ is comparable with that by the emission of β^--particle. The recoil energy by the emission of γ-ray of the highest energy (2.1 MeV for $^{129}Te^g$) was calculated to be 18.3 eV by the equation (Li47)

$$E_r^\gamma = \frac{536}{M} E_\gamma^2, \qquad (3.7)$$

where, E_γ is the energy of the γ-ray in MeV. The effective recoil energy is calculated to be 8.1 eV by equation 3.6. As expected, however, most of γ-rays have lower energies and the recoil energies by the γ-rays are low as well as by the β^--particles.

Since the exact values are not known for the bond energy of the Te-O bonds, we crudely adopt the value of ∿4 eV which is the dissociation energy of diatomic molecules TeO (We77a). Although, in aqueous solutions, the solvation energies of ions compensate to some degree the bond energy, a considerable high recoil energy must be required for the recoiling atom to escape the ionic cage (∿25 eV). Since the recoil energies are low (<10 eV) as mentioned above, most of the recoiling atoms would not be allowed to escape the ionic cage.

(C) Electronic excitation and ionization

After any type of decay involving a change in the nuclear charge, there is a sudden change in the electrostatic field controlling the electron cloud of the atom. In most cases, the cloud then contracts or expands adiabatically to accommodate itself to the new situation. This involves an energy adjustment ΔE, which has been estimated as

$$\Delta E = 22.8\ Z^{0.4}, \qquad (3.8)$$

in eV for each unit charge in Z (Se52). For antimony (Z = 51), equation 3.8 gives ΔE = 110 eV. The effect is for the atom to become electronically excited and to become ionized. This ionization process is often called the electron shake off.

Another ionization is the internal conversion of γ-rays emitted following β-decay. Furthermore, in a part of the atoms ionized by the shake off and the internal conversion, the ionization is progressed by the Auger cascade. Speaking chemically, a highly ionized atoms is very reactive and would result in bond rupture due to the coulombic repulsion as mentioned in Chapter 1.

In the case of β-decay of ^{127}Sb and ^{129}Sb, the ionization probabilities of the internal conversion and the electron shake off were estimated to be $\sim$0 % (Br78) and $\sim$25 % (Ca68), respectively... About 25 % of the daughter atoms has a more positive charge by 2

than the original nuclides and is in good accordance with the fraction of ∿20 % as Te(IV) in the β-decay process 3.4. It should be noted, however, that the ionization is not solely responsible for the chemical effects since the excited products may also be reduced by the medium. Considering that the recoil energy hardly result in bond rupture, it would be concluded that the electronic excitaion and ionization by emission of a β^--partcle are essential factor in the chemical effects of the β-decay process 3.4.

Similarly, the electronic excitation and ionization must play an important role in the chemical effects of the β-decay processes 3.2 and 3.3. However, Table 3.5 shows that the β-decay processes 3.2 and 3.3 are necessarily accompanied with the changes of the products in chemical structure. This means that the thermodynamic stability of the primary products and their subsequent reaction are important as well as the electronic excitaion and ionization in this case (Ne62, Ne64).

In the β-decay process 3.2, a primary product is expected to have the chemical structure of $SbSO_4^{3+}$, which is unstable in the experimental atmosphere. Two competitive pathways are open for the excited $SbSO_4^{3+}$, (i) deactivation, leading to the formation of $Sb(OH)_6^-$ (∿60 %), and (ii) the chemical reduction by the medium, leading to SbO^+ (∿40 %). The excitation of the primary product would be high enough to supply the activation energy for the chemical reduction by the medium. Similar

interpretations are offered for the β-decay process 3.3. The decay sequence is

$$SbO^{+} \xrightarrow{\beta^{-}} TeO^{2+} \rightarrow \begin{matrix} HTeO_2^{+},\ H_2TeO_3 & (>95\ \%), \\ H_2TeO_4,\ H_6TeO_6 & (<5\ \%). \end{matrix} \qquad (3.9)$$

The chemical oxidation of the primary product TeO^{2+} hardly occurred in this case. The excitation of the primary product would not be so high that it could not supply the activation energy for the chemical oxidation by the medium. Comparing both cases, it is concluded that the yield of the chemical reaction of the primary products would vary from case to case since the excitation following β-decay was comparatively low.

3.4.3. Comparison between β-decay and isomeric transition

It is of interest to compare the present results of β-decay with the ones of the $^{127}Te^{m} \rightarrow {}^{127}Te^{g}$ and $^{129}Te^{m} \rightarrow {}^{129}Te^{g}$ isomeric transitions since both isomeric transistions are highly internally converted. As mentioned above, the internal conversion is accompanied by the Auger cascade, and the net result is the loss of at least one, and usually several electrons. The loss of these electrons naturally results in bond rupture due to the coulombic repulsion.

The chemical effects of both isomeric transitions have been studied in aqueous solutions (Si40, Ha64, Hi71).

According to Hillman and Weiss (Hi71), at low pH, higher yields (>90 %) of Te(IV) were obtained when starting with both Te(IV) and Te(VI). The corresponding yields of the β-decay processes 3.3 and 3.4 are >95 % and ∿20 %, respectively. The results of the isomeric transitions are similar to the present results of the β-decay processes 3.3 and 3.4 although the differences are found among the yields. The internal conversion of the former is more complete than that of the latter and would result in the drastic chemical effects. Thus, the differences are probably attributed to the different extents of the electronic excitation and ionization.

3.5. Conclusions

The chemical effects of the β-decay processes: $^{128}Sn \rightarrow {}^{128}Sb^{m}$, $^{127}Sb \rightarrow {}^{127}Te^{g}$, and $^{129}Sb \rightarrow {}^{129}Te^{g}$ were investigated in sulfuric acid solutions. The chemical separation of Sb(III) and Sb(V) and that of Te(IV) and Te(VI) were performed with anion exchange methods. The experiments were performed under various conditions and the results were discussed in order to know some details of the mechanism of the chemical effects of β-decay.

First, the hot reactions were distinguished from the thermal reactions. The tracer experiments showed that any thermal reaction including the radiation-induced reactions did not occur in all the cases. Using oxygen as a radical scavenger, negligible scavenger effects were observed in both liquid and frozen systems. Furthermore, the results in the frozen system were in good accordance with the ones in the liquids. Therefore, it was concluded that the present results are not of the thermal reactions but of the hot reactions.

Next, the chemical effects of the β-decay processes $^{127, 129}Sb(V) \rightarrow {}^{127g, 129g}Te$ were discussed. Both Te(IV) and Te(VI) were formed with the yields of ∿20 % and ∿80 %, respectively. The memory effect was attributed to the similarity in chemical structure between Sb(V) and Te(VI); ∿20 % as Te(IV) was probably due to bond rupture caused by

either the recoil or the electronic excitation and ionization. Since the effective recoil energies were estimated to be comparatively low (<10 eV), it was concluded that most of the recoiling atoms would not be allowed to escape the ionic cage, and that the electronic excitation and ionization by emission of a β^--particle would be the essential factor in the chemical effects in this case.

In the β-decay process $^{128}Sn(IV) \rightarrow {}^{128}Sb^m$, both Sb(III) and Sb(V) were formed with the yields of ∿40 % and ∿60 %, respectively. On the other hand, in the β-decay processes $^{127, 129}Sb(III) \rightarrow {}^{127g, 129g}Te$, both Te(IV) and Te(VI) were formed with the yields of >95 % and <5 %, respectively. Since both decay processes are necessarily accompanied with the changes of the primary products in chemical structure, the essential factors were considered to be the thermodynamic stability of the primary products and their subsequent reaction as well as the electronic excitation and ionization. It was concluded that some of the primary products would suffer chemical reaction by the medium because of the electronic excitation and ionization, but that the yield of the chemical reaction would greatly depend on its activation energy since the excitation following β-decay was comparatively low.

Finally, the present results of β-decay were compared with the ones of the $^{127m, 129m}Te \rightarrow {}^{127g, 129g}Te$ isomeric transitions which are highly internally converted (Hi71).

The results of β-decay are less drastic than the ones of the isomeric transitions. The differences among the yields would be attributed to the different extents of the electronic excitation and ionization.

CHAPTER 4

OXIDATION STATES OF INDEPENDENTLY FORMED FISSION PRODUCTS

4.1. Introduction

Fission fragments are all exceedingly energetic when first formed, each fragment carrying ca. 35 - 110 MeV. The fragments also lose a large number of electrons in the initial fission act, giving them charges in the region of +20. Finally they may find themselves in a foreign environment, as for example, krypton and xenon atoms formed in uranium metal. Perhaps the most drastic effect as the result of nuclear decay comes from fission.

Generally speaking, the fission products formed independently favor the reduced states, whereas the oxidized states tend to persist during β-decay of the precursors. However, the situation is far from clear, since the previous studies were only qualitative (see Chapter 1). In order to learn more about the nature of high energy chemical reactions, it is of interest to study quantitatively and systematically the oxidation state of the other neighbouring elements in the periodic table.

In this Chapter, the measurements are reported of the oxidation states of the tin fission product: ^{128}Sn, the antimony

fission products: $^{128}Sb^{m}$, ^{132}Sb, and ^{133}Sb, and the tellurium fission products: $^{131}Te^{m}$, $^{133}Te^{m}$, and ^{134}Te formed in dilute acid solutions. These isotopes are formed almost independently by thermal neutron induced fission of ^{233}U. The distribution of the above isotopes between the reduced and oxidized states is studied carrying out corrections for the thermal reactions including the radiation-induced reactions. The mechanism is discussed on the basis of physical concepts (Wo65, Bo40).

4.2. Experimental

Either liquid or frozen aqueous solution of ^{233}U was irradiated with thermal neutrons. Sample solutions also contained the reduced and oxidized states of either Sn, Sb, and Te. Sn(II) and Sn(IV) were separated by precipitation of SnS from HCl, HF solution following the method of Brown and Wahl (Br67). For Sb and Te, the reduced and oxidized states were separated with anion exchange methods. Radioactivities were measured as a function of time. The decay data were resolved into components associated with the isotopes of interest.

4.2.1. Preparations

The guaranteed reagents obtained from Nakarai Chemicals, Ltd., were used without further purification. Triplly distilled

water was used to make up all the solutions.

(A) $^{233}UO_2SO_4$

Uranyl sulfate was prepared with U_3O_8 enriched to 100 % in ^{233}U, which was obtained from Atomic Fuel Industrial, Ltd. The U_3O_8 was dissolved in a small amount of hot concentrated nitric acid. The solution was evaporated to dryness and dissolved in concentrated sulfuric acid. Excess nitric acid was removed by boiling and the solution was diluted to 0.4 M in sulfuric acid.

(B) Tracers and carriers

The solutions of Sb(III), Sb(V), Te(IV), and Te(VI) labeled with ^{124}Sb, ^{125}Sb, $^{123}Te^m$, and $^{123}Te^m$, respectively, were prepared following the procedures given in Section 2.2.1. The Sn(II) solution labeled with ^{113}Sn was prepared by dissolving the irradiated tin metal, which was given in Section 2.2.1.B, in concentrated hydrochloric acid under argon atmosphere. The labeled Sn(IV) solution was prepared by oxidizing the Sn(II) with hydrogen peroxide.

The carriers Sn(II), Sn(IV), Sb(III), Sb(V), Te(IV), and Te(VI) were made up in the same manner as the corresponding tracers, but the carriers excluding Te(VI) were in hydrochloric acid solutions. The Te(VI) carrier was in water. Also, the Sr carrier for monitoring the total number of fission events was

prepared by dissolving a weighed amount of strontium carbonate in 1 M hydrochloric acid.

(C) Samples

Sample solutions for the tin study contained four components: 1.0 M HCl, 4.3 mM UO_2^{2+}, 8.4 mM Sn(II), and 8.4 mM Sn(IV), those for the antimony study contained four components: 0.4 M H_2SO_4, 4.3 mM UO_2^{2+}, 0.5 mM Sb(III), and 0.5 mM Sb(V), and those for the tellurium study contained four components: 0.4 M H_2SO_4, 4.3 mM UO_2^{2+}, 1.5 mM Te(IV), and 1.5 mM Te(VI). For the tin study, either Sn(II) or Sn(IV) was labeled with ^{113}Sn in order to know the yields of the thermal reactions including the radiation-induced reactions. Similarly, Sb(III) and Sb(V) were labeled with ^{124}Sb and ^{125}Sb, respectively, and either Te(IV) or Te(VI) was labeled with $^{123}Te^m$.

The sample solutions were either aerated or deaerated and sealed in 1 ml polyethylene tubes. The frozen samples were prepared in a dry ice box.

3.2.2. Irradiations

The liquid and frozen sample solutions were irradiated for 2 - 20 seconds at the pneumatic facility of the Kyoto University reactor, where the thermal neutron flux was $\sim 1.3 \times 10^{13}$ cm^{-2} sec^{-1}, the epithermal neutron flux was $\sim 1 \times 10^{12}$ cm^{-2} sec^{-1}, and the fast neutron flux was $\sim 4 \times 10^{12}$ cm^{-2} sec^{-1}, and the γ-dose rate was $\sim 3 \times 10^4$ r sec^{-1}. The temperature was somewhat higher

than the room temperature. The frozen samples were irradiated together with the dry ices. Figure 4.1 shows the target assembly in polyethylene pneumatic "rabbit" cartridges with a capacity of ∿30 ml.

4.2.3. Procedures

(A) Separation of Sn(II) and Sn(IV) and purification

The frozen sample was dissolved in a boiling water. The irradiated sample solution was transferred into 10 ml of 1 M HCl - 0.2 M HF solutions containing 10 mg of Sn(II) and 10 mg of Sn(IV) for the measurement of chemical yields and 10 mg of Sr for monitoring the number of fission events. Sn(II) and Sn(IV) were separated by precipitating SnS with H_2S following the method of Brown and Wahl (Br67). The fraction of Sn(IV) in the precipitation is less than 1 % and the fraction of Sn(II) in solution is about 3 %. It was also found that the exchange reaction between Sn(II) and Sn(IV) in separation process within 2 minutes is negligible as mentioned later. Sn(IV), which remained as a fluoride complex in the solution, was precipitated with H_2S after adding boric acid to the solution.

Each separated tin fraction was purified. Tin sulfide was dissolved in 12 M HCl containing 1 mg of Sb(V). After the complete reduction of Sb(V) to Sb(III) with NH_2OHHCl, Sb_2S_3 was precipitated from 3 M HCl solution. The filtrate which contained Sn(IV) was diluted to 1 M in HCl and SnS_2 was precipitated twice

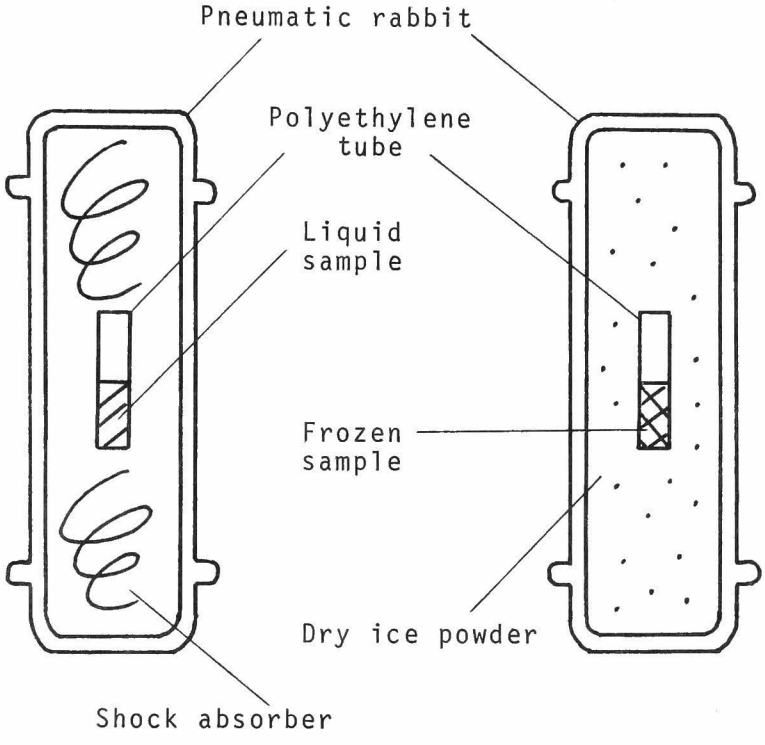

Fig. 4.1. Target assembly in pneumatic rabbits.

by hydrogen sulfide. They were mounted for the radioactivity measuerments.

(B) Separation of Sb(III) and Sb(V) and purification

After dissolving the frozen sample in boiling water, the irradiated sample solution was transferred into 10 ml of 1 M HCl solution containing 10 mg of Sb(III), 10 mg of Sb(V), and 10 mg of Sr carriers. Sb(III) and Sb(V) were separated with the anion exchange method described in Section 2.2.3. The separation was performed in several seconds under reduced pressure. As mentioned in Section 2.3.1.A, no thermal reaction occurred in the separation process within 2 minutes.

Each separated antimony fraction was purified by distilling SbH_3 following the method described in Section 3.2.2.B (Gr63). For the radioactivity measurements, antimony sulfide was mounted. In some runs, liquid samples were prepared for the rapid measurements. The separation and purification were carried out in about 5 minutes after the end of irradiation. The contamination in each fraction was found to be less than 0.1 % which was the detection limit of ^{128}Sn.

(C) Separation of Te(IV) and Te(VI) and purification

After dissolving the frozen sample in a boiling water, the irradiated sample solution was transferred into 10 ml of 6 M HCl containing 10 mg of Te(IV), 10 mg of Te(VI), and 10 mg of

Sr carriers. Te(IV) and Te(VI) were separated with the anion exchange method described in Section 2.2.4. The separation was performed in several seconds under reduced pressure. As mentioned in Section 2.3.1.B, no thermal reaction occurred in the separation process within 2 minutes.

Each separated tellurium fraction was purified. Te(VI) was reduced to Te(IV) in the boiling 6 M HCl solution which contained hydrazine hydrochloride. The solution was then adjusted to 2.4 M in HCl with the addition of 5 ml of 1.3 % tartaric acid solution, and Te(IV) was reduced to the metallic form by $NaHSO_3$. Tartaric acid prevented the contamination of antimony to less than 0.1 %. Each metallic tellurium was mounted for radioactivity measurements. The purification was carried out in about 10 minutes after the end of irradiation.

(D) Recovery of strontium

Strontium was recovered from each residual solution and the radioactivity was measured to get the total number of fission events in the irradiated sample.

The residual solution, to which sulfuric acid was added, was boiled. The precipitate of strontium sulfate was filtered and boiled with sodium carbonate. The precipitate of strontium carbonate was dissolved in 6 M hydrochloric acid containing 1 mg of palladium carrier and palladium sulfide was precipitated with hydrogen sulfide. The filtrate containing a iron carrier

was made basic with NH_4OH. The purification of the strontium was effected by palladium sulfide and ferric hydroxide scavenging steps. Strontium oxalate was precipitated from the filtrate which was adjusted to pH 5 with a buffer solution of CH_3COOH - CH_3COONH_4. The strontium oxalate was mounted for the radioactivity measurements.

4.2.4. Measurements

The radioactive decay of each fraction was followed with a 38 cm^3 Ge(Li) detector connected to a 4096 channel analyzer. The photo peaks of interest in the spectra were summarized in Table 4.1 together with the data used in the analysis of the experimental data. The radioactive decay data were ressolved by the method of least squares using Cumming's program (Cu63) modified for the use with a Facom 230-60 computer.

The chemical yields of the carriers Sn(II), Sn(IV), Sb(III), Sb(V), Te(IV), Te(VI), and Sr were determined by a neutron activation method after the measurements of the radioactivities and found to be more than 80 %.

4.2.5. Interfering thermal reactions

Both thermal and radiation-induced reactions would cause the isotopic mixing and the fission products would undergo the oxidation state changes before they could be investigated. The interfering thermal reactions were studied with the use of the

Table 4.1. Nuclear data and fission yields used in the analysis of experimental data.

Nuclide	Half life[†]	γ-Energy[†] in KeV	Intensity[†]	Branching fraction in % to	(Ref.)	Independent or Cumulative[*] fission yield in % (Im76)[∂]
^{134}Te	41.8 m	181	0.184			3.77[*§]
^{133}Sb	2.43 m	daughter activity		$^{133}Te^{m}$	15(Fu74,Fu76)	0.84[*]
$^{133}Te^{m}$	55.4 m	913	0.88[#]			2.03
^{132}Sn	39. s			$^{132}Sb^{g}$	100 (Hi76)	0.11[*]
$^{132}Sb^{m}$	4.1 m	974	1.00	$^{132}Sb^{g}$	0 (Hi76)	0.84
$^{132}Sb^{g}$	2.8 m	974	1.00			0.30
$^{131}Sn^{m,g}$	39 s, 50 s					0.51[*]
^{131}Sb	23. m	944	0.44	$^{131}Te^{m}$	6.8(Au76)	1.42
$^{131}Te^{m}$	30. h	150	0.21[#]			0.94
^{128}Sn	59.1 m	482	0.58	$^{128}Sb^{m}$	100 (Im75)	0.62[*]
$^{128}Sb^{m}$	10.0 m[@]	743	1.00	$^{128}Sb^{g}$	3.6(Im75)	0.062
$^{128}Sb^{g}$	9.1 h[@]	743	1.00			0.070

Table 4.1. Continued

Nuclide	Half life†	γ-Energy† in KeV	Intensity†	Branching fraction in % to (Ref.)	Independent or cumulative* fission yield in % (Im76) ∂
^{92}Sr	2.71 h	1384	0.90		6.6*¶

† Taken from Ref. (Bl77).

Taken from Refs. (Fu74, Fu76).

§ Obtained in the present work with the uncertainty of ±7 %.

@ Taken from Ref. (Im75).

¶ Taken from Refs. (Ka60, Tr71).

∂ In thermal neutron induced fission of ^{233}U.

tracers and the results were used for corrections.

(A) Tin

Both thermal and radiation-induced reactions were in some detail reported by Brown and Wahl (Br67). In the preliminary experiments with ^{113}Sn as shown in Table 4.2, it was confirmed that the thermal reactions were negligible in the sample solution during the 30 minutes that elapsed between preparation and separation except for irradiation.

On the other hand, irradiation induced the isotopic exchange between Sn(II) and Sn(IV). The percent exchange induced by the 5 sec irradiation was found to be $\sim$10 % both for the liquid and frozen solutions. This leads to a G-value of about 6 although the mechanism is still far from clear.

(B) Antimony and tellurium

As studied in Section 2.3.1, negligible thermal reaction occurs both in 0.4 M H_2SO_4 solutions and in the separation process within a few minutes.

On the other hand, irradiation induced the oxidation of Sb(III) and Te(IV) and the reduction of Sb(V) and Te(VI). Tables 4.3 and 4.4 show the observed yields of the radiation induced reactions of Sb and Te, respectively. The total absorbed dose is due to the reactor radiations (mainly composed of γ-rays) and the fission fragments in the sample. The energy absorption from the reactor radiations was determined from G(Fe(III)) =

Table 4.2. Thermal and radiation-induced reactions of Sn(II) and Sn(IV) in 1 M HCl under argon atmosphere.#

Temperature	$[Sn(II)]_0$, mM	$[Sn(IV)]_0$, mM	$[^{233}UO_2^{2+}]$, mM	Time elapsed	Δ[Sn(II)→Sn(IV)], mM	Δ[Sn(IV)→Sn(II)], mM
Room	8.4	-	-	30 min	<0.1	
Room	-	8.4	-	30 min		<0.1
Room	8.4	8.4	-	30 min	<0.1	<0.1
Reactor*	8.4	8.4	4.3	5 sec*	0.5	0.4
Dry ice*	8.4	8.4	4.3	5 sec*	0.4	0.4

All the separations were performed within 1 minute.

* Irradiated in the reactor.

Table 4.3. Radiation-induced oxidation of Sb(III) and reduction of Sb(V) in 0.4 M H_2SO_4 solutions containing 4.3 mM $^{233}UO_2^{2+}$, 0.5 mM Sb(III), and 0.5 mM Sb(V).

Phase	Oxygen	$G(Sb(III) \rightarrow Sb(V))^*_{obsd}$	$G(Sb(V) \rightarrow Sb(III))^*_{obsd}$
Frozen	Deaerated	0.20 ± 0.05 (0.2 ± 0.1)	<0.05 (<0.1)
Frozen	Aerated	0.30 ± 0.05 (0.3 ± 0.1)	<0.05 (<0.1)
Liquid	Deaerated	0.45 ± 0.05 (0.4 ± 0.1)	<0.05 (<0.1)

* The G-values were calculated from eq. 2.5. The rates of energy absorption from the reactor radiations and the fission fragments were $\sim 2 \times 10^{18}$ eV g^{-1} sec^{-1} and $\sim 3 \times 10^{18}$ eV g^{-1} sec^{-1}, respectively. The G-values in the parentheses were obtained from the samples which contain no $^{233}UO_2^{2+}$; the energy absorption came only from the reactor radiations.

Table 4.4. Radiation-induced oxidation of Te(IV) and reduction of Te(VI) in 0.4 M H_2SO_4 solutions containing 4.3 mM $^{233}UO_2^{2+}$, 1.5 mM Te(IV), and 1.5 mM Te(VI).

Phase	Oxygen	$G(Te(IV) \rightarrow Te(VI))^*_{obsd}$		$G(Te(VI) \rightarrow Te(IV))^*_{obsd}$	
Frozen	Deaerated	<0.02	(<0.05)	0.04 ± 0.04	(0.10 ± 0.05)
Frozen	Aerated	<0.02	(<0.05)	<0.02	(<0.05)
Liquid	Deaerated	0.04 ± 0.01	(0.10 ± 0.03)	0.06 ± 0.01	(0.15 ± 0.03)
Liquid	Aerated	0.57 ± 0.04	(1.5 ± 0.1)	<0.04	(<0.1)

* See the footnote of Table 4.3.

8.20 (Fr66) for the oxygen free ferrous sulfate dosimeters which had been irradiated with the sample solutions. Energy absorption from fission fragments was calculated from their average energy of 169.4 MeV (Va73) with the total number of fission events. The rate of energy absorption from the reactor radiations and the fission fragments were $\sim 2 \times 10^{18}$ eV g^{-1} sec^{-1} and $\sim 3 \times 10^{18}$ eV g^{-1} sec^{-1}, respectively.

The results are interpreted in Section 2.3.6 according to the mechanisms of the radiation-induced reactions of the antimony and tellurium compounds given in Chapter 2.

4.3. Results

The fission product tin isotope was found in both the +2 and +4 oxidation states, the antimony isotopes were in both the +3 and +5 oxidation states, and the tellurium isotopes were in both the +4 and +6 oxidation states. Some of the irradiated solutions were examined for other oxidation states, but none was found. The sums of the yields of the isotopes in the reduced states and those in the oxidized states were also confirmed to be equivalent to the known fission yields.

4.3.1. Oxidation states of tin fission products

The measured fraction of an isotope found in the +2 oxidation state was corrected for the radiation-induced exchange that mentioned in Section 4.2.5.A. During irradiation, the rate at which radioactive atoms were formed, $\frac{dN}{dt}$, is the sum of the rate of formation by fission, R_f and the rate of decay of themselves, $-\lambda N$. The rates of formation of radioactive atoms in the reduced and oxidized states, $\frac{dN_r}{dt}$ and $\frac{dN_o}{dt}$, respectively, are given by

$$\frac{dN_r}{dt} = F_f R_f - \lambda N_r - R_e\left(\frac{N_r}{N_{rc}} - \frac{N_o}{N_{oc}}\right), \tag{4.1}$$

$$\frac{dN_o}{dt} = (1 - F_f)R_f - \lambda N_o + R_e\left(\frac{N_r}{N_{rc}} - \frac{N_o}{N_{oc}}\right), \tag{4.2}$$

where, F_f is the fraction of radioactive atoms formed in the reduced state from fission, R_e is the rate of the radiation induced exchange, and N_{rc} and N_{oc} are the numbers of carrier atoms in the reduced and oxidized states, respectively.

The activities in each state at the end of irradiation were first obtained from decay curves. Also, the rate of the radiation-induced exchange, R_e was obtained from the tracer experiments as mentioned in Section 4.2.5.A using the Mckay's equation (Mc71b):

$$R_e = \frac{N_{rc}N_{oc}}{(N_{rc} + N_{oc})T} \ln(1 - F), \qquad (4.3)$$

where, T is the duration of irradiation and F is the fraction exchange induced during the irradiation. The corrections were comparatively small (<5 %). Table 4.5 shows the results corrected for the radiation-induced exchange. The reproducibility of several runs was fairly good. The uncertainty was arrived at by the method described in Section 2.2.5.

4.3.2. Oxidation states of antimony and tellurium fission products

The measured fraction of an isotope in each state was corrected for the mixing that occurred during irradiation. During irradiation, the rate at which radioactive atoms were formed,

Table 4.5. Percent as Sn(II) of the isotopes formed by fission of ^{233}U in 1 M HCl solutions containing 4.3 mM UO_2^{2+}, 8.4 mM Sn(II), and 8.4 mM Sn(IV).

Phase	Oxygen	Percent as Sn(II)	
		^{128}Sn	^{132}Sn
Frozen	Deaerated	36 ± 6	
Liquid	Deaerated	58 ± 6	~65*
Solid		32.5#	
Contribution of precursors in %		5†	1†

* Taken from Ref. (Li73).
\# In $[(CH_3)_4N]_2{}^{235}UCl_6$(s) in Ref. (Br67).
† Estimated from Ref. (Wo74).

$\frac{dN}{dt}$, is the sum of the rate of formation by fission, R_f and the rate of decay of themselves, $-\lambda N$. The contributions both of β-decay and of isomeric transition were excepted since they were of little importance (<9 %) as shown in Table 4.1. Also, the contribution of neutron capture was excepted since it was very small (<1 %) even in the case of $^{131}Te(n,\gamma)^{131}Te^{m}$. Assuming that the rates of the radiation-induced oxidation and reduction are constant, we obtain for the rates of formation of radioactive atoms in the reduced and oxidized states, $\frac{dN_r}{dt}$ and $\frac{dN_o}{dt}$, respectively:

$$\frac{dN_r}{dt} = F_f R_f - \lambda N_r - R_o \frac{N_r}{N_{rc}} + R_r \frac{N_o}{N_{oc}}, \qquad (3.4)$$

$$\frac{dN_o}{dt} = (1 - F_f) R_f - \lambda N_o + R_o \frac{N_r}{N_{rc}} - R_r \frac{N_o}{N_{oc}}, \qquad (3.5)$$

where, F_f is the fraction of radioactive atoms formed in the reduced state from fission, R_o and R_r are the rates of radiation-induced oxidation and reduction, respectively, and N_{rc} and N_{oc} are the numbers of carrier atoms in the reduced and oxidized states, respectively.

The activities in each state at the end of irradiation were first obtained from decay curves. Also, the rates of the radiation-induced oxidation and reduction, R_o and R_r, respectively, were obtained from the tracer experiments as shown in Tables

4.3 and 4.4, using the following equations:

$$\frac{dN_{rc}}{dt} = - R_o + R_r , \qquad (4.6)$$

$$\frac{dN_{oc}}{dt} = R_o - R_r . \qquad (4.7)$$

Equations 4.4 and 4.5 were solved for F_f using these experimental data together with the nuclear data and fission yields shown in Table 4.1. The results of Sb and Te corrected for the radiation-induced oxidation and reduction are summarized in Table 4.6 and 4.7, respectively. The reproducibility of several runs was very good. The uncertainty was arrived at by the method described in Section 2.2.5.

Table 4.6. Percent as Sb(III) of the isotopes formed by fission of ^{233}U in 0.4 M H_2SO_4 solutions containing 4.3 mM UO_2^{2+}, 0.5 mM Sb(III), and 0.5 mM Sb(V).

Phase	Oxygen	Percent as Sb(III)			
		$^{128}Sb^g$	^{132}Sb	^{133}Sb	Average*
Frozen	Deaerated	81 ± 5	85 ± 3	81 ± 5	83 ± 3
Frozen	Aerated	84 ± 5	84 ± 3	82 ± 5	83 ± 3
Liquid	Deaerated	95 ± 6	86 ± 5	99 ± 6	93 ± 4
Contribution of precursors in %		5	9	2#	

Estimated from Ref. (Wo74).

* The weighted average shown in the last column is obtained by weighting the result of each isotope by the inverse square of its assigned standard deviation σ_i. The errors caused by the contribution of the precursors are not included since their effects are unknown. The uncertainty shown is either the quantity Δ, which also includes the deviations of the individual results from the weighted average Δ_i

$$\Delta = \left(\frac{1}{n-1} \frac{\Sigma(\Delta_i/\sigma_i)^2}{\Sigma(1/\sigma_i)^2} \right)^{1/2},$$

or the quantity σ obtained from $1/\sigma^2 = \Sigma(1/\sigma_i^2)$, whichever larger.

Table 4.7. Percent as Te(IV) of the isotopes formed by fission of ^{233}U in 0.4 M H_2SO_4 solutions containing 4.3 mM UO_2^{2+}, 1.5 mM Te(IV), and 1.5 mM Te(VI).

Phase	Oxygen	Percent as Te(IV)			
		$^{131}Te^m$	$^{133}Te^m$	^{134}Te	Average
Frozen	Deaerated	81 ± 4	83 ± 3	84 ± 4	83 ± 2
Frozen	Aerated	80 ± 4	83 ± 3	80 ± 4	81 ± 3
Liquid	Deaerated	97 ± 6	97 ± 4	99 ± 3	98 ± 2
Liquid	Aerated	93 ± 6	91 ± 5	91 ± 4	92 ± 3
Contribution of precursors in %		1	3	4#	

Estimated from Ref. (Wo74).

4.4. Discussion

A fission fragment undergoes a long journey from the initial fission event to its final resting place where it becomes part of the chemical environment. The energy of the fission fragment, of the order of 100 MeV, exceeds considerably normal ionization or chemical bound energies. It is why, in the first period subsequent to its formation, the fragment can not form a chemical compound.

Chemically speaking, the fragment would be able to react with the medium when it losed most of its recoil energy. Thus, the final oxidation state of the fission product mainly results from the hot reactions at the final stage of the long journey. However, there is also the possibility of the product being involved in the thermal reactions in the medium, and undergoing the final oxidation state changes.

The main interest of this Chapter is to distinguish the hot from the thermal reactions and to discuss the mechanism which lead the fission product to rest in the final oxidation state.

4.4.1. Distinction between hot and thermal reactions

The fission product would be involved in the thermal reactions (i) with the diffusing radicals from its own track or (ii) with the bulk-radiolysis products in the medium.

In the present work, the latter reactions were followed with the use of tracers and Tables 4.5 - 4.7 show the results corrected for the thermal reactions with the bulk-radiolysis products. However, the former reactions are hardly followed since the former radicals are localized in the fission tracks. Considering that the former localized radicals are formed at very high energy transfer values of ∿250 eV/Å (Mo69), they seem very important in this case. Oxygen was adopted as a radical scavenger of the diffusing radicals from the fission tracks.

In the case of the frozen systems, the average fraction of the reduced state for the antimony isotopes shown in Table 4.6 is 83 ± 3 % in the absence of oxygen and 83 ± 3 % in the presence of oxygen; that for the tellurium isotopes shown in Table 4.7 is 83 ± 2 % in the absence of oxygen and 81 ± 3 % in the presence of oxygen. From no scavenger effect for each element, it is concluded that the fractions are resulted from the hot reactions and that fission products are not involved in the thermal reactions with the diffusing radicals from their own tracks. Unfortunately, the scavenger effect for the tin isotopes could not be confirmed since the chemical oxidation of Sn(II) occurred in the presence of oxygen.

In contrast with the above case, an apparent scavenger effect is observed for the tellurium isotopes in the liquid systems. The average fraction of the reduced state for the

tellurium isotopes shown in Table 4.7 is 98 ± 2 % in the absence of oxygen and 92 ± 3 % in the presence of oxygen. This effect evidently indicates that the tellurium isotopes are partially involved in the thermal reactions with the diffusing radicals from their own tracks since the fractions shown in Table 4.7 have been already corrected for the thermal reactions with the bulk-radiolysis products. The scavenger effects for the antimony isotopes could not be confirmed since most of the carrier Sb(III) was oxidized during the irradiation in the aerated liquid solutions.

Taking it into consideration for oxygen to scavenge the reducing species, an qualitative explanation can be suggested. The fission fragment leaves the track of radicals and rests at a relatively large distance of the order of hundred angströms from the spot where it formed, even in the solid phase (Sp76). Since the reducing species such as H diffusing faster than the oxidizing species (Sc69), they can encounter and reduce the oxidized forms of the tellurium fission products. Thus, in deaerated liquid solutions, the fraction of the reduced state goes to nearly 100 %. In the presence of oxygen, the reducing species are scavenged before diffusing to the oxidized tellurium products. The fraction of 92 % in the presence of oxygen is nearer to the results in the hot reactions in the frozen systems than in the absence of oxygen. Comparative low concentration ($\sim 10^{-4}$ M) of oxygen seems not to scavenge the

reducing species thoroughly.

The other thermal reactions with the oxidizing species such as OH and HO_2 radicals diffusing from the tracks seem unprobable although that is not confirmed experimentally. The oxidizing species diffuse slower than the reducing species (Sc69) and the rate constants $k_{Te(IV) + OH}$ and $k_{Te(IV) + HO_2}$ are lower (4.7×10^6 M^{-1} sec^{-1} and 46 M^{-1} sec^{-1}, respectively) than the rate constant $k_{Te(VI) + H} = 1.05 \times 10^8$ M^{-1} sec^{-1} (Ha68).

From the above consideration, it is concluded that the oxidation state of the fission products in the frozen system is nearer to that of the hot reactions than in the liquid system. Except for the differences caused by the diffusing radicals from their own tracks, the oxidation states of the fission products are expected to be insensitive to phase changes, indicating the validity of the hot-zone model (Ha79).

4.4.2. Chemical behavior of primary fission products

Figure 4.2 shows the fractions of the reduced states of the tin, antimony, and tellurium fission products as a function of their redox potentials. Standard reduction potential is 0.139 V for Sn(IV) - Sn(II) in 1 M HCl, 0.69 V for Sb_2O_5 - Sb_2O_3, and 1.02 V for $H_6TeO_{6(s)}$ - $TeO_{2(s)}$ (We77b) It should be noted that the oxidation state of the fission products in the frozen system is nearer to that of the hot reactions than in the liquid system. The higher the reduction potential is, the

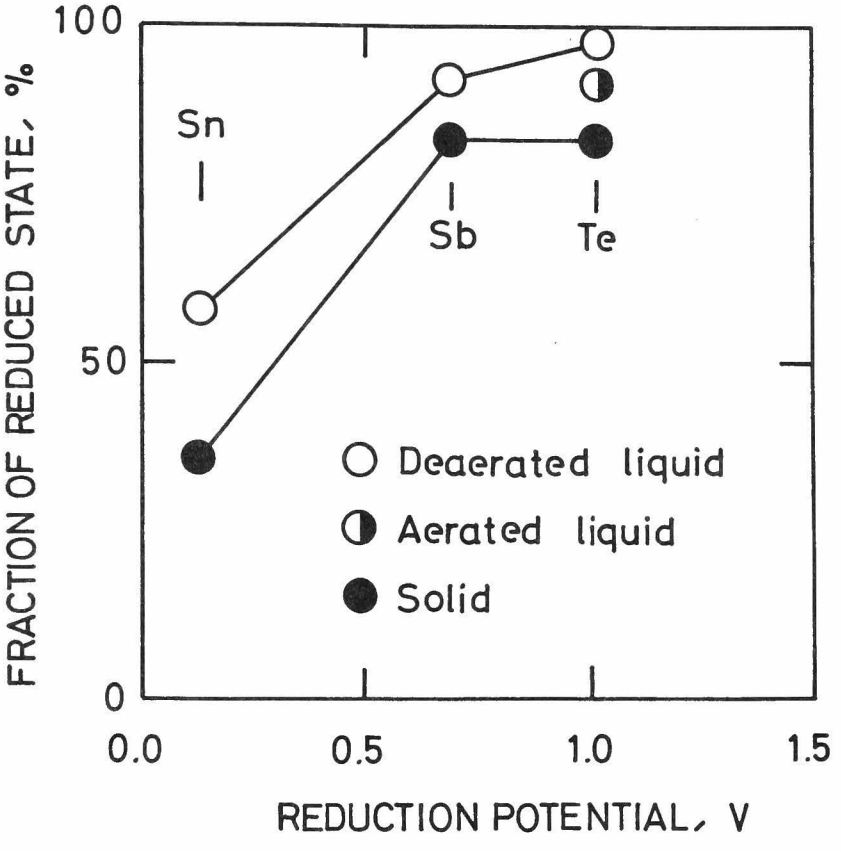

Fig. 4.2. Fractions of the reduced states of the tin, antimony, and tellurium isotopes formed by fission as a function of their reduction potentials (We77b).

larger the fraction of the reduced state is. It is interesting to seek for the trail of the newly formed atoms that leads predominently the reduced states from fission. Our procedure will be first, to review the chemical explanation for the iodine fission products (Ha61), then to review the explanation based on physical concepts for tin (Br67), and finally to discuss the mechanism systematically with the present results.

(A) Chemical explanation for iodine (Ha61)

As shown in Table 4.8, the fractions of the reduced states of the iodine fission products increase in the case of uranyl iodate (Ha61), uranyl nitrate (Sp73), and uranyl chloride (Sp76) in the order of ^{131}I, ^{133}I, ^{135}I. Especially, the ^{135}I is predominently formed in the reduced states in all the cases. Since about 40 % of the ^{135}I is formed independently in fission, it can be concluded that the oxidation states of the iodine fission products formed independently do not depend on the matrix in which they are formed. This indicates that a preference of the fission products for stabilizing in their reduced states is not the consequence of the thermal reactions but the hot reactions. It is necessary to take into account the details of the fission process itself.

At the moment of their formation the fission fragment are stripped of 15 - 20 electrons and this correspond to a highly oxidized form. Obviously, this form is unlikely to be stable

Table 4.8. Percent as reduced states of the iodine fission products in crystals.

Crystals	Percent as reduced states*			Ref.
	^{131}I	^{133}I	^{135}I	
Uranyl iodate	∿14	∿18	54 - 68	Ha61
Uranyl nitrate	35 - 42	42 - 50	71 - 88	Sp73
Uranyl chloride	68 - 73	68 - 70	76 - 77	Sp76
Contribution of precursors in %	>99	95	58	Wo74

* The percentages of reduced states R were considered:

$$R = \frac{[I^-] + [I_2]}{[I^-] + [I_2] + [IO_3^-] + [IO_4^-]} \times 100.$$

and it might follow that if complete neutralization does not occur, they will assume the valency state most suited to their partially stripped condition; this would lead to the fission products appearing in their most oxidized states. Since the experimental results show a preference of the fission products for stabilizing in their reduced states, the problem is to explain the reduction mechanism.

To explain the reduction mechanism, Hall and Walton (Ha61) suggested that the oxidation state is probably determined by the affinities of the primary fragments for the medium in which they are formed, and the relative ionization potentials of the different product elements would have a great importance. Thus, the oxidized ^{131}I may be explained because the mass 131 chain arises mainly as tin and antimony which have low electron binding energies. Since the mass 135 is formed mainly as iodine, which has a high electron binding energy, it would be expected to reach the reduced state more easily.

According to this chemical explanation, it is clear that the tin and antimony formed independently in fission must be found in the oxidized states. As shown in Fig. 4.2, the fractions of the reduced states of the tin and antimony are $\sim$36 % and $\sim$83 %, respectively, in the frozen system. The present results evidently indicate that appearance in a reduced state of isotopes formed independently in fission is partly related to the properties of the individual atom.

(B) Explanation based on physical concepts for tin (Br67)

An explanation of the oxidation state of primary fission products based on physical concepts was firstly by Walton (Wa64) and then Brown and Wahl (Br67) for the tin fission products in an aqueous medium. Primary fission products formed with kinetic energies of ∿70 MeV (Ni61) and ionic charges of ∿+15 (Fu58) lose kinetic energies by ionizing and exciting molecules along their paths and also lose charge through charge exchange with the medium.

Since the steady-state charge of a product depends on its velocity, the recoil energy can be estimated when the charge is reduced from the initial abnormal charge. The estimate can be made by extrapolation of experimental data (Be72) or by application of theoretical concepts such as the adiabatic principle (Wo65). This principle states that the maximum probability for electron exchange during a collision occurs when the reciprocal of the collision time equals the frequency of the electronic transition. Another theoretical approach is the Bohr approximation (Bo48) that ions gain electrons whose orbital velocity is less than the velocity of the ions and lose electrons whose orbital velocity is greater. All approaches give the result that when the steady-state charge in the +4 the recoil energy is still many MeV (∿5 MeV).

Thus, the recoil atom must lose much more charge before it starts to react with the medium. Then, in the 0 or +1 states,

the primary tin fission product would be oxidized by H^+ or other oxidizing agents to Sn(II). To account for the presence of the Sn(IV), it was assumed that the newly formed tin ions of low charge was still excited and that some was oxidized to Sn(IV) by the medium before becoming chemically equivalent to Sn(II) carriers. This analysis has also been used for the iodine fission products in solids (Sp73, Sp76).

(C) Further explanation

We now turn to a systematic consideration of the mechanism with the present results as shown in Fig. 4.2. The above mentioned analysis based on physical concepts is useful for a more general explanation. At the stage of charge exchange and nuclear scattering processes, there is no essential difference due to the different elements. At about 100 eV, the fission fragment becomes electrically neutral. This stage is particularly important, because the particle is able to react chemically. For example, the newly formed antimony ions of very low charges are unstable in the medium. They are oxidized to Sb(III) in the same way as tin but are hardly oxidized to Sb(V) because of a high reduction potential. The same situation holds also for the tellurium fission products Figure 4.2 indicates these situations.

However, Fig. 4.2 shows that the fraction of the reduced states of the antimony and tellurium isotopes in the frozen

system is only about 80 % in spite of their high reduction potentials. The hot-zone model would explain these phenomena. As mentioned in Chapter 1, in condensed phases, the hot reactions may occur in a hot zone created with a thermal spike.

As regards the thermal spike, a very important line of evidence comes from sputtering studies in solid state physics. These have been recently reviewed by Nelson (Ne68): each atom in the thermal spike has an average energy

$$E = E_T + \frac{3}{2} kT_0, \qquad (4.8)$$

where,

$$E_T = E_p/(\pi r^2 L N_0) = \frac{3}{2} kT_s$$

is the excess energy over that due to the ambient temperature T_o and where E_p is the energy of the primary particle, input to the spike. N_0 is the atomic density and $\pi r^2 L$ the cylindrical spike volume. Then T_s is the spike temperature. Using Maxwell - Boltzmann statistics to describe the energy spectrum within the spike, Thompson and Nelson (Th62) derive an expression for the energy spectrum of evaporated atoms and show that this fits the results of sputtering studies in quite satisfactory detail. The effective spike temperature comes out of this fit. For gold bombarded by 45 KeV Xe^+ ions, the spike temperature

T_s was 900 K above ambient. The spike had a radius of 100 Å and lasted 3×10^{-12} sec.

Similarly, a fission fragment is expected to carry enough energy to raise some 10^8 molecules to 5000 K. These molecules would occupy a region 200 Å in diameter along the fission track. The region of the thermal spike would overlap the radical sheath mentioned above. The fate of the fission product may, of course, be affected by these effects in the medium. When the fragment finally slows down, it will be situated at the end of the thermal spike it has produced. However, the thermal diffusivity in the water is estimated to be of the order of 10^{-3} cm^2 sec^{-1} and is larger by 10^2 than the diffusion coefficients of the radicals (Ha79). The large thermal diffusivity allows the fission product being involved in the thermal spike as well as in the chemical reactions with the diffusing radicals from its own track (see above).

Seitz and Koehler (Se56) considered the occurrence of reactions such as the formation of Frenkel defects and exchange of atoms in order-disorder processes in the hot zone in alloys: Harbottle et al. (Ha79) extended this to include chemical reactions such as redox. They showed how the quantity n_j, the number of jumps for a particular atom involved in a rate process of activation energy F in the hot zone, could be calculated by evaluating the integral:

$$n_j = \int_{t_0}^{\infty} \gamma_0 e^{-F/kT(t)} dt, \qquad (4.9)$$

where, T(t) is the temperature history of the hot zone at the particular atomic site. Since the spike temperature is very high in fission compared with the other nuclear reactions, it would play an important role in the hot reactions of fission products.

Another important factor expected is the electronic excitation of the fission products themselves. There is the most drastic change in the electrostatic field controlling the electron cloud of the fissioning system; the effect is for the fission products to become highly electronically excited. For the same reason mentioned in Section 3.4.2.C, the electronic excitation of the fission products might play an important part of the chemcal behaviors of fission products besides a very high spike temperature. It would be concluded that, together with a very high temperature of the thermal spike of fission, the electronic excitation of the fission products could allow themselves to undergo the chemical reaction requiring a high activation energy. The fact that the fraction of the reduced states of Sb and Te isotopes is only 80 % in spite of their high reduction potentials seems to support this illustration.

As to be mentioned later, a comparison between fission

and neutron capture reaction suggests the importance of the electronic excitation of the products in fission.

4.5. Conclusions

The oxidation states were investigated of the tin fission product: ^{128}Sn, the antimony fission products: $^{128}Sb^{g}$, ^{132}Sb, and ^{133}Sb, and the tellurium fission products: $^{131}Te^{m}$, $^{133}Te^{m}$, and ^{134}Te formed in dilute acid solutions. These isotopes are formed almost independently by thermal neutron induced fission of ^{233}U. The labeled carriers were used in order to protect the newly formed atoms from the radiation-induced reactions. Immediately after irradiation, Sn(II) and Sn(IV) were separated by precipitation of SnS from HCl, HF solution. The reduced and oxidized states of Sb and Te were separated with anion exchange methods. The experiments were performed under various conditions and the results were discussed leading to some details of the mechanism of the chemical behavior of the fission products.

First, the distribution of the fission products between the reduced and oxidized states was corrected for the radiation induced reactions. Irradiation in the reactor induced the exchange between Sn(II) and Sn(IV), the oxidation of Sb(III) and Te(IV), and the reduction of Sb(V) and Te(VI). The rates of the radiation-induced reactions were measured by the use of the tracers and were used for the corrections.

In 0.4 M sulfuric acid solutions containing 4.3 mM $^{233}UO_2^{2+}$, 1.5 mM Te(IV), and 1.5 mM Te(VI), the fraction of Te(IV) is

98 ± 2 % in the absence of oxygen and 92 ± 3 % in the presence of oxygen. In the frozen solutions of the same composition, the fraction of Te(IV) is 83 ± 2 % in the absence of oxygen and 81 ± 3 % in the presence of oxygen. Similar differences are also found in the case of the antimony isotopes in 0.4 M sulfuric acid solutions and the tin isotopes in 1 M hydrochloric acid solutions. It is concluded that, (i) in the frozen system, the distribution of the fission products between the reduced and oxidized states is resulted from the hot reactions but that, (ii) in the liquid system, there is the possibility of the fission products being involved in the thermal reactions with the diffusing radicals from their own tracks. Except for this difference, the oxidation state of the fission products is expected to be insensitive to phase changes, indicating the validity of the hot-zone model.

The results in the frozen system showed two interesting features: (i) the higher the reduction potential is, the larger the fraction of the reduced state is, and (ii) the fraction of the reduced states of Sb and Te isotopes is only 80 % in spite of their high reduction potentials. The mechanism of the chemical behaviors of the fission products were discussed based on physical concepts (Wo65, Bo48). The physical concepts suggest that, at the stage of charge exchange and nuclear scattering processes, there is no essential difference due to the different elements, and that, at 100 eV, the fission

fragment becomes electronically neutral and can react chemically. The hot-zone model was applied to the hot reactions at the final stage. From the present results, it was suggested that, together with a very high spike temperature, the electronic excitation of the fission products could allow themselves to undergo the chemical reaction requiring a high activation energy.

CHAPTER 5

OXIDATION STATES OF CUMULATIVELY FORMED FISSION PRODUCTS

5.1. Introduction

We now turn to different effects due to different nuclear reactions. The fission products may be formed either directly in fission or indirectly by β-decay. As reviewed in Chapter 1, several investigators have reported differences in the oxidation states of the iodine and tin isotopes from fission and have qualitatively attributed the differences to different modes of formation. However, attempts to develop a quantitative situation have often been handicapped by the lack of studies of isotopes formed with known large fractional independent fission yields.

Fortunately, the oxidation states have been measured of the tin, antimony, and tellurium isotopes formed with the large fractional independent yields in the perceding Chapter 4. These results can allow us to distinguish the precursor effects from the effects of fission itself even if the fission products are formed cumulatively. Accordingly, a quantitative situation can be developed on the connection between the nuclear and the chemical phenomena.

In this Chapter, measurements are analyzed of the oxidation

states of the antimony fission products: ^{129}Sb, $^{130}Sb^{g}$, and ^{131}Sb, and the tellurium fission products: $^{131}Te^{g}$, ^{132}Te, and $^{133}Te^{g}$ formed in sulfuric acid solutions. These isotopes are considerably formed through β-decay in thermal neutron induced fission of ^{235}U, although some of them are formed independently. After a quantitative corrections, the oxidation states of the above isotopes formed by β-decay are obtained and compared with the results described in the preceding Chapters. Since the oxidation state of the precursors is known to influence that of the daughters (see Chapter 3), the oxidation state of beta-decaying precursors are measured in the similar samples.

In the separate experiment, the chemical effects associated with neutron capture reaction are studied because the radioactivities of the $^{131}Te^{g}$ produced in $^{130}Te(n,\gamma)^{131}Te^{g}$ would interfere with the exact measurement of the oxidation states of the $^{131}Te^{g}$ formed in fission.

5.2. Experimental

Either liquid or frozen aqueous solution of ^{235}U was irradiated with thermal neutrons from the Kyoto University reactor. Sample solutions contained the reduced and oxidized states of either Sb or Te. In the irradiated sample containing Sb carriers, the oxidation states were studied of both the tin precursors and the antimony daughters. In the irradiated sample containing Te carriers, the oxidation states were studied of both the antimony precursors and the tellurium daughters. Most of the experimental procedures were similar to those described in Section 4.2. Some differences are given in this Section.

5.2.1. Preparations and irradiations

Uranyl sulfate was prepared with U_3O_8 enriched to 90 % in ^{235}U, which was obtained from Atomic Fuel Industrial, Ltd. The preparations and the irradiations of the samples were the same as described in Section 4.2.1 and 4.2.2, respectively.

5.2.2. Procedures

The procedures to separate the reduced from the oxidized states of either Sn, Sb, or Te were the same as those described in Section 4.2.3. It should be noted that the isotopes under

investigation are formed both directly in fission and indirectly by β-decay. In order to distinguish the chemical effects of β-decay from those of fission, it is very important to know the behaviors of the precursors in the chemical separation processes. The behaviors of the tin and antimony precursors are shown in Figs. 5.1 and 5.2, respectively.

As mentioned later, the tin and antimony precursors would be oxidized to Sn(IV) and Sb(V), respectively, by reactor radiations in the case of no carrier.

5.2.3. Measurements

The radioactive decay of each fraction was followed with a calibrated 38 cm^3 Ge(Li) detector connected to a 4096 channel pulse height analyzer. The photo peaks of interest in the spectra are summarized in Table 5.3 together with the data used in the analysis of experimental data.

5.2.4. Chemical effects associated with neutron capture reaction

In the separate experiment, the chemical effects associated with neutron capture reaction were studied for the nuclear reaction $^{130}Te(n, \gamma)^{131}Te^{g}$. The 0.4 M H_2SO_4 solutions containing Te(IV) and Te(VI) were prepared and irradiated. The procedures were the same as those described in the preceding Sections.

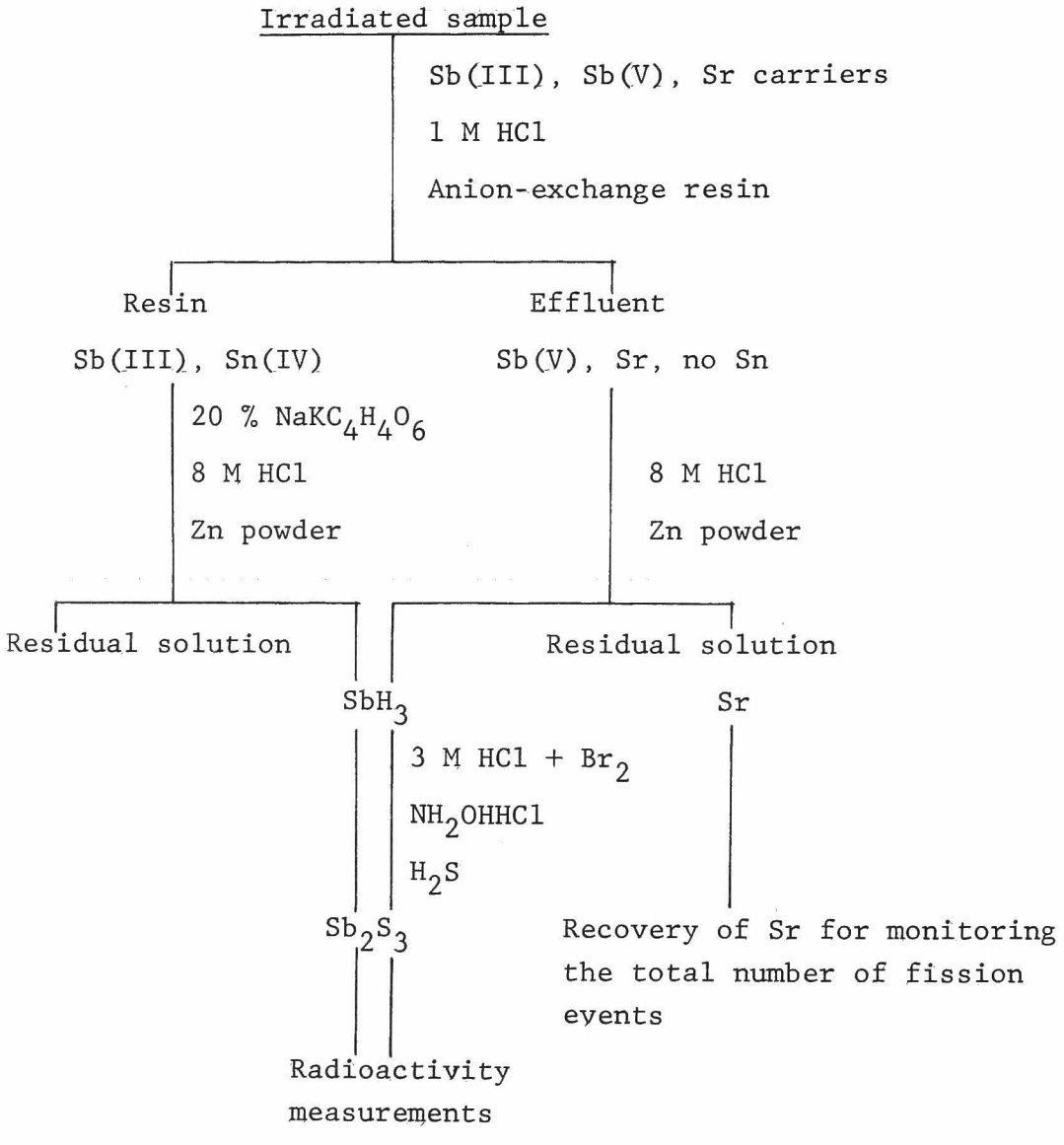

Fig. 5.1. Chemical separation between Sb(III) and Sb(V) and behavior of Sn precursors.

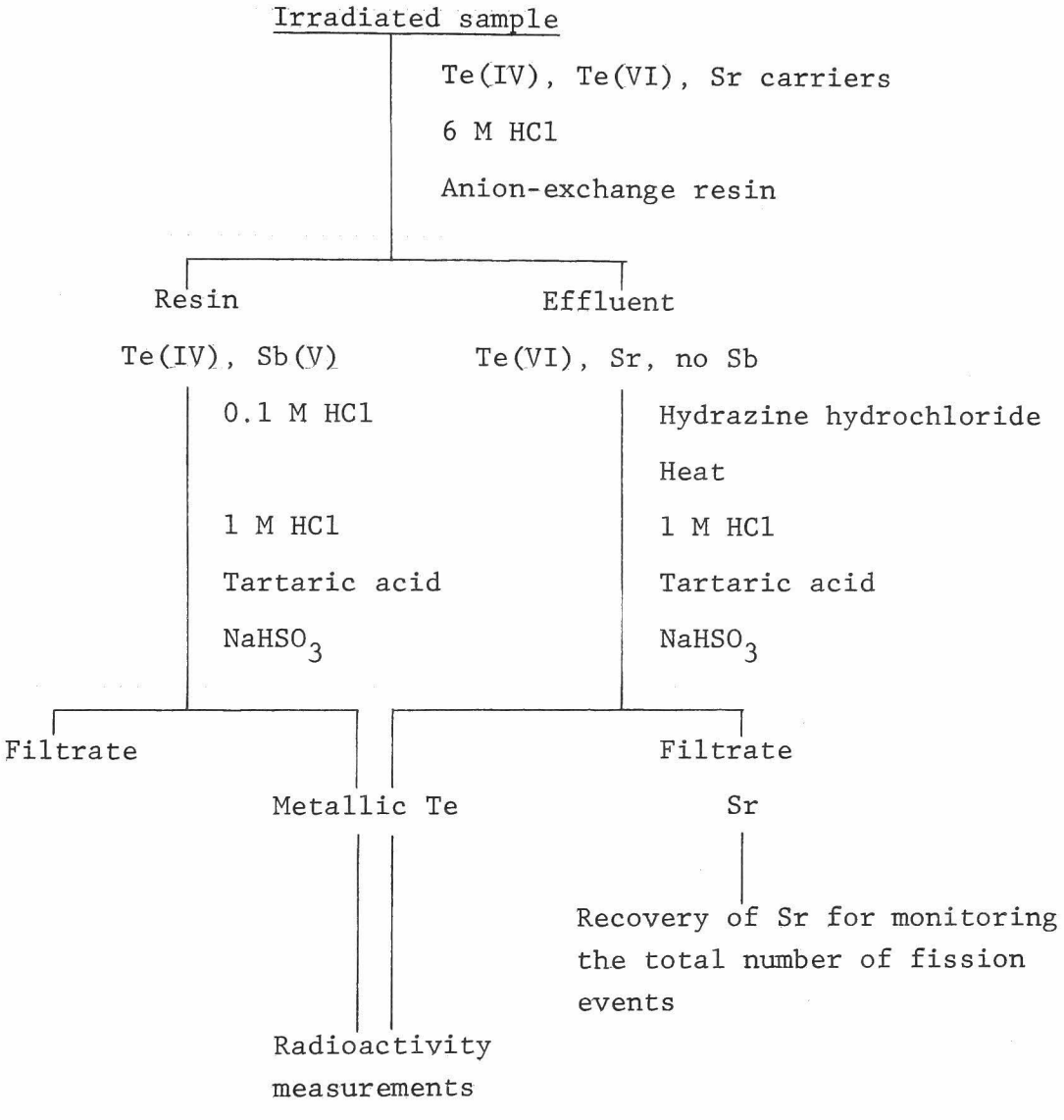

Fig. 5.2. Chemical separation between Te(IV) and Te(VI) and behavior of Sb precursors.

Table 5.1. Nuclear data and fission yields used in the analysis of experimental data.

Nuclide	Half life[†]	γ-Energy[†] in KeV	Intensity[†]	Branching fraction in % to	(Ref.)	Independent or cumulative[*] fission yield in % (Im76)[∂]
^{133}Sb	2.43 m	daughter activity		$^{133}Te^{m}$	15(Fu74,Fu76)	2.29*
$^{133}Te^{m}$	55.4 m	913	0.88[#]	$^{133}Te^{g}$	29(Fu74,Fu76)	1.96
$^{133}Te^{g}$	12.43 m	312	0.59[#]			1.56
^{132}Sn	39. s			$^{132}Sb^{g}$	100 (Hi76)	0.55*
$^{132}Sb^{m}$	4.1 m	974	1.00	$^{132}Sb^{g}$	0 (Hi76)	0.38
$^{132}Sb^{g}$	2.8 m	974	1.00			1.62
^{132}Te	3.24 d	228	0.88			1.20[§]
$^{131}Sn^{m,g}$	39 s, 50 s					0.80*
^{131}Sb	23. m	944	0.44	$^{131}Te^{m}$	6.8(Au76)	1.54
$^{131}Te^{m}$	30. h	150	0.21[#]	$^{131}Te^{g}$	21(Fu74,Fu76)	0.21
$^{131}Te^{g}$	25. m	150	0.75[#]			0.11
$^{130}Sn^{m}$	1.7 m	daughter activity		$^{130}Sb^{m}$	100 (Hi74)	0.11*
$^{130}Sn^{g}$	3.7 m	daughter activity		$^{130}Sb^{g}$	100 (Hi74)	1.1*

Table 5.1. Continued

Nuclide	Half life[†]	γ-Energy[†] in KeV	Intensity[†]	Branching fraction in % to	(Ref.)	Independent or cumulative[*] fission yield in % (Im76)[∂]
$^{130}Sb^{m}$	40.3 m	839	0.998	$^{130}Sb^{g}$ 0	(Hi74)	0.27
$^{130}Sb^{g}$	6.3 m	839	1.00			0.22
$^{129}Sn^{m}$	7.5 m	daughter activity		^{129}Sb 100	(Fo72)	0.357[*Ω]
$^{129}Sn^{g}$	2.52 m	daughter activity				0.529[*Ω]
^{129}Sb	4.32 h	813	0.435	$^{129}Te^{m}$ 16.6	(Ho72)	0.114[Ω]
^{128}Sn	59.1 m	482	0.58	$^{128}Sb^{m}$ 100	(Im75)	0.25[§]
$^{128}Sb^{m}$	10.0 m[@]	743	1.00	$^{128}Sb^{g}$ 3.6	(Im75)	
$^{128}Sb^{g}$	9.1 h[@]	743	1.00			
^{92}Sr	2.71 h	1384	0.90			6.0[*¶]

† Taken from Ref. (Bl77).
# Taken from Refs. (Fu74, Fu76).
§ Obtained in the present work with the uncertainty of 7 %.
@ Taken from Ref. (Im75).
¶ Taken from Refs. (Ka60, Tr71).
Ω Taken from Ref. (Fo72).
∂ In thermal neutron induced fission of ^{235}U.

5.3. Results

The distribution of the oxidation states of the cumulatively formed fission products varied with the isotopes. Fig. 5.3 shows a typical example in a deaerated 0.4 M H_2SO_4 solutions containing ^{235}U and carriers. Since the independently formed fission products are formed in the reduced states almost completely (see Chapter 4), the differences are attributed to the different modes of formation. In the following Sections, the chemical effects of β-decay are distinguished from those of fission.

5.3.1. Oxidation states of precursors

When the isotopes are formed by β-decay, their oxidation states must be greatly affected by those of the precursors (see Chapter 3). The oxidation state of the tin precursors was studied after the method proposed by Lin and Wahl (Li67). The tin precursors are found to be present in the +4 oxidation state when the irradiated solution contains no tin carrier even though it contains both oxidation states of the antimony carriers, as shown in Table 5.2. The oxidation state of the antimony precursors without carriers was also studied and was found to be in the +5 oxidation state, as shown in Table 5.3. Those precursors are produced mostly by fission and would be formed in the reduced states, as shown in the preceding Chapter 4. The precursors, however, would be oxidized by reactor

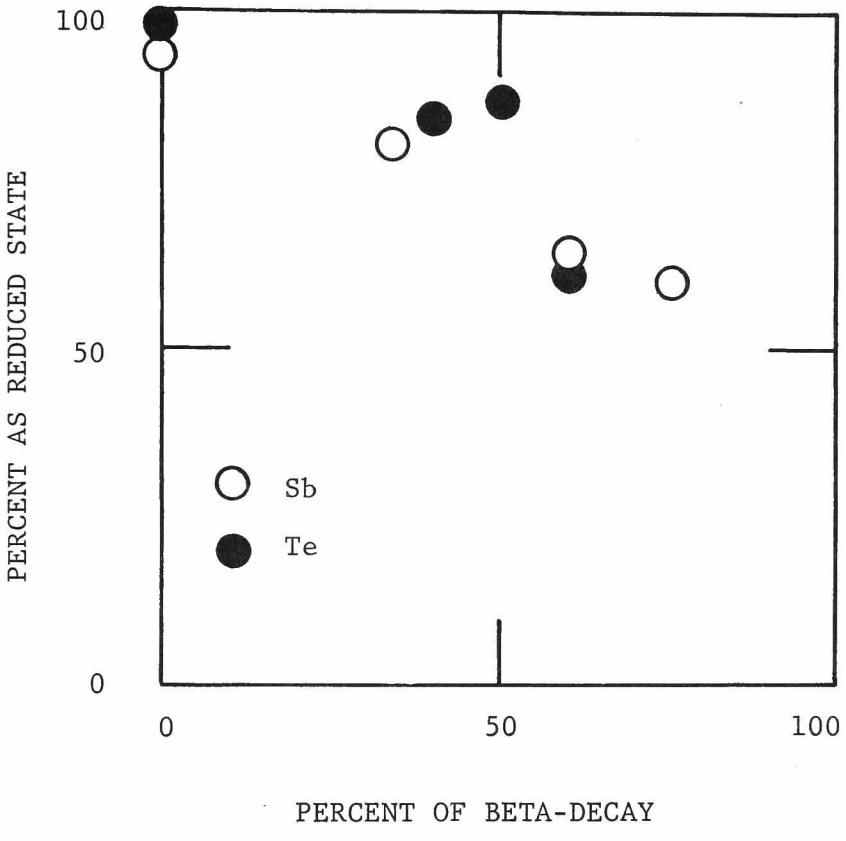

Fig. 5.3. Fraction as reduced state of antimony and tellurium fission products as a function of contribution of β-decay. Sample solution is deaerated 0.4 M H_2SO_4 solution containing ^{235}U and carriers. Results have been corrected for radiation-induced reactions.

Table 5.2. Percent as Sb(III) of antimony isotopes formed by β-decay of tin precursors in irradiated 0.4 M H_2SO_4 solutions containing 4.3 mM UO_2^{2+}, 0.5 mM Sb(III), 0.5 mM Sb(V), and no Sn carrier.#

Phase	Oxygen	Percent as Sn(II) of precursor			Percent as Sb(III) of product			
		^{128}Sn	$^{129}Sn^{m,g}$	$^{130}Sn^{g}$	$^{128}Sb^{g}$	^{129}Sb	$^{130}Sb^{g}$	^{131}Sb
Liquid	Deaerated	∿0	<4	<5	41 ± 4	49 ± 6	45 ± 5	35 ± 9
β-Decay energy in MeV					1.3	4.0	2.0	4.8
(Ref.)					(Au73)	(Fo72)	(Hi74)	(Au76)

The averages and uncertainties were arrived at by the method described in Section 2.2.5.

Table 5.3. Percent as Te(IV) of tellurium isotopes formed by β-decay of antimony precurcers in irradiated 0.4 M H_2SO_4 solutions containing 4.3 mM UO_2^{2+}, 1.5 mM Te(IV), 1.5 mM Te(VI), and no Sb carrier.#

Phase	Oxygen	Percent as Sb(III) of precursor			Percent as Te(IV) of product		
		^{131}Sb	$^{132}Sb^{m,g}$	^{133}Sb	$^{131}Te^{g}$	^{132}Te	$^{133}Te^{g}$
Frozen	Aerated	80 ± 5	84 ± 4	82 ± 5	80 ± 6	74 ± 8	76 ± 10
Frozen	Deaerated	82 ± 5	83 ± 4	84 ± 5	84 ± 6	76 ± 8	78 ± 10
Liquid	Aerated	<1	<3	<4	34 ± 8	70 ± 10	55 ± 12
Liquid	Deaerated	<1	<6	<7	35 ± 8	74 ± 10	60 ± 12
β-Decay energy in MeV (Ref.)					3.1 (Au76)	5.6 (Hi76)	4.0 (He74)

The averages and uncertainties were arrived at by the method described in Section 2.2.5.

radiation in the sample solution because of no carrier.

5.3.2. Oxidation states of β-decay products with higher recoil energies

In the thermal neutron induced fission of ^{235}U, the antimony isotopes such as ^{129}Sb, $^{130}Sb^{g}$, and ^{131}Sb and the tellurium isotopes $^{131}Te^{g}$, ^{132}Te, and $^{133}Te^{g}$ are mostly formed by β-decay of the precursors, which are so short-lived and inconvenient to look for chemical behaviors. For those isotopes, the results of the radioactivity measuremente were analyzed with the following assumptions: (i) the isotopes themselves produced independently by fission are formed in the reduced states with the yields as shown in Tables 4.6 and 4.7, and (ii) their precursors are formed in the oxidized states because of no carrier.

The measured fraction of an isotope found in each state was corrected as follows for mixing that occurred during irradiation. During irradiation, the rate of formation of radioactive atoms, $\frac{dN}{dt}$, is the sum of the rates of formation by fission, R_f, by β-decay, $b_a\lambda_a N_a + b_b\lambda_b N_b$ (rates of β-decay from a pair of precursors a and b), by isomeric transition, $b_m\lambda_m N_m$, and by neutron capture of carriers, R_n, and the rate of decay of themselves, $-\lambda N$. Therefore, the rates of formation of radioactive atoms in the reduced and oxidized states, $\frac{dN_r}{dt}$ and $\frac{dN_o}{dt}$, respectively, are given by

$$\frac{dN_r}{dt} = F_f R_f + F_n R_n + F_\beta (b_a \lambda_a N_a + b_b \lambda_b N_b) + F_m b_m \lambda_m N_m$$

$$- \lambda N_r - R_o \frac{N_r}{N_{rc}} + R_r \frac{N_o}{N_{oc}} , \qquad (5.1)$$

$$\frac{dN_o}{dt} = (1 - F_f) R_f + (1 - F_n) R_n + (1 - F_\beta)(b_a \lambda_a N_a + b_b \lambda_b N_b)$$

$$+ (1 - F_m) b_m \lambda_m N_m - \lambda N_o + R_o \frac{N_r}{N_{rc}} - R_r \frac{N_o}{N_{oc}} , \qquad (5.2)$$

where, F_f, F_n, F_β, and F_m are the fraction of radioactive atoms formed in the reduced state from fission, neutron capture, β-decay and isomeric transition, respectively, and N_{rc} and N_{oc} are the numbers of carrier atoms in the reduced states and oxidized states, respectively. The fractions of the reduced states through two possible β-decay paths were not discriminated, and F_β is assumed to be equal for two branches. As the rate of oxidation and reduction induced by reactor radiation of the antimony and tellurium atoms, R_o and R_r, were properly assumed to be constant for each element (see Chapter 2), the last two terms of the above equations denote the effects of reactor radiation on the rates of formation in the respective oxidation states.

During the time interval between the end of irradiation and the separation of the oxidation states of the element concerned, the rates of growth of radioactive atoms from the

precursors in the respective oxidation states are

$$\frac{dN_r}{dt} = F_\beta(b_a\lambda_a N_a + b_b\lambda_b N_b) + F_m b_m \lambda_m N_m - \lambda N_r \ , \qquad (5.3)$$

$$\frac{dN_o}{dt} = (1 - F_\beta)(b_a\lambda_a N_a + b_b\lambda_b N_b) + (1 - F_m)b_m\lambda_m N_m - \lambda N_o \ , \qquad (5.4)$$

The precursors in the irradiated solution containing no carrier were in the oxidized states, as shown in Tables 5.2 and 5.3 for Sn and Sb, respectively. The oxidized forms of the precursors were adsorbed in the anion exchange resin and eluted with the reduced forms of their descendants Sb(III) and Te(IV), as shown in Figs. 5.1 and 5.2, respectively. Therefore, the rates of growth of radioactive atoms from the precursors in the respective oxidation states during the time interval between the separation of the oxidation states and the final purification are given by

$$\frac{dN_r}{dt} = (b_a\lambda_a N_a + b_b\lambda_b N_b) + f_m b_m \lambda_m N_m - \lambda N_r \ , \qquad (5.5)$$

$$\frac{dN_o}{dt} = (1 - f_m)b_m\lambda_m N_m - \lambda N_o \ , \qquad (5.6)$$

where, f_m is the fraction of the precursors of isomeric transition in the reduced states at the separation of the oxidation states and each measured value was used as f_m.

The values of F_m for the tellurium isomers were measured previously to be 0.95 for $^{131}Te^m$ and 0.57 for $^{133}Te^m$ (Fu74, Fu76), and those for the antimony isomers were neglected because of little or no branching decay to the ground states. The value of F_n was measured in the separate experiment to be about unity for the nuclear reaction $^{130}Te(n, \gamma)^{131}Te^g$ as shown in Table 5.4, and was neglected for the antimony isotopes because of no contribution.

The radioactivities in each oxidation state at the final purification were obtained by decay analysis (Cu63). Equations 5.1 - 5.6 were solved for F_β using these experimental data together with the values of F_f given in Tables 4.6 and 4.7. The values of F_β thus obtained, are shown in Tables 5.2 and 5.3 for Sb and Te, respectively. The reproducibility of several runs was fairly good.

Table 5.4. Percent as Te(IV) of $^{131}Te^{g}$ formed by neutron capture reaction of ^{130}Te in 0.4 M H_2SO_4 solutions containing Te(IV) and Te(VI) carriers.#

Phase	Oxygen	Percent as Te(IV)	
		in 5.0 mM Te(IV) and 0.5 mM Te(VI) solution	in 0.5 mM Te(IV) and 5.0 mM Te(VI) solution
Frozen	Aerated	>94	96 ± 1
Frozen	Deaerated	>99	>95
Liquid	Aerated	96 ± 3	95 ± 2
Liquid	Deaerated	>98	>98

The averages and uncertainties were arrived at by the method described in Section 2.2.5.

5.4. Discussion

The main interest of this Chapter is to discuss some differences among nuclear processes. These bring out the connection between the nuclear and the chemical phenomena.

5.4.1. Comparison between fission and neutron capture

Historically speaking, the effect of initial recoil energy has been studied in differing nuclear processes such as (n, γ), (γ, n), and (n, 2n) which produce atoms having initial recoil energies differing by a factor as large as 10^3 (Ac72). The overwhelming conclusion is that, although isotopic effects produce some yield differences, the effect of initial recoil energy is relatively minor.

In the preliminary experiment, the oxidation states of the product $^{131}Te^g$ was studied in the neutron capture reaction $^{130}Te(n, \gamma)^{131}Te^g$. Since the recoil energy is relatively low in neutron capture, it is very instructive to compare the neutron capture with fission in which a most drastic recoil energy is imparted. It will improve a knowledge of the effect of changes in initial recoil energy on the hot reactions.

Table 5.4 shows the fractions of the reduced state Te(IV) of $^{131}Te^g$ formed by neutron capture reactions of ^{130}Te in 0.4 M H_2SO_4 solutions containing Te(IV) and Te(VI) carriers. Higher yields (>90 %) of Te(IV) were obtained when starting

with both Te(IV) and Te(VI). No scavenger effect of oxygen was observed in all the cases. These facts indicate that (i) rupture of parent molecules are almost complete and that (ii) they are not of the thermal reactions but of the hot reactions. As shown in Chapter 4, the fraction of Te(IV) of the tellurium fission products is only 80 % in the hot reactions. There is an apparent difference between fission and neutron capture.

In the $^{130}Te(n, \gamma)^{131}Te^{g}$ reaction, the maximum capture gamma-ray energy is 5.9 MeV. It leads to a maximum recoil energy of 142 eV for $^{131}Te^{g}$ following the equation 3.7. Although the spectra of effective recoil energies of atoms are typically very broad, they seem high enough to rupture the parent compounds. Once a rupture happens, the recoil atoms are expected to form the thermal spikes as described for fission products in Section 4.4.2.C. The Seitz-Koehler spike theory, combined with what is known of changes in mean free path of atoms slowing down in condensed phases, leads to the expectation that the temperature history of the terminal hot-zone ought not to reflect in any significant way the initial energy of the recoil atom.

It should be remembered that the atoms formed by neutron capture reactions are hardly electronically excited whereas the fission fragments may be highly excited. In contrast to the latter, the low electronic excitation of the former might not allow the atoms to undergo the chemical reaction which

requires a high activation energy.

5.4.2. Recoil effects in β-decay

The fractions of the tellurium isotopes as Te(IV) formed by β-decay of the antimony precursors in the +5 oxidation state are, in particular in liquid systems, dependent on the isotopes as shown in Table 5.3. Figure 5.4 shows the fractions of the tellurium isotopes as Te(VI) formed by β-decay of Sb(V) isotopes in deaerated liquid as a function of β-decay energy. The higher β-decay energy is, the less the fraction as Te(VI) is.

In a dilute H_2SO_4 solution, Sb(V) is probably exist as a mixture of $Sb(OH)_6^-$ and $(Sb_3O_6(OH)_6)^{3-}$ (Da70), and Te(VI) as a mixture of H_6TeO_6 and H_2TeO_4 (Ho60). The similarity between the chemical structures of $Sb(OH)_6^-$ and H_6TeO_6 may support that the antimony complex $Sb(OH)_6^-$ leads to the tellurium complex H_6TeO_6 through β-decay without bond rupture. As shown in Chapter 3, the following factors are very important in bond rupture caused by β-decay: (i) stability of daughter complex, (ii) electronic excitation and ionization, and (iii) recoil energy. Since the former two factors hardly explain the different behaviors among the isotopes, it is plausible that the different recoil energies of the isotopes in the emission of β-particles owe to the different degrees of bond rupture. A large recoil energy must increase the probability of the

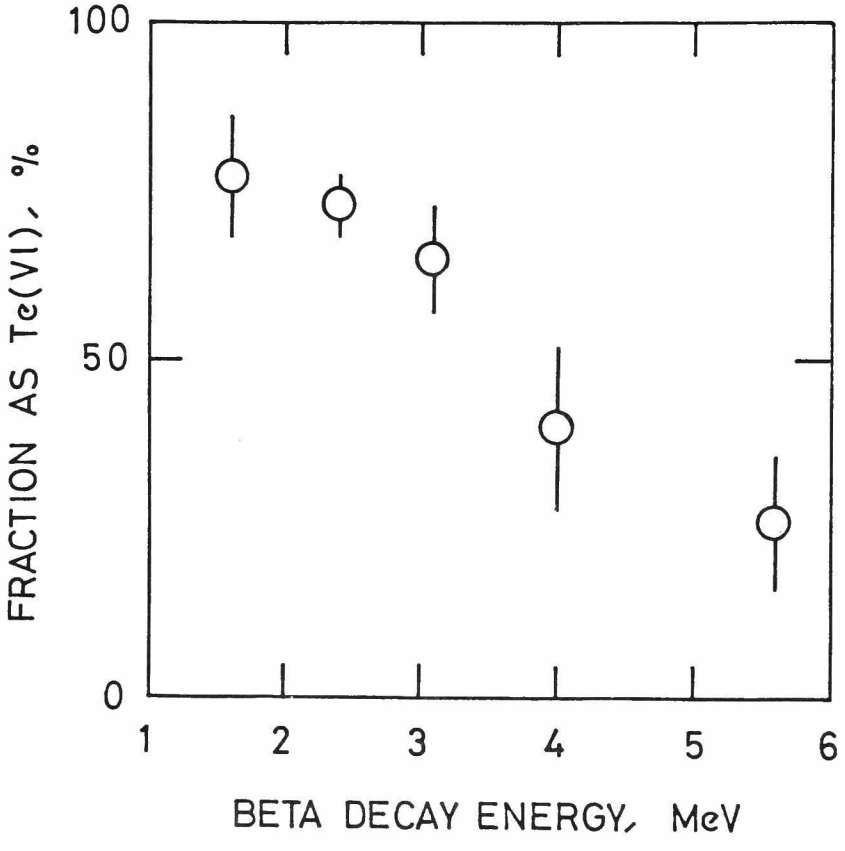

Fig. 5.4. Fractions of tellurium isotopes: $^{127}Te^{g}$, $^{129}Te^{g}$, $^{131}Te^{g}$, ^{132}Te, and $^{133}Te^{g}$ as Te(VI) formed by β-decay of antimony precursors in the +5 state as a function of β-decay energy.

bond rupture of the daughter tellurium complex H_6TeO_6. Then, the tellurium atom in the +6 oxidation state is still excited and will be reduced probably by the medium to Te(IV) that is more stable than Te(VI) in the experimental atmosphere.

In contrast to the Te isotopes, the fractions of the antimony isotopes as Sb(III) formed by β-decay of the tin precursors in the +4 oxidation state are nearly constant irrespective of their β-decay energies as shown in Table 5.2. The β-decay of a tin isotope in the +4 oxidation state would result in antimony atoms in the +5 oxidation state. In a dilute H_2SO_4 solution, Sn(IV) is probably present as $SnSO_4^{2+}$ (Br55) and has different chemical structure from that of Sb(V). Thus, the newly formed antimony atom in the +5 oxidation state must rearrange its chemical structure irrespective of that of Sn(IV). This is the reason why the fractions as Sb(V) are independent of the recoil energies, as shown in Table 5.2. Since the newly formed Sb atoms in the +5 state have recoil energy and electronic excitation energy of about 100 eV (Se52), they would suffer chemical reduction by the medium and about one-half of them is found in the reduced state.

Finally, we note the possibility of application of the oxidation states in aqueous solutions to measures of fractional fission yields. According to Lin and Wahl (Li73), the fraction as Sn(II) from β-decay increases with mass number, possibly

because of increasing recoil energy, and overlaps the fraction as Sn(II) of 0.6 - 0.7 for independently formed tin fission products. Thus, oxidation states are not useful measures of fractional independent yields for tin fission products. In the case of antimony and tellurium fission products, the present study shows that oxidation states are some effective measures of fractinal yields if the radiation-induced reactions are negligible.

5.5. Conclusions

The oxidation states were investigated of the antimony fission products: ^{129}Sb, $^{130}Sb^{g}$, and ^{131}Sb, and the tellurium fission products: $^{131}Te^{g}$, ^{132}Te, and $^{133}Te^{g}$ formed in sulfuric acid solutions. These isotopes are formed either directly in fission or indirectly by β-decay in thermal neutron induced fission of ^{235}U. The differences in the oxidation states of the antimony and tellurium isotopes were observed and attributed to different modes of formation.

First, the oxidation states of the beta-decaying precursors were measured since the precursor state was known to influence the daughter atom. The tin and antimony precursors produced mostly by fission were concluded to be oxidized by reactor radiations in the sample solutions because of no carrier.

Next, the distribution of the daughters of β-decay between the reduced and oxidized states was analyzed using the results of the independently formed fission products that had been obtained in Chapter 4. The fractions of the tellurium isotopes as Te(IV) formed by β-decay of the antimony percursors in the +5 oxidation state were dependent on the isotopes; the higher β-decay energy is, the more the fraction as Te(IV) is. The differences were attributed to different recoil energies of the isotopes in the emission of β-particles because of the similarity between the chemical structures of precursors and those of

daughters.

In contrast to the Te isotopes, the fractions of the Sb isotopes as Sb(III) formed by β-decay of the tin precursors in the +4 oxidation state were nearly constant irrespective of their β-decay energies. This was explained by considering that the newly formed antimony atom in the +5 oxidation state must rearrange its chemical structure.

Considering the differences of the oxidation states due to modes of formation, it was noted that the oxidation states would be some effective measures of fractional fission yields.

In the preliminary experiment, the oxidation states of the $^{131}Te^{g}$ was studied in the $^{130}Te(n, \gamma)^{131}Te^{g}$. Higher yields (>90 %) of Te(IV) were obtained when starting with both Te(IV) and Te(VI). A comparison between fission and neutron capture suggested the importance of the electronic excitation of the products, in particular for the former.

CHAPTER 6
SUMMARY AND CONCLUSION

The present study is a summary of the author's works on chemical behaviors of the tin, antimony, and tellurium fission products in aqueous solutions, and parts of the experimental evidences have been reported previously (Mo80a, Mo80b, Mo80c).

A fission fragment undergoes a long journey from the initial fission event to its final resting place where it becomes part of the chemical environment. In the preceding Chapters, the experimental evidences have been described to discuss the mechanisms which lead the fission product to rest in the final oxidation state.

The results te be noted is given as follows:

In Chapter 2, the radiation-induced reactions of antimony and tellurium compounds in sulfuric acid solutions were investigated using double tracers for each element. The double tracers were very effective to improve the knowledge of reaction kinetics, and the new reaction mechanisms in deaerated solutions were proposed for each element.

The tracer technique was employed to distinguish the hot from the thermal reactions in the behavior of the newly formed

atoms in nuclear events. The oxygen effect and the phase effect were studied on the distribution of the oxidation states of the newly formed atoms.

In Chapter 3, the chemical effects of β-decay were investigated out of reactors for the tin and antimony isotope having considerably low β-decay energies. The oxidation state of the daughter isotopes was not interfered with any thermal reactions and showed a remarkable variety of the chemical effects of β-decay. The essential factors were considered to be the thermodynamic stability of the primary products and their subsequent reaction as well as the electronic excitation and ionization.

In Chapter 4, the oxidation states were investigated of the independently formed fission products. It was shown that, in the irradiated solutions, there was the possibility of the fission products being involved in the thermal reactions with the diffusing reactive species from their own tracks or the bulk-radiolysis products in the medium. The present results suggested that, together with a very high temperature of the thermal spike of fission, the electronic excitation of the fission products could allow themselves to undergo the chemical reaction requiring a high activation energy.

In Chapter 5, the oxidation states were analyzed of the cumulatively formed fission products. The differences in the oxidation states among the isotopes were observed and attributed

to different modes of formation. In β-decay, the fractions of the tellurium isotopes in the oxidized state depend on the β-decay energies of their precursors, whereas those of the antimony isotopes are nearly constant irrespective of the β-decay energy. It was explained that the different behaviors between those two elements would reflect the chemical properties of their precursors. In the separate experiment, a comparison between fission and neutron capture reaction suggested that the electronic excitation of the product, in particular in the former, would be more important in the final distribution of the oxidation state of the product than the spike temperature.

In conclusion, the author's present view is summarized on the overall process of the chemical behaviors of fission products:

(i) Because the energy of the fission fragment, of the order of 100 MeV, exceeds considerably normal ionization energies, the fragment can not form a chemical compound in the first period subsequent to its formation ($<10^{-14}$ sec).

(ii) Chemically speaking, the fragment would be able to react with the medium when it losed most of its recoil energy. Physical concepts (Bo40, Wo65) suggest that a fission fragment becomes nearly neutral before it starts to react chemically ($\sim 10^{-14}$ sec).

(iii) The primary fission product of very low charge, in a highly reduced state, would then react with the medium (10^{-14} - 10^{-12} sec). It should be noted that the electronic excitation of the product would play an important part as well as a very high temperature of the thermal spike of fission. The electronic excitation of the fission product are considered to be very high compared with other nuclear reactions such as neutron capture.

(iv) After the fission product becomes part of the chemical environment, there is the possibility of the product being involved in thermal reactions with the diffusing radicals from its own track or bulk-radiolysis products in the medium (10^{-12} - 10^{-6} sec). The former localized radicals are very important in this case since they are formed at very high energy transfer values.

(v) Furthermore, the fission product suffering in various stages may be involved in thermal reactions such as exchange, reduction, oxidation, etc. ($>10^{-6}$ sec).

(vi) In general, most of the fission products undergo radioactive decay. Chemical observations on the fission products refer usually to the later members of the decay chains and these arise mainly through decay of precursors instead of directly in fission.

(vii) Although discussion has centered on aqueous system, there is no reason to think that the slowing-down of fast atoms

in other condensed systems will not also lead to the similar effects. The major difference, of course, is that the chemical properties of the media might affect the oxidation state of the newly formed atom. Thus essential phenomena are repeated in other condensed systems.

It is very difficult to reach a quantitative theory on the behaviors of hot atoms since they are often governed by their inherent properties as normally observed in thermal reactions. In future, it is, however, desired to develop a general quantitative theory considering the experimental evidences and the theories in other neighboring fields such as radiation chemistry inclusively.

ACKNOWLEDGEMENTS

The works described in this thesis have been carried out under the direction of Professor Tomota Nishi. I would like to express my sincere thanks to Professor T. Nishi, who has led me to these works, for his many valuable suggestions, helpful advices, interesting discussions and kind encouragements.

I am greatly indebted to Professor Ichiro Fujiwara, Institute of Atomic Energy of Kyoto University, for contributing his experimental skill and grasp of objectives to the accomplishment of this work. Besides, I am exceedingly pleased with his able guidance and critical reading of this thesis in the course of its preparation.

I would like to thank heartily Professor Nobutsugu Imanishi for his co-operation in determining gamma-ray measurements. Grateful acknowledgements are due to Dr. Michihiro Ishibashi, Dr. Teruaki Ohnishi, and Mr. Kokichi Hotta for their significant suggestions and continuous encouragements.

Thanks are due to Professor Shiro Iwata, Research Reactor Institute of Kyoto University, for his help and interest in this work. I also indebted to the peaple at this institute during achivements of the experiments with the reactor and other equipments. A part of this work was done under the Visiting Researcher's program of Kyoto University Research Reactor Institute.

Thanks are also extended to Mr. Rintaro Katano, Institute for Chemical Research of Kyoto University, for his advice in carrying out irradiations by gamma-rays.

Finally many thanks go to Professor Jun Oishi, Department of Nuclear Engineering of Kyoto University, and Dr. Kameo Asada who is now at Nihon Denchi Co., for their continuous encouragement and advice in preparation of this thesis. I am pleased to thank Dr. Kazuhiro Wada, Department of Nuclear Engineering, for his encouragement.

I cannot mention the names of all my friends either at Kyoto University or other. Their friendship and encouragement were indispensable to this work. I thank my parents, Yaeko and Minoru Moriyama, for their kind support.

REFERENCES

Ac72 R. E. Ackerhalt and G. Harbottle, Radiochim. Acta 17, 126(1972).

Al60 J. T. Allen and G. Scholes, Nature 187, 218(1960).

Al74 A. Alian and A. Haggag, J. Inorg. Nucl. Chem. 36, 679 (1974).

Am35 E. Amaldi, O. D'Agostino, E. Fermi, B. Pontecorvo, F. Rasetti and E. Segre, Proc. Roy. Soc. A149, 522(1935).

Am71 S. Ambe and N. Saito, Radiochim. Acta 16, 40(1971).

Am75 S. Ambe and F. Ambe, J. Chem. Phys. 63, 4077(1975); F. Ambe and S. Ambe, Inorg. Nucl. Chem. Lett. 11, 139 (1975).

An66 T. Andersen, F. Christensen, and K. Olesen, Trans. Faraday Soc. 62, 248(1966); T. Andersen, H. E. Lundager-Madsen and K. Olesen, ibid. 63, 1730(1966).

Au72 R. L. Auble, Nucl. Data Sheets B8, 77(1972).

Au73 R. L. Auble, Nucl. Data Sheets 9, 157(1973).

Au76 R. L. Auble, H. R. Hiddleston and C. P. Browne, Nucl. Data Sheets 17, 573(1976).

Be72 H. D. Betz, Rev. Mod. Phys. 44, 465(1972).

Bi75 N. E. Bibler, J. Phys. Chem. 79, 1991(1975).

Bl77 J. Blachot and C. Fiche, Atomic Data and Nuclear Data Tables 20, 241(1977).

Bo40 N. Bohr, Phys. Rev. 58, 654(1940).

Bo59 J. W. Boyle, S. Weiner and C. J. Hochanadel, J. Phys. Chem. 63, 892(1959).

Br55 C. H. Brubaker, J. Am. Chem. Soc. 77, 5265(1955).

Br67 L. C. Brown and A. C. Wahl, J. Inorg. Nucl. Chem. 29, 2133(1967).

Br78 E. Browne, J. M. Dairiki and R. E. Doebler, Table of Isotopes, 7th ed., Wiley-Interscience, New York(1978).

Bu48 W. H. Burgus, T. H. Davies, R. R. Edwards, H. Gest, C. W. Stanley, R. R. Williams and C. D. Coryell, J. Chim. Phys. 45, 165(1948).

Bu51 W. H. Burgus and T. H. Davies, Nat. Nuclear Energy Ser., The Fission Products, Paper 19, McGraw-Hill, New York (1951).

Ca60 T. A. Carlson, J. Chem. Phys. 32, 1234(1960).

Ca68 T. A. Carlson, C. W. Nesto, Jr., T. C. Tucker and F. B. Marik, Phys. Rev. 169, 27(1968).

Cu63 J. B. Cumming, U. S. Atomic Energy Commission, Rep. No. NAS-NS-3107, p. 25(1963).

Cz63 G. Czapski and B. H. J. Bielski, J. Phys. Chem. 67, 2180 (1963).

Da70 J. L. Dawson, J. Wilkinson and M. I. Gillibrand, J. Inorg. Nucl. Chem. 32, 501(1970).

De39 D. C. DeVault and W. F. Libby, Phys. Rev. 55, 322(1939).

De63 H. O. Denschlag, N. Henzel and G. Herrmann, Radiochim. Acta 1, 172(1963).

Do67 L. Dogliotti and E. Hayon, J. Phys. Chem. 71, 3802(1967).

Er68 B. R. Erdal and A. C. Wahl, J. Inorg.Nucl. Chem. 30, 1985(1968).

Er69a B. R. Erdal, A. C. Wahl and B. J. Dropesky, J. Inorg. Nucl. Chem. 31, 3005(1969).

Er69b B. G. Ershov and A. K. Pikaev, Radiation Res. Rev. 2, 1(1969).

Es60 P. J. Estrup and R. Wolfgang, J. Am. Chem. Soc. 82, 2665(1960).

Fe63 F. Feher, Handbook of Preparative Inorganic Chemistry, p. 437, Academic Press, London(1963).

Fo72 M. M. Fowler, C. C. Lin and A. C. Wahl, unpublished results; M. M. Fowler, Ph. D. Thesis, Washington, St. Louis, Mo.(1972).

Fr39 O. R. Frisch, Nature 143, 276(1939).

Fr66 H. Fricke and E. J. Hart, Radiation Dosimetry, 2nd ed., p. 167, Academic Press, New York(1966).

Fu58 C. B. Fulmer and B. L. Cohen, Phys. Rev. 109, 94(1958).

Fu74 I. Fujiwara, N. Imanishi and T. Nishi, J. Inorg. Nucl. Chem. 36, 1921(1974).

Fu76 I. Fujiwara, N. Imanishi and T. Nishi, J. Inorg. Nucl. Chem. 38, 1594(1976).

Gr63 A. E. Greendale and D. L. Love, Anal. Chem. 35, 632(1963).

Ha39 O. Hahn and F. Strassman, Naturwissenschaften 27, 11 and 89(1939).

Ha58 G. Harbottle and N. Sutin, J. Phys. Chem. 62, 1344(1958).

Ha61 D. Hall and G. N. Walton, J. Inorg. Nucl. Chem. 19, 16 (1961).

Ha64 R. L. Hahn, J. Chem. Phys. 39, 3482(1963); ibid. 41, 1986(1964).

Ha66 M. Haissinsky, G. Lunde and P. Patgny, J. Chim. Phys. 63, 1093(1966).

Ha67 M. Haissinsky, The Chemistry of Ionization and Excitation, p. 277, Taylor and Francis, London(1967).

Ha68 M. Haissinsky, J. Chim. Phys. 65, 1368(1968).

Ha79 G. Harbottle, Chemical Effects of Nuclear Transformations in Inorganic Systems, p. 39, North-Holland, Amsterdam (1979).

He74 E. A. Henry, Nucl. Data Sheets 11, 495(1974).

Hi71 M. Hillman and A. J. Weiss, Sonderdruck aus Radiochimica Acta 15, 79(1971).

Hi74 H. R. Hiddleston and C. P. Browne, Nucl. Data Sheets 13, 133(1974).

Hi76 H. R. Hiddleston and C. P. Browne, Nucl. Data Sheets 17, 225(1976).

Ho60 J. Hoarau, Noveau Traite Chim. Minerale 13, 2023(1960).

Ho72 D. J. Horen, Nucl. Data Sheets B8, 123(1972).

Im75 N. Imanishi, I. Fujiwara and T. Nishi, Nucl. Phys. A238, 325(1975).

Im76 N. Imanishi, I. Fujiwara and T, Nishi, Nucl. Phys. A263, 141(1976).

Ka60 S. Katcoff, Nucleonics 18, 201(1960).

Ka61 T. Kambara, Y. Oba and K. Shiozawa, Radioisotopes 10, 217(1961).

Ka65 T. Kambara, K. Yamaguchi and Y. Yasuba, Exchange Reaction, p. 101, IAEA, Vienna(1965).

Ka70 R. Katano, Bull. Inst. Chem. Res., Kyoto Univ. 48, 66 (1970).

Ke64 J. P. Keene, Radiat. Res. 22, 1(1964).

Le67 B. Lesigne, C. Ferradini and J. Pucheault, J. Phys. Chem. 77, 2156(1967).

Le70 R. A. Lebedev, A. M. Babeshkin, A. N. Nesmeyanov and N. L. Fatieva, Radiochem. Radioanal. Lett. 5, 83(1970).

Li47 W. F. Libby, J. Am. Chem. Soc. 69, 2523(1947).

Li73 C. C. Lin and A. C. Wahl, J. Inorg. Nucl. Chem. 35, 1 (1973).

Ma58 A. Mahlman and J. W. Boyle, J. Am. Chem. Soc. 80, 773 (1958).

Ma61 N. Matsuura, Y. Kurimura and M. Takizawa, Sci. Papers Inst. Phys. Chem. Res. 55, 224(1961).

Ma62 N. Matsuura, Y. Kurimura and M. Takizawa, Reports Inst. Phys. Chem. Res. (in Japanese) 38, 555(1962).

Ma65 M. S. Matheson and J. Rabani, J. Phys. Chem. 69, 1324 (1965).

Ma72 R. W. Matthews, H. A. Mahlman and T. J. Sworski, J. Phys. Chem. 76, 1265(1972).

Mc71a H. A. C. Mckay, Principles of Radiochemistry, p. 446, Butterworths, London(1971).

Mc71b H. A. C. Mckay, Principles of Radiochemistry, P. 296, Butterworths, London(1971).

Me39 L. Meinter and O. R. Frisch, Nature 143, 239(1939).

Mi50 J. M. Miller and R. W. Dodson, J. Chem. Phys. 18, 865 (1950).

Mo69 A. Mozumder, Adv. Rad. Chem. 1, p. 82, Wiley-Interscience, New York(1969).

Mo80a H. Moriyama, I. Fujiwara and T. Nishi, J. Radioanal. Chem. 55, 45(1980).

Mo80b H. Moriyama, I. Fujiwara and T. Nishi, J. Phys. Chem. 84, 1801(1980).

Mo80c H. Moriyama, I. Fujiwara and T. Nishi, J. Inorg. Nucl. Chem. in press(1980).

Ne62 V. D. Nefedov, I. S. Kirin and V. M. Zaitsev, Soviet Radiochem. 4, 311(1962).

Ne64 V. D, Nefedov, I. S. Kirin and V. M. Zaitsev, Radiokhimiya 6, 67(1964).

Ne68 R. S. Nelson, The Observation of Atomic Collisions in Crystalline Solids, North-Holland, Amsterdam(1968).

Ni61 J. B. Niday, Phys. Rev. 121, 1471(1961).

Pa64 Y. Paiss and S. Amiel, J. Am. Chem. Soc. 86, 2332(1964).

Pi57 A. L. Pitman, M. Pourbaix and N. deZoubov, J. Electrochem. Soc. 104, 594(1957).

Sc63a W. Schenk, Handbook of Preparative Inorganic Chemistry, p. 606, Academic Press, London(1963).

Sc63b H. A. Schwarz, J. Phys. Chem. 67, 2827(1963).

Sc69 H. A. Schwarz, J. Phys. Chem. 73, 1928(1969).

Se39 E. Segre, R. Halford and G. T. Seaborg, Phys. Rev. 55, 321(1939).

Se40 G. T. Seaborg, G. Friedlander and J. W. Kennedy, J. Am. Chem. Soc. 62, 1309(1940).

Se52 R. Serber and H. Snyder, Phys. Rev. 87, 152(1952).

Se56 F. Seitz and J. S. Koehler, Solid State Physics 2, p. 305, Academic Press, New York(1956).

Se73 K. Sehested, E. Bjergbakke and H. Fricke, Radiat. Res. 56, 385(1973).

Si66 O. Sibert and R. H. Tomlinson, Radiochim. Acta 5, 217 (1966).

Sm73 J. D. Smith, Comprehensive Inorganic Chemistry, p. 580, Pergamon Press, Oxford(1973).

Sp73 S. Spiridon and A. Calusaru, J. Inorg. Nucl. Chem. 35, 713(1973).

Sp76 S. Spiridon and A. Calusaru, J. Inorg. Nucl. Chem. 38, 1429(1976).

St51 C. W. Stanley and T. H. Davies , Nat. Nuclear Energy Ser., The Fission Products, Paper 18, McGraw-Hill, New York (1951).

Su40 H. Suess, Z. Phys. Chem. B45, 297 and 312(1940).

Sz34 L. Szilard and T. A. Chalmers, Nature 134, 462(1934).

Th62 M. W. Thompson and R. S. Nelson, Phil. Mag. 7, 2015(1962).

Th69 J. K. Thomas, Adv. Radiat. Chem. 1, p. 170, Wiley Interscience, New York(1969).

Tr71 D. E. Troutner, J. Inorg. Nucl. Chem. 33, 4327(1971).

Va73 R. Vandenbosch and J. R. Huizenga, Nuclear Fission, p. 290, Academic Press, New York(1973).

Wa57 G. N. Walton, Prog. Nucl. Phys. 6, 192(1957).

Wa64 G. N. Walton, Radiochim. Acta 3, 108(1964).

Wa79 U. Wagner-Zahn, Chemical Effects of Nuclear Transformations in Inorganic Systems, p. 355, North-Holland, Amsterdam (1979).

We60 S. Wexler and G. R. Anderson, J. Chem. Phys. 33, 850 (1960).

We77a R. C. Weast, Handbook of Chemistry and Physics, p. F216, CRC Press, Cleveland(1977).

We77b R. C. Weast, Handbook of Chemistry and Physics, p. D143, CRC Press, Cleveland(1977).

Wi53 J. E. Willard, Ann. Rev. Nucl. Sci. 3, (1953).

Wo63 R. Wolfgang, J. Chem. Phys. 39, 2983(1963).

Wo65 R. Wolfgang, Prog. Reaction Kinetics 3, 108(1965).

Wo74 K. Wolfsberg, Los Alamos Scientific Lab., Rep. No. LA-5553-MS(1974).